

**ENGINEERED BARRIER SYSTEM PERFORMANCE ASSESSMENT CODES  
(EBSPAC) PROGRESS REPORT -  
OCTOBER 1, 1992, THROUGH SEPTEMBER 25, 1993**

*Prepared for*

**Nuclear Regulatory Commission  
Contract NRC-02-88-005**

*Prepared by*

**Center for Nuclear Waste Regulatory Analyses  
San Antonio, Texas**

**October 1993**



462.2 --- T199310180003  
Engineered Barrier System  
Performance Assessment Codes  
(EBSPAC) Progress Report  
October 1, 1992, through

**Engineered Barrier System Performance Assessment Codes  
(EBSPAC) Progress Report —  
October 1, 1992, through September 25, 1993**

*Prepared for*

**Nuclear Regulatory Commission  
Contract NRC-02-88-005**

*Prepared by*

**N. Sridhar  
J.C. Walton  
G.A. Cragolino  
P.K. Nair**

**Center for Nuclear Waste Regulatory Analyses  
San Antonio, Texas**

**October 1993**

## PREVIOUS REPORTS IN SERIES

<b>Number</b>	<b>Name</b>	<b>Date Issued</b>
CNWRA 92-019	TWITCH—A Model for Transient Diffusion, Electromigration, and Chemical Reaction in One Dimension	August 1992
CNWRA 92-020	MARIANA—A Simple Chemical Equilibrium Module, Version 1.0	August 1992
Letter Report	Selection and Evaluation of Models for Substantially Complete Containment Example Problem	September 1992
Letter Report	Preliminary Assessment of Pitting Corrosion Models	September 1992

## ABSTRACT

The progress in developing the Engineered Barrier System Performance Assessment Codes (EBSPAC) during FY93 is described in this report. The evolution of the waste package environment in an unsaturated (or partially saturated) environment is modeled in terms of evaporative concentration and migration of water towards the container. The corrosion performance of the waste containers is modeled in terms of corrosion potentials and critical potentials for localized corrosion and stress corrosion cracking. The upgrades to a detailed crevice corrosion model (TWITCH) are discussed and the code extended to predict the corrosion product formation in copper pits. The mechanical failure of the container is discussed in terms of buckling and fracture. The release rate of radionuclides from spent fuel is examined using a transport model assuming fixed solubility. The effect of moisture transport towards the container on the release rate from the engineered barrier system (EBS) is examined. The electrochemical dissolution mechanism for calculating the dissolution rate of spent fuel and its congruent release rate is discussed. Limitations of the existing models and future directions of the EBSPAC are described.

# CONTENTS

Section	Page
FIGURES .....	vi
TABLES .....	viii
ACKNOWLEDGMENTS .....	ix
EXECUTIVE SUMMARY .....	x
1 INTRODUCTION .....	1-1
2 WASTE PACKAGE ENVIRONMENTAL MODELS .....	2-1
2.1 INTRODUCTION AND RATIONALE .....	2-1
2.2 SIMPLIFIED THERMAL MODEL .....	2-2
2.3 SITUATIONS LEADING TO WATER CONTACTING THE WASTE PACKAGE ...	2-5
2.4 EVAPORATION .....	2-7
2.5 SOLUTE EFFECTS ON WATER DYNAMICS .....	2-10
2.6 GENERAL CASE FOR NEAR-FIELD AQUEOUS CONDITIONS .....	2-12
2.7 FUTURE DIRECTIONS .....	2-14
3 CONTAINMENT MODELS .....	3-1
3.1 OVERALL APPROACH .....	3-1
3.1.1 The Approach for Corrosion-Resistant Metallic Materials .....	3-1
3.1.2 Approach for Corrosion-Allowance Type Metallic Alloys .....	3-3
3.2 CORROSION POTENTIAL .....	3-3
3.3 LOCALIZED CORROSION MODELS .....	3-9
3.3.1 Update to TWITCH .....	3-10
3.3.1.1 Governing Equations .....	3-10
3.3.1.2 Application of TWITCH to Modeling Copper Pitting .....	3-18
3.3.1.3 Future Developments .....	3-19
3.4 CRITICAL POTENTIALS .....	3-20
3.4.1 Stochastic Models .....	3-23
3.4.2 Deterministic Mechanistic Models .....	3-25
3.4.3 Empirical Models .....	3-26
3.5 STRESS CORROSION CRACKING MODELS .....	3-28
3.5.1 Mechanistic Models .....	3-29
3.5.1.1 Slip-Dissolution Model .....	3-31
3.5.1.2 Film-Induced Cleavage Model .....	3-35
3.5.1.3 Surface Mobility Model .....	3-36
3.5.2 Empirical Models .....	3-38
3.5.3 Future Directions .....	3-41
3.6 MECHANICAL FAILURE MODELS .....	3-42
3.6.1 Buckling Failure Model .....	3-42
3.6.2 Yield Failure Model .....	3-43
3.6.3 Fracture Failure Model .....	3-44

# CONTENTS

Section		Page
4	RELEASE RATE MODELS .....	4-1
4.1	CURRENT CONCEPTUAL MODELS .....	4-1
4.1.1	Mass Transport Analysis .....	4-1
4.1.2	Elevation of Temperature Above Boiling Point of Water .....	4-2
4.1.3	Gradient Reversal .....	4-2
4.1.4	Container Corrosion .....	4-2
4.1.5	Release Controlling Phenomena Currently Included in SCCEX Code .....	4-3
4.2	RADIONUCLIDE RELEASE SIMULATIONS .....	4-3
4.3	ELECTROCHEMICAL DISSOLUTION MODEL .....	4-8
5	SUMMARY .....	5-1
6	REFERENCES .....	6-1

## APPENDIX A

## FIGURES

Figure		Page
2-1	Calculated heat generation rate from radioactive decay (DOE, 1993c) . . . . .	2-3
2-2	Thermal history of repository center as a function of time and thermal loading (1 kW/acre = 0.247 W/m <sup>2</sup> ) . . . . .	2-4
2-3	Temperature drop between individual waste container and surrounding rock . . . . .	2-4
2-4	Schematic of desiccated zone and fractures surrounding waste packages . . . . .	2-6
2-5	Evaporation rate of pure water as a function of temperature drop between the waste container and the surrounding rock . . . . .	2-9
2-6	Vapor pressure as a function of temperature for several saturated salt solutions . . . . .	2-11
2-7	Temperature difference between saturated salt solutions and pure water at the same vapor pressure . . . . .	2-12
2-8	Predicted salinity on the surface of the waste package as a function of time and radial distance from the center of the waste package . . . . .	2-14
3-1	Overall approach to predicting corrosion failure modes (in this case, localized corrosion) of a corrosion-resistant alloy . . . . .	3-2
3-2	A sample calculation of the corrosion potential using oxygen reduction and hydrogen evolution as cathodic processes and passive current as the anodic process . . . . .	3-8
3-3	Comparison of calculated activity coefficients for calcium chloride with experimental data . . . . .	3-16
3-4	Geometry of copper pit assumed in modeling. Narrowing at the mouth was imposed to simulate mass transport limitations caused by a cap of corrosion products. Total pit depth was assumed to be 10 mm. . . . .	3-20
3-5	pH in copper pit . . . . .	3-21
3-6	Negative log [cuprous ion concentration] as a function of depth in pit . . . . .	3-21
3-7	Bicarbonate, dissolved carbon dioxide plus carbonic acid, and dissolved oxygen inside the pit. Concentrations drop precipitously near the mouth where malachite precipitation occurs. . . . .	3-22
3-8	Potential drop in copper pit . . . . .	3-22
3-9	Precipitation of solids in copper pit in moles/liter of crevice solution . . . . .	3-23
3-10	The capture of a vacancy by the stressed tip of the crack is the elementary step for crack propagation in the surface-mobility SCC mechanism (Galvele, 1987) . . . . .	3-37
3-11	Schematic of crack velocity versus stress intensity showing the three stages of crack propagation . . . . .	3-39
4-1	Waste container temperature based on heat conduction for scenarios a, b, and c . . . . .	4-5
4-2	Water coverage of container surface for scenarios a, b, and c . . . . .	4-5
4-3	Predicted salinity for scenarios a, b, and c . . . . .	4-6
4-4	Waste container temperature based on heat conduction for scenarios c, d, and e . . . . .	4-6
4-5	Water coverage of container surface for scenarios c, d, and e . . . . .	4-7
4-6	Predicted salinity for scenarios c, d, and e . . . . .	4-7

## FIGURES

Figure	Page
4-7 Steady state dissolution current of unirradiated $\text{UO}_2$ as a function of applied potential and environmental species. ■ — 0.1 M $\text{Na}_2\text{SO}_4$ ; ○ — 0.1 M $\text{NaHCO}_3$ ; X — 0.1 M $\text{Na}_2\text{HPO}_4$ (Sunder and Shoemith, 1991) . . . . .	4-11

## TABLES

Table		Page
2-1	Water chemistry of the groundwater from a saturated zone near the repository and evolution of water chemistry due to evaporation and condensation cycles . . . . .	2-7
3-1	Parameters used to calculate the kinetics of cathodic reactions and corrosion potentials shown in Figure 3-2. For all cases: $T=95\text{ }^{\circ}\text{C}$ ; $\text{pH}=8$ ; $i_0(\text{H}^+)=1\times 10^{-4}\text{ A/m}^2$ ; $i_{\text{pass}}=1\times 10^{-3}\text{ A/m}^2$ . Activation energies for exchange current densities for oxygen and hydrogen reactions were 100 and 40 kJ/mol, respectively. . . . .	3-7
3-2	Initial and boundary conditions for species used in copper pit model . . . . .	3-19
4-1	Parameters used for calculating temperature profile of an assemblage of waste packages . . . . .	4-3
4-2	Common parameters used for simulating radionuclide release rate from waste packages . . . . .	4-4

## **ACKNOWLEDGMENTS**

The authors wish to acknowledge the assistance of Tony Torng in performing many of the computer simulations and in providing input to the mechanical failure models. Discussions with William Murphy, Randy Manteufel, and Peter Lichtner are also gratefully acknowledged. The authors wish to thank Stephen Lukezich and Peter Lichtner for providing technical reviews of the various sections. The assistance of Bonnie L. Garcia in producing this document in the finished form and the Southwest Research Institute (SwRI) publications staff is also acknowledged.

The report was prepared to document work performed by the Center for Nuclear Waste Regulatory Analyses (CNWRA) for the U.S. Nuclear Regulatory Commission (NRC) under Contract NRC-02-88-005. The activities reported here were performed on behalf of the NRC Office of Nuclear Material Safety and Safeguards (NMSS), Division of High Level Waste Management (DHLWM). The report is an independent product of the CNWRA and does not necessarily reflect the views or the regulatory position of the NRC.

## EXECUTIVE SUMMARY

This report describes the progress in FY93 of the Engineered Barrier System Performance Assessment Codes (EBSPAC) that are under development to determine compliance of EBS with NRC regulations. EBSPAC is the suite of auxiliary analyses, codes, and models that support the performance assessment (PA) codes, such as the Iterative Performance Assessment (IPA) code and the Substantially Complete Containment Example Problem (SCCEX) code. Activities in both containment and release rate modeling are discussed, and future directions are outlined. Specific areas of integration with the experimental program, Integrated Waste Package Experiments (IWPE), are indicated.

A systematic approach to PA of EBS requires a definition of the environment around the waste packages, materials of the waste packages, modes/submodes of failure, statistical description of failure, failure criteria, and accelerated testing. In a partially saturated environment such as the repository horizon at Yucca Mountain, high thermal loading can cause the formation of a relatively dry zone around the waste packages. In such a case, issues related to corrosion of waste package components and transport of radionuclides through an aqueous medium become unimportant and only gaseous release of  $^{14}\text{C}$  is an issue in meeting the EBS and repository performance requirements. However, condensation of evaporated water and drainage through fractures back to the waste packages is a possibility. Based on the latter scenario, the evolution of the chemical composition of the environment contacting the container surface is modeled. It is predicted that evaporation can occur even for relatively modest thermal loading and can lead to precipitation of scale-forming compounds (such as silicates). Concentration of salts containing chloride and other ions can result in an elevated boiling point. The diffusion of water vapor away from the hot container and convection of liquid water towards the container due to vapor pressure depression is modeled. In this scenario, a highly saline solution containing about 5 M chloride is predicted to form on scale deposits at the container surface. However, this calculation does not rigorously consider the complex chemistry of the groundwater, high ion-strength fluids, and the kinetics of interaction of the incoming condensate water with the rock. For example, if the incoming water is devoid of chloride, then a gradual dilution of chloride in the initial evaporated solution can be expected. Nevertheless, the complex nature of the chemistry of the environment near the waste packages even for modest thermal loading is highlighted.

The overall approach used for modeling the corrosion of container materials consists of modeling the corrosion potential and the critical potentials of various corrosion modes such as pitting, crevice corrosion, and stress corrosion cracking. A simple model for corrosion potential calculation involving oxygen and hydrogen ion as the cathodic species and steady-state molecular diffusion as the transport process is used. The anodic reaction is considered to be the potential-independent passive current. This is included as a subroutine in the SCCEX code. The uncertainties in the various parameters in the cathodic reactions are pointed out. Further improvements in the modeling of corrosion potential under anticipated repository conditions are necessary. The critical potentials for pitting and crevice corrosion are obtained through various empirical models constructed from data available in the literature as well as the IWPE program. If a high saline condition is predicted near the waste package, the differences in critical potentials between alloy 825 and type 304L stainless steel are insignificant, and no performance improvement of alloy 825 over type 304L stainless steel is predicted. However, if a more dilute chloride environment exists, there will be a significant improvement in corrosion resistance of alloy 825 over type 304L stainless steel. This overall approach is robust with respect to the changing design of the waste package since a corrosion potential and critical potentials can be identified for any new material or

material combination. The evaluation of corrosion and critical potentials will be the focus of ongoing literature review as well as the IWPE research program.

Detailed models for pitting and crevice corrosion are discussed. Improvements in a crevice corrosion model, TWITCH, are discussed. The major limitation of this model, as well as similar models for crevice corrosion of stainless steels, is its inability to predict a critical potential assuming a potential-independent passive current density. Future modifications to the model to predict a critical potential will include consideration of potential-dependent dissolution of manganese sulfide inclusions for alloys such as type 304L stainless steel and lateral propagation of crevice corrosion nuclei in a realistic crevice between rough surfaces of other alloys that do not contain MnS inclusions. The pitting of copper using TWITCH predicts the formation of malachite [ $\text{CuCO}_3\text{Cu}(\text{OH})_2$ ] on the pit mouth, cuprite ( $\text{Cu}_2\text{O}$ ) inside the pit, and nantokite ( $\text{CuCl}$ ) at the pit bottom. The formation of these corrosion products is in qualitative agreement with experimental observations.

Models for SCC in which crack growth is stimulated by the anodic process were evaluated with a focus on the slip-dissolution model. While this model has enjoyed some success in predicting SCC behavior in many environments, the predictions have had a considerable element of experimental calibration. Also, uncertainties exist in the values of relevant parameters. From the point of view of long-term prediction, two alternative approaches can be used: (i) empirically developed crack growth rate relationships and (ii) empirically developed critical potentials for SCC. The critical potential concept is attractive because it can be used as a criterion to prevent crack growth. Further benefits can be derived if it can be shown to be related to the critical potentials for localized corrosion. However, there is little agreement regarding the existence of a critical potential for SCC and its relationship to other localized corrosion phenomena.

Models for release of radionuclides from spent fuel are discussed. Release rate calculations from vitrified wastefrom is not the focus of current efforts in the EBSPAC program. Release of radionuclides from spent fuel involves three components: (i) release of volatile components, such as Cs and I, from the fuel-cladding gap; (ii) release of components such as Tc from the grain boundaries of the spent fuel; and (iii) release of radionuclides held in the matrix of the fuel. The release rate calculation by the last mechanism involves assumptions regarding the spent fuel dissolution behavior. Most of the current release rate models involve calculation of transport of a radionuclide, such as  $^{235}\text{U}$ , with the boundary condition at the wastefrom surface corresponding to its solubility limit in the waste package environment. The solubility limit is usually assumed to be dependent on the environmental  $E_h$ . A more reasonable model, considering the semiconductive nature of  $\text{UO}_{2+x}$ , is the electrochemical dissolution model, which attempts to calculate the dissolution rate as a function of reaction rates of oxidation and reduction processes at the spent fuel surface. This approach is similar to the calculation of the corrosion potential of metallic container materials. The limitations of this approach include the lack of reaction rate data for various cathodic and anodic processes on the spent fuel surface. Future areas of activity in spent fuel leaching rate modeling must include the electrochemical dissolution mechanism coupled to transport calculations and precipitation reactions at a distance from the waste packages.

# 1 INTRODUCTION

Engineered Barrier System Performance Assessment Codes (EBSPAC) form a suite of auxiliary codes, models, and analyses that are used to understand and evaluate the performance of the various components of the engineered barrier system (EBS). The objectives of the EBSPAC development task are to (i) develop and evaluate credible compliance determination models for assessing the performance of EBS components and subsystems, and (ii) develop an understanding of the near-field wasteform performance issues. The detailed models and analyses developed within EBSPAC will support the more simplified models that will be used in the Source Term Code (SOTEC) for Total System Performance Assessment calculations. Another activity within Task 2 of the EBS program, which is supported by EBSPAC, is a code for calculation of compliance with the substantially complete containment requirement in 10 CFR 60.113(a)(1)(ii)(A). The substantially complete containment example problem code (SCCEX) considers only those processes that contribute to containment goals and uses simplified models similar to SOTEC. While understanding that the performance of various waste package components is the objective of the EBSPAC program, it is recognized that fundamental mechanistic understanding of many corrosion processes is a goal yet to be attained. Even when mechanistic models are available for some processes, such as stress corrosion cracking and localized corrosion, these models are not universally accepted or applicable to all corroding systems. Therefore, where necessary, empirical models will be incorporated in SOTEC and SCCEX analyses. Hence, another objective of the EBSPAC program is to evaluate empirical models or correlations available in the literature as well as through Center for Nuclear Waste Regulatory Analyses (CNWRA) experimental programs for suitability of use in performance calculations.

Recently, various Advanced Conceptual Designs (ACDs) of waste packages and the EBS were discussed by the U.S. Department of Energy (DOE) (DOE, 1993a, 1993b; Doering, 1993; Benton, 1993). In addition to the Site Characterization Plan (SCP) reference design, which consists of a single-wall container, bimetallic containers have been proposed. In the bimetallic container designs, the inner container is made of a corrosion-resistant alloy (alloy 825, alloy C-4, or Titanium Grade 12), and the outer container is made of a corrosion-allowance material such as carbon steel. These bimetallic designs are proposed to be used as either multipurpose units (MPU) whose functions span from the reactor site through the Monitored Retrievable Storage (MRS) system to the disposal facility, or as part of the multipurpose canister (MPC) design in which the inner container would remain fixed in design and the outer cask will be changed from transportation through storage to disposal. While these alternate design concepts entail changes in the consideration of failure processes, the methodology of the EBSPAC program should be such that the overall approach is not altered substantially. This philosophy is consistent with the Corrosion-Based Design Approach advocated by Staehle (1991), which consists of the following ten steps.

- (i) Definition of environment
- (ii) Material definition
- (iii) Failure mode and submode definition
- (iv) Superposition of environmental and mode/submode definitions
- (v) Failure definition (establishing failure criteria)
- (vi) Statistical treatment
- (vii) Accelerated testing to define environmental parameters and failure modes
- (viii) Prediction of container life
- (ix) Feedback from component performance (before permanent closure)
- (x) Modification and optimization of design, materials, environment, operations

While Staehle (1991) described this approach for designing a system, the approach can also be used for performance assessment (PA). The last two steps, however, are not applicable to the EBSPAC program since they are part of the performance confirmation requirements as specified in 10 CFR 60.140, 60.142, and 60.143. The accelerated testing is being performed under the Integrated Waste Package Experiments (IWPE) program. The statistical treatment is provided in the overall PA and Iterative Performance Assessment (IPA) codes through a Monte Carlo or Fast Probabilistic Analysis technique. The EBSPAC program, then, focuses on the first five of the previously mentioned steps. In subsequent sections, the applicability of this approach to a variety of waste package designs is outlined.

## 2 WASTE PACKAGE ENVIRONMENTAL MODELS

### 2.1 INTRODUCTION AND RATIONALE

Development of detailed models for engineered barriers subsystem and component performance requires fairly precise information concerning the chemical and physical environment in the vicinity of and inside the waste package over time. For example, estimates of radionuclide solubility used in release rate calculations are highly dependent upon knowledge of the aqueous chemistry and temperature. Important variables for EBS performance include: (i) relative humidity, (ii) water flow rate, (iii) temperature, and (iv) aqueous chemistry. Knowledge of the important variables is complicated by the partially saturated fractured rock present at Yucca Mountain and heat loading from radioactive decay.

The initial plan for EBSPAC was to abstract the results of detailed environmental codes such as TOUGH for the hydrothermal environment and EQ3/6 for the geochemical environment. The abstraction could take the form of look-up tables or simplified models with lumped parameters. The abstracted models could then supply the environmental parameters for further EBSPAC development. However, while the EQ6 code has been used to model the rock-water interactions to predict the changes in environmental concentrations (Murphy, 1991), the effect of these changes in the groundwater on the stability of water on the container surface was not included in this calculation. Additionally, the effect of extensive vaporization leading to concentrated solutions and drying was not examined. The thermohydrological models, such as TOUGH, on the other hand, do not consider the effects of water chemistry on the stability of water near the waste package. In order to support the development of EBSPAC models, a model of the waste package environment was developed.

Essentially three types of conditions are anticipated to occur near the waste packages.

- Dry conditions (less than about 10 percent saturation) brought on by a high thermal loading strategy. The high thermal loading is the current strategy proposed by the DOE and is also implicit in the MPC and MPU concepts, which contain up to 21 pressurized water reactor (PWR) assemblies. The container material performance under these conditions is determined by oxidation rate in either dry air or air and water vapor environment.
- Wet conditions (greater than about 85 percent saturation) due to either climatic changes resulting in large infiltration of meteoric water or rising water table due to seismic/tectonic activities. Under this condition, aqueous corrosion is expected to prevail. However, the environment surrounding the containers is essentially a rather dilute groundwater and is not anticipated to be corrosive to the corrosion-resistant container materials. Additionally, if wet conditions prevail for a significant period of time, the environmental redox potential can be expected to decrease, assuming that radiolysis is not significant.
- Drip-dry conditions by repeated evaporation of the water coming in contact with the container. The thermal load can result in the evaporation of the pore water that condenses in cooler regions at the top of the repository and can lead to shedding of condensate water towards the container through fractures intersecting a borehole or drift. Such a condition can lead to more corrosive conditions than either completely dry or completely wet conditions through concentration of salts on the container surface. Hence, modeling these evaporation-induced changes in chemistry of water contacting the container is important for a

conservative prediction of container performance. This effort is the focus of the waste package environment modeling effort.

- Another condition that may lead to a dripping environment is the heat pipe condition (Pruess and Tsang, 1993). This condition, where water vapor condenses remotely and water flows towards the container due to vapor pressure differential, may result in the temperature not exceeding 96 °C at a location near the waste package.

## 2.2 SIMPLIFIED THERMAL MODEL

Assuming heat transfer by conduction only, uniform and constant thermal conductivity and heat capacity, and a rectangular repository leads to a Green's function solution for an infinite, homogeneous domain ( $G$ ) of the form (Carslaw and Jaeger, 1959)

$$G = \frac{(G_x G_y G_z)}{8 \rho C_p w L h} \quad (2-1)$$

$$\begin{aligned} G_x &= \text{Erf} \left( \frac{\frac{L}{2} + x}{\sqrt{4\alpha t}} \right) + \text{Erf} \left( \frac{\frac{L}{2} - x}{\sqrt{4\alpha t}} \right) \\ G_y &= \text{Erf} \left( \frac{\frac{w}{2} + y}{\sqrt{4\alpha t}} \right) + \text{Erf} \left( \frac{\frac{w}{2} - y}{\sqrt{4\alpha t}} \right) \\ G_z &= \text{Erf} \left( \frac{\frac{h}{2} + z}{\sqrt{4\alpha t}} \right) + \text{Erf} \left( \frac{\frac{h}{2} - z}{\sqrt{4\alpha t}} \right) \end{aligned} \quad (2-2)$$

where

- $\rho C_p$  = density times heat capacity =  $2.4 \times 10^6 \text{ J/m}^3/\text{°K}$
- $w$  = width of square repository (m)
- $L$  = length of repository (m)
- $h$  = height of repository (m)
- $x, y, z$  = distance from center of repository (assumed zero) (m)
- $\kappa$  = thermal conductivity ( $\text{W/m/°K}$ )
- $\alpha$  = thermal diffusivity =  $\kappa/\rho C_p \cdot (\text{m}^2/\text{s})$

The time and spatially dependent temperature is obtained from a convolution integral with the heat generation rate

where

$$T = \left( \int_0^t Q(\tau) \beta G(t - \tau) d\tau \right) + T_{ref} \quad (2-3)$$

where

- $t$  = time
- $Q$  = heat generation rate per kg initial heavy metal (J/s/kg)
- $\beta$  = amount of heavy metal (kg)
- $T_{ref}$  = initial temperature (23 °C).

The rate of heat generation ( $Q$ ) is illustrated in Figure 2-1, based upon data in U.S. DOE (1993c). The calculation assumes 70,000 metric tons of 60-percent PWR fuel at 33,000 MWd/MTU burnup and 40-percent boiling water reactor (BWR) fuel at 27,500 MWd/MTU burnup.

An illustration of anticipated thermal effects is given in Figure 2-2 which depicts the average temperature in the center of the repository ( $x=y=z=0$ ), plotted as a function of time for different thermal loadings. The temperature drop between the waste container and the surrounding rock is shown in Figure 2-3. This simplified thermal model assists the parametric studies of the influence of thermal loading and location within the repository on EBS performance. Alternatively, EBS calculations can be based upon the output of numerical models of heat transport and fluid flow, such as V-TOUGH (Nitao, 1989).

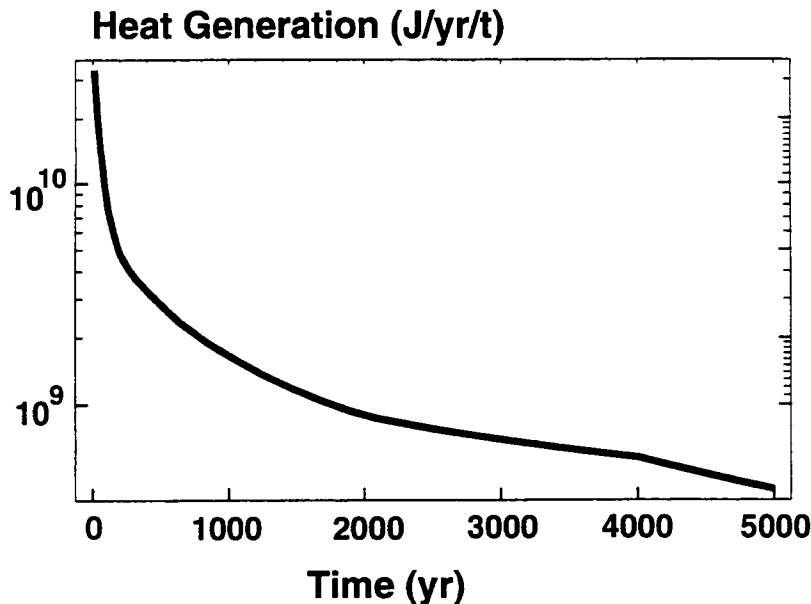


Figure 2-1. Calculated heat generation rate from radioactive decay (DOE, 1993c)

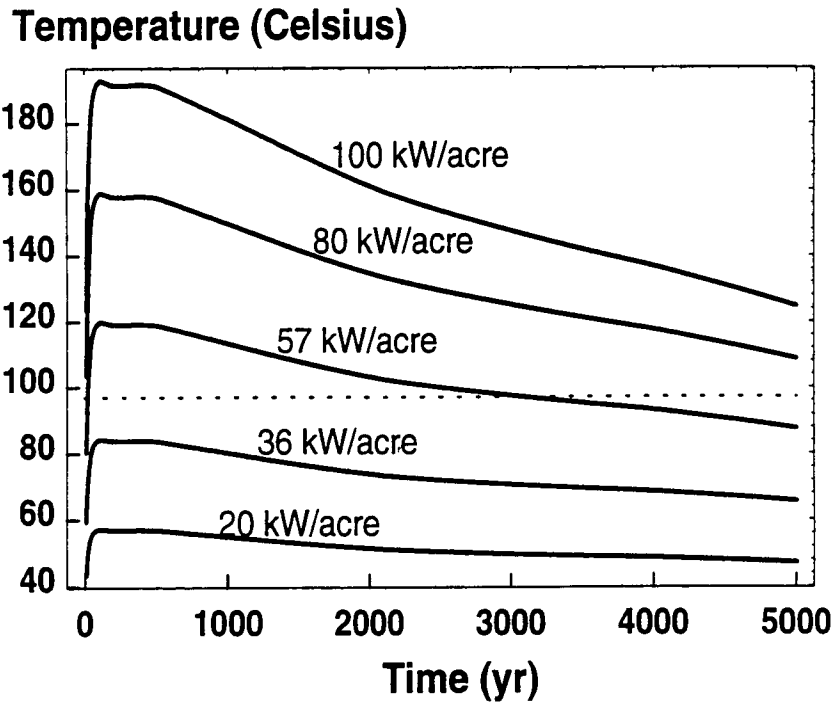


Figure 2-2. Thermal history of repository center as a function of time and thermal loading (1 kW/acre = 0.247 W/m<sup>2</sup>)

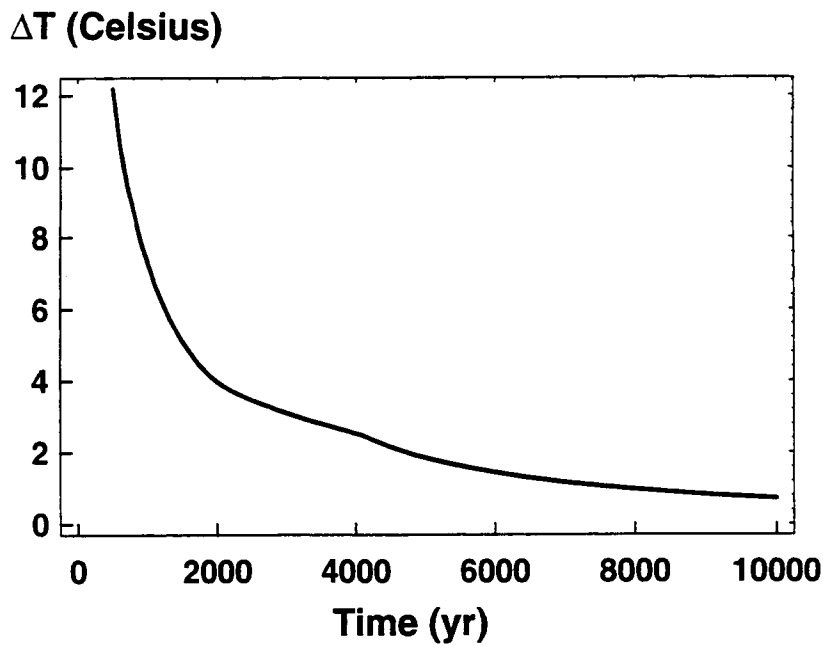


Figure 2-3. Temperature drop between individual waste container and surrounding rock

In addition to the overall heating of the repository and mountain, there is a more localized temperature difference between individual waste containers and the rock a few meters from the waste containers. The localized temperature difference works in a similar manner to overall repository temperature in keeping individual waste packages dry. An estimate of the temperature difference between a waste container and the rock a few meters away is obtained assuming steady-state heat conduction in a layered, radial geometry. The steady-state solution can be justified because the time constant for heat conduction over a scale of a few meters is rapid relative to the rate of change in the heat generation curve, particularly during the later time periods in which we are most interested. The appropriate equation is

$$\Delta T = \frac{\beta Q}{2 \pi l} \left( \frac{\ln\left(\frac{r_2}{r_1}\right)}{\kappa_p} + \frac{\ln\left(\frac{r_3}{r_2}\right)}{\kappa_r} \right) \tag{2-4}$$

where

- $r_1, r_2, r_3$  = radial distance of container wall, packing/rock interface, and outer boundary from container centerline (m)
- $\kappa_p, \kappa_r$  = thermal conductivity of rock and packing materials (W/m/°K)
- $l$  = length of container (m)

In order to illustrate anticipated results of the thermal model, calculations are performed assuming 2.3 metric tons of spent fuel per container ( $\beta$ ) with a 2-cm air gap surrounding the container. The air gap is assumed to be half filled with tuff rock, with a thermal conductivity half that of intact rock. The radius of the container is 0.33 m, and the container is 4 m long. The outer boundary ( $r_3$ ) is assumed to be 5 m. Because of the radial geometry, the estimated  $\Delta T$  is not very sensitive to the outer distance assumed in the calculations. The "steady-state"  $\Delta T$  is a function of  $Q$ , which varies more slowly with time. Hence,  $\Delta T$  can be plotted as a function of time using the variation in  $Q$ . The calculations illustrated in Figure 2-3 indicate that the difference in temperature between the waste container and the rock a few meters away is initially high and gradually declines over time.

### 2.3 SITUATIONS LEADING TO WATER CONTACTING THE WASTE PACKAGE

The initial factor to be determined is the method by which water reaches the waste package and container surface in the partially water-saturated environment. In the absence of thermal effects, water can reach the container surface by fracture flow and dripping. Water dripping from the ceiling through fractured rock in the unsaturated zone is a commonly observed phenomenon in mine tunnels, even in arid climates. Dripping water has been observed, for example, in the G-tunnel on the Nevada Test Site (Zimmerman et al., 1986). In a repository with no thermal effects, dripping from the ceiling, generally related to fracture flow of meteoric water, is anticipated to wet some unknown percentage of the waste packages sometime after closure.

In the presence of thermal effects, the problem is more complex. Higher temperatures raise the vapor pressure of water in the region around waste packages and the repository as a whole, leading to migration of water vapor to cooler regions, at which point condensation occurs. A schematic diagram of the situation around the waste package is given in Figure 2-4. Although Yucca Mountain is a relatively dry site, a significant quantity of water is initially present in the rock pores. For the Topopah Spring unit at the repository horizon, a porosity of 10 percent and an initial saturation of 65 percent have been estimated (Pruess, et al., 1990). Assuming a waste package 0.66 m in diameter and 4 m long surrounded by rock, more than 2 m<sup>3</sup> (2,000 liters) of water are initially present in the rock within 1 m of the waste package. The condensate water migrates either downward through fractures under the influence of gravity, or through the rock matrix under the influence of gravity and capillary forces.

Although most of the condensate water is expected to drain around the repository horizon by the hydrothermal umbrella effect (Buscheck and Nitao, 1992), a portion of the water may enter fractures intersecting waste packages, resulting in localized wetting. Empirical evidence for wetting of this type comes from the Climax test and the G-tunnel test. During the Climax test conducted in the unsaturated zone on the Nevada Test Site, 1 out of 17 waste containers experienced saturated conditions related to fracture flow during the test (Patrick, 1986). In heater tests in the G-tunnel, Zimmerman and Blanford (1986) removed ~0.5 liter of vapor condensate from a heater-handling pipe in one of two tests with vertical waste emplacement. They also found evidence of condensate drainage near thermocouples in a horizontal heater test. Thus, the experimental evidence suggests condensate drainage may wet some percentage of the waste containers during the initial thermal transient. Additional water may contact the containers as the repository cools. As a result, the condensate water being shed from the repository center may intersect with the cooler outer fringes of the repository, leading to increased fracture flow and dripping around the periphery of the repository.

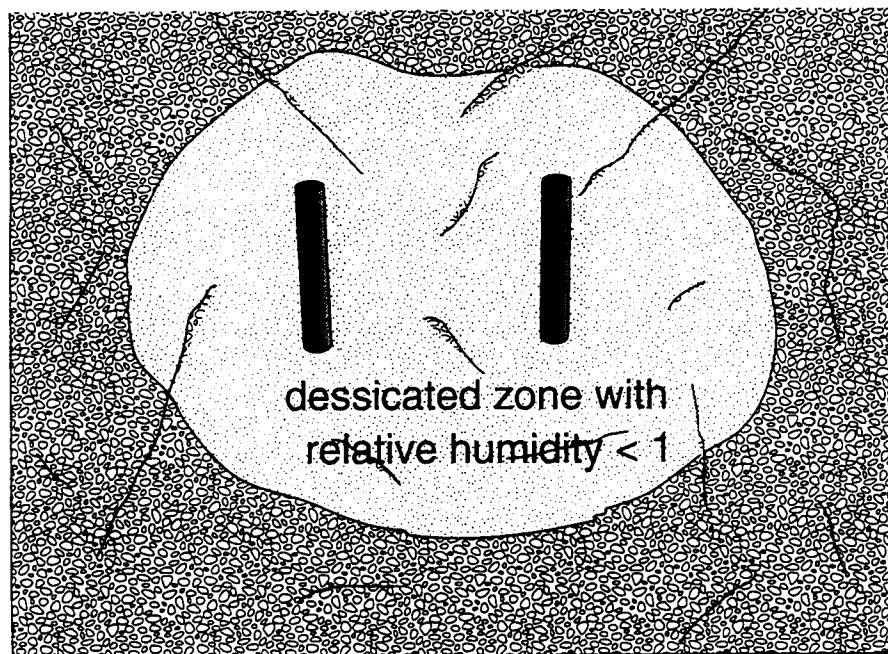


Figure 2-4. Schematic of desiccated zone and fractures surrounding waste packages

The composition of the water contacting the waste containers is likely to be as variable as its quantity because the water can come from several sources. The anticipated sources of water are (i) water initially present in the rock pores prior to repository operations, (ii) water spilled or modified during repository operations, (iii) infiltrating water from precipitation events, and (iv) condensate water resulting from vapor migration with cooling at distance. The initial water composition from each of these sources may also be modified by rock-water interactions at elevated temperatures and by evaporation. An approximation of the initial pore water composition, used extensively in DOE tests of waste package performance, can be obtained from the groundwater below the site as measured from well J-13 (DOE, 1989). Extracted pore waters from tuff rocks from a

**Table 2-1. Water chemistry of the groundwater from a saturated zone near the repository and evolution of water chemistry due to evaporation and condensation cycles**

	J-13 (mg/l except pH)	Experimental (Rimstidt et al., 1991) (ppm except pH)
pH	7.2	6.36 ± 1.12
Ca <sup>2+</sup>	12.0	57 ± 30
Mg <sup>2+</sup>	2.1	—
Na <sup>+</sup>	42.0	115 ± 50
K <sup>+</sup>	5.0	135 ± 74
HCO <sub>3</sub> <sup>-</sup>	124.0	—
Cl <sup>-</sup>	7.1	—
NO <sub>3</sub> <sup>-</sup>	7.2	—
SO <sub>4</sub> <sup>2-</sup>	17.0	—
SiO <sub>2</sub>	57.0	183 ± 35

variety of locations have also been measured (Peters et al., 1992). The composition of J-13 well water is given in Table 2-1. The chemical evolution of the water near the waste packages becomes more complex as the water continually evaporates and condenses, reacts with the rock, and mixes with other waters. Condensate initially has the composition of distilled water. However, as soon as it condenses, it begins to react with the rock and mix with other waters present (e.g., pore waters) leading to a highly variable composition. A series of experiments with evaporation and condensation cycles was performed by Rimstidt et al. (1991). Average cation concentrations measured in the experiments are given in Table 2-1, along with their standard deviations. The observed variability in concentrations is very high, even in a small-scale, simplified laboratory situation. Additional changes to water chemistry may be caused by processes such as radiolysis. Radiolysis is known to lead to nitrate formation in air or steam environments (Reed, 1991).

## 2.4 EVAPORATION

The evaporation of water around the waste package is driven by the difference in temperature between the waste package and the rock a few meters from where liquid water is present in the pores (Figure 2-4). When water reaches the container surface by any of the mechanisms discussed previously, the temperature of the water is raised. The increase in temperature of the water on the container surface causes the vapor pressure to be elevated relative to that of the water present outside of the dry-out zone. The vapor pressure difference promotes evaporation of the water from the container surface. Because of

the small amounts of water anticipated and the large mass of the container, the loss of sensible and latent heat by water heating and evaporation from the container surface is insignificant in the overall energy balance. The rate of evaporation is thus limited by mass transport of water vapor across the dry-out zone if the system is below the boiling point. When the container temperature exceeds the boiling point, evaporation is effectively instantaneous.

Below the boiling point of the solution, the rate of evaporation is a function of overall temperature and temperature drop between the container and surrounding rock. At the scale assumed in this work (diffusion distance of 5 m), the rate of advection would have to exceed 200 m/yr to give a Peclet number greater than 1. For this reason, the calculations assume mass transport only by diffusion. The flux equation for binary diffusion of water vapor through air is given by Bird et al. (1960).

$$N_{\text{H}_2\text{O}} = x_{\text{H}_2\text{O}}(N_{\text{H}_2\text{O}} + N_{\text{air}}) - c_g D_{\text{H}_2\text{O}} \tau \phi \nabla x_{\text{H}_2\text{O}} \quad (2-5)$$

where

- $N_{\text{H}_2\text{O}}$  = molar flux of water vapor
- $N_{\text{air}}$  = molar flux of air
- $x_{\text{H}_2\text{O}}$  = mole fraction of water vapor
- $c_g$  = total molar concentration of gas
- $D_{\text{H}_2\text{O}}$  = binary diffusion coefficient
- $\tau$  = tortuosity factor
- $\phi$  = rock porosity (0.1)

Solving for steady-state evaporation in a radial geometry gives

$$E = 2 \pi l c_g D_{\text{H}_2\text{O}} \tau \phi \frac{\ln\left(\frac{1-x_1}{1-x_3}\right)}{\ln\left(\frac{r_1}{r_3}\right)} \quad (2-6)$$

where

- $x_1, x_3$  = mole fraction of water vapor at container surface and at distance, respectively.
- $E$  = molar evaporation rate from the entire container surface without end effects

The tortuosity and porosity factors are related (van Brakel and Heertjes, 1974), although, in the current analysis, they are treated as independent parameters. The air gap zone around the waste container can be ignored because it has greater diffusion rates than the surrounding rocks. The diffusion coefficient in the air/water vapor system in  $\text{m}^2/\text{s}$  is assumed to be given by (Treybal, 1980).

$$D_{\text{H}_2\text{O}} = 3.05 \times 10^{-5} \left( \frac{760}{680} \right) \left( \frac{T}{T_{\text{ref}}} \right)^{1.5} \quad (2-7)$$

where the pressure at the repository horizon is taken as 680 mm Hg, and the reference temperature of 232 °K (59 °C) is the experimental temperature for the measured diffusion coefficient. The vapor pressure of water as a function of temperature is taken from Perry's Handbook (Perry and Chilton, 1973). Conversions between vapor pressure, concentration, and mole fraction are performed with the ideal gas law. The tortuosity factor is taken from Jury et al. (1991). Jury et al. (1991) discuss mechanisms that may enhance water vapor migration in soil by a factor of 2 to 3 times greater than predicted by the above equations, although the theoretical rationale is limited to temperatures of less than 60 °C and high relative humidity.

The evaporation rate for a container entirely covered with pure water (ignoring end effects) as a function of temperature and  $\Delta T$  is given in Figure 2-5. The figure is truncated at higher evaporation rates where the assumption that latent heat is unimportant in the energy balance of the system would be incorrect. Evaporation is greater at higher temperatures because of increased slope of the vapor/liquid equilibrium curve, higher diffusion coefficients at greater temperatures, and the bulk flow term in the diffusion equation, which becomes significant at higher mole fractions of water. The simple evaporation calculations were made with a number of simplifying assumptions including (i) steady-state, (ii) no advection, and (iii) the presence of water at the vapor/liquid equilibrium curve 5 m from the container surface. The major simplifying assumptions will tend to underestimate the potential evaporation rates in the repository.

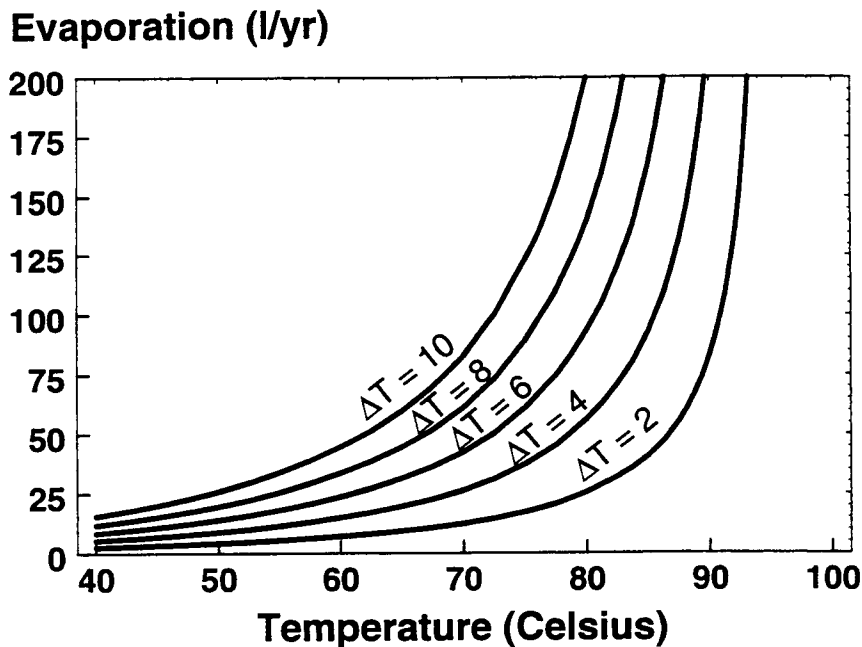


Figure 2-5. Evaporation rate of pure water as a function of temperature drop between the waste container and the surrounding rock

Since the rate and timing of dripping onto the container surface are spatially and temporally variant and difficult to predict, scenarios can only approximate the actual system. However, the estimated evaporation rates are high and exceed anticipated rates of water dripping on the container until both the repository temperature and the temperature around the container have dropped considerably. The conclusion is that most of the water initially impinging on the containers is expected to evaporate, and this conclusion is valid for both the hot and cold repository concepts.

## 2.5 SOLUTE EFFECTS ON WATER DYNAMICS

The above calculations provide significant evidence that even at temperatures well below the boiling point of water, and in the presence of pure water dripping related to fractures and heterogeneity in the system, the waste containers should remain dry. However, the water dripping on the waste containers is not likely to be pure. As discussed previously, the water that drips on the waste containers is expected to have a variable composition of dissolved constituents. During evaporation, the nonvolatile constituents of the water remain on the container surface. As the water evaporates, the less soluble dissolved constituents precipitate, forming a "boiler scale" on the container surface. The more soluble constituents remain in solution, perhaps in pore water inside the scale, underneath the scale, or on the surface of the scale.

Partial evaporation of groundwaters similar to J-13 water has been considered by Garrels and MacKenzie (1966). They conclude that evaporation at equilibrium with the atmosphere results in precipitation of silicate and carbonate minerals, leading to an alkaline brine solution. Evaporation of southern Nevada waters with the geochemical codes PHREEQE and EQ3/6 likewise leads to alkaline brine solutions (Murphy, 1991; Vaniman et al., 1992). As evaporation continues, the remaining aqueous solution becomes more concentrated, and the vapor pressure of the water is decreased. The maximum extent of the vapor pressure decrease depends upon the final composition of the water on the container surface at the endpoint of the evaporation process (i.e., the final composition of the solution prior to complete drying). The composition of water at the evaporation endpoint is currently unknown and may depend upon evaporation rate relative to drip rate, container temperature, vapor composition, presence or absence of rock particles in the solution, and the composition of the dripping water—all of which vary between containers and even along a single container. The solutes present at the endpoint can play a pivotal role in controlling water access to the waste container by lowering the vapor pressure of water.

The initial pore waters in the region and the current groundwater have sodium and calcium as major cations, with bicarbonate, chloride, and nitrate present in significant quantities as anions. Additional nitrate may be formed by radiolysis. Several of the most soluble compounds of the ions present are  $\text{Na}_2\text{CO}_3$ ,  $\text{NaCl}$ ,  $\text{NaNO}_3$ ,  $\text{KCl}$ , and  $\text{CaCl}_2$ . The actual brine solution formed is expected to be a mixture of soluble ions. The pure salt solutions are intended to illustrate the range of vapor pressure decrease expected from plausible evaporation endpoints. The vapor pressure of saturated solutions of these compounds (National Research Council, 1928; Ananthaswamy and Atkinson, 1985; Patil et al., 1991; Liu and Lindsay, 1972; Rard and Platford, 1991) is illustrated in Figure 2-6. Depending upon the salt forming, the vapor pressure of water could be lowered significantly. In some cases, the boiling point of the solution can be significantly elevated above the boiling point of pure water. For this reason, elevation of the container surface temperature above the boiling point of water cannot be taken as a demonstration that liquid water cannot be present on the container. It must be noted that the above arguments for water retention reflect the basis for isopiestic measurements of osmotic coefficients (Rard and Platford, 1991).

### Vapor Pressure of Saturated Solutions (atm)

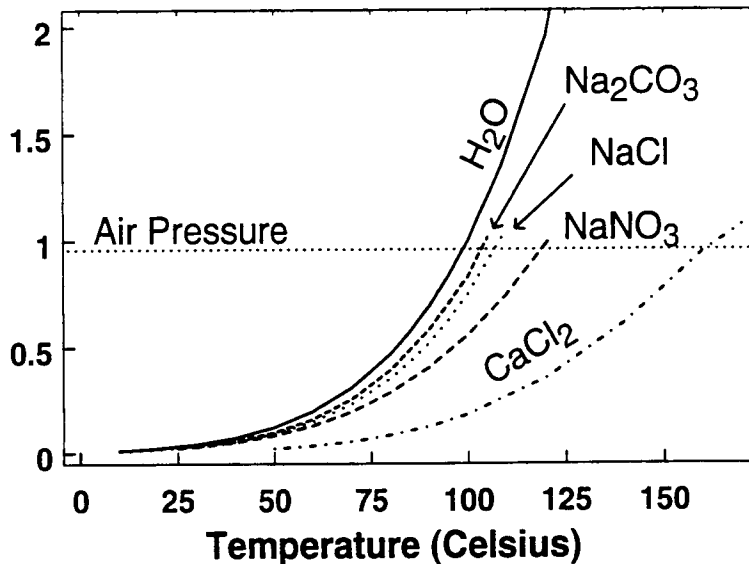


Figure 2-6. Vapor pressure as a function of temperature for several saturated salt solutions

In the presence of a concentrated salt solution, the evaporation process can be expected to proceed until the vapor pressure of water on the container surface is equal to the vapor pressure of nearly pure water at a distance from the container and at a lower temperature. A useful exercise is to calculate the temperature drop required to lower the vapor pressure of water to equilibrate with a saturated salt solution. The calculated "effective" temperature drop can then be compared with the predicted thermal temperature drop around the container. If the solute-related temperature drop exceeds the actual change in temperature, the salt solution could maintain water on the waste package surface. The effective temperature drops are illustrated in Figure 2-7. Note that even for salts of relatively low solubility (e.g., NaCl), the solute effect exceeds the anticipated temperature drop around the container shown in Figure 2-3 except during early time periods.

The amount of water held on the container by solute forces is dependent upon the vapor pressure of water in the repository horizon and the mass of salts present on the container. The amount of salts present is proportional to the volume of water evaporated and the initial composition of the dripping water. As discussed previously, the actual amount of dripping water and the composition of the dripping water are likely to be highly variable in time and space and are difficult to predict with precision. Nonetheless, the overall range expected can be examined with calculations. Assuming that the dripping water has the composition of J-13 well water and the final solution is composed of sodium chloride and sodium nitrate, at 25 weight percent dissolved salt, the solute effects are significant. Assuming the brine film on the container remains at 25 percent dissolved salt by weight, then for each liter of water dripping on the container, the brine film grows by 0.065 ml (0.0065 percent of the water dripping on the waste package remains in the salt film). The water lost by evaporation can be replenished by diffusion of water vapor towards the waste package to maintain the salt concentration. Thus, chemical

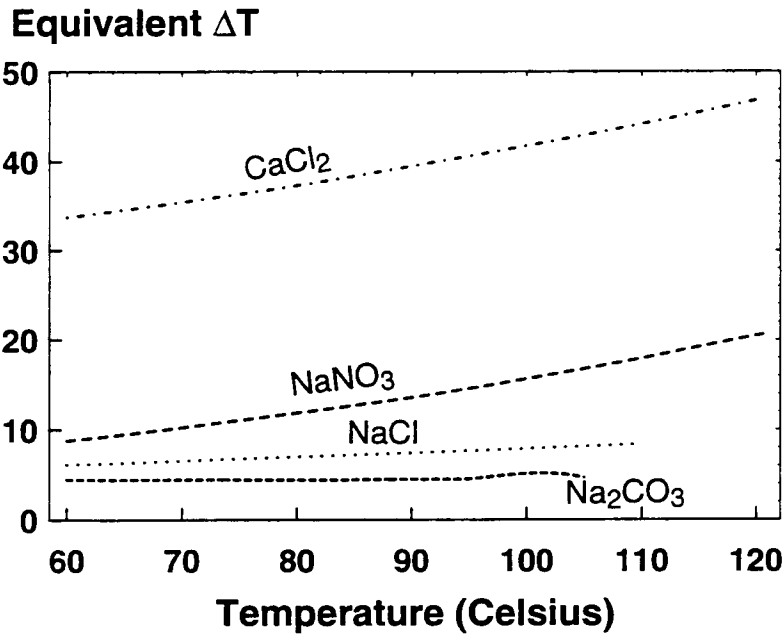


Figure 2-7. Temperature difference between saturated salt solutions and pure water at the same vapor pressure

reactions on or in the waste package that consume water do not lower the amount of water present in the salt film unless the salt itself is consumed in the chemical reactions. Generation of additional salts by chemical reactions on the container or waste (e.g., by wasteform alteration or corrosion), would tend to increase the volume of water on the salt film.

## 2.6 GENERAL CASE FOR NEAR-FIELD AQUEOUS CONDITIONS

Heat loading, combined with limited water supply, leads to creation of a desiccated zone around the waste package in which the relative humidity is decreased well below 1. Three conditions can cause water to be present within this zone: (i) adsorbed or capillary water, (ii) solute-caused lowering in vapor pressure, and (iii) transient water related to fracture drainage. Vapor pressure lowering in capillaries is described with Kelvin's equation.

$$f_{\text{capillary}} = \frac{P_{\text{capillary}}}{p^0} = \exp\left[\frac{\psi Mg}{RT}\right] \quad (2-8)$$

where

$\psi$  = matrix potential

- $M$**  = molecular weight of water  
 **$g$**  = gravitational constant  
 **$R$**  = gas constant

Vapor pressure lowering from solutes is a function of concentration and solute composition.

$$f_{\text{solute}} = \left( \frac{P_{\text{solute}}}{P^0} \right) = f(C_1, C_2, \dots, C_i) \quad (2-9)$$

Total vapor pressure lowering is a combination of solute and capillary effects.

$$\frac{P_{\text{total}}}{P^0} = f_{\text{capillary}} \cdot f_{\text{solute}} \quad (2-10)$$

If the waste container is surrounded with an air gap or with crushed rock (gravel), then the unsaturated hydraulic conductivity of the packing will be near zero. In this situation, the vapor pressure of water inside the waste package is determined by the vapor pressure of water in the rock near the waste package. At a constant vapor pressure of water, the relative humidity at any point is a function only of temperature (i.e., temperature determines  $P^0$ ). At any point, water will evaporate or condense until the waste package vapor pressure of water is reached. On the average, temperature will decrease from the centerline of the waste package outward in a radial direction. The salinity or composition of water in this system is then determined by temperature, presence of small pores, and presence of soluble salts. In an idealized, homogeneous, porous medium, water and soluble salts would tend to redistribute towards a state where vapor pressure of water and capillary pressure were both constant. Gradients in vapor pressure of water lead to vapor diffusion, which is very fast at high temperatures and waste package size scales. Gradients in capillary pressure lead to liquid flow, a relatively slow process at high capillary pressure. This liquid flow, combined with the heat-generated circulation, leads to greater salinity towards the waste package centerline.

A waste package far into the future is not well approximated as a homogeneous, isotropic, porous medium. Initially, the host rock is a fractured material, whereas the steel, cladding, and fuel pellets represent relatively smooth surfaces. Over time, they corrode, leading to variable secondary mineral formation. The resulting pore structure is highly variable in space (and in time). As structural components fail, the shape or geometry of the system can change dramatically. For example, as cladding fails, spent fuel pellets (or their remains) could fall to the bottom of the container. Air gaps (e.g., inside a failed container) are likely to lead to hydraulic discontinuities for unsaturated flow. The presence of soluble salts may be controlled by dripping, leading to a nonuniform distribution of salts.

If a drop of water is placed at a point, it begins to evaporate. As the water evaporates, it fills smaller pores (leading to vapor pressure decrease) and solutes become concentrated (leading to additional vapor pressure decrease). Evaporation ends when the vapor pressure of water prevailing in the waste package is reached. Depending upon pore structure, temperature, and presence of soluble salts, final

solution composition could range from pure water to concentrated brine and capillary pressure from very high to zero.

A useful exercise is to examine the predicted solution composition in the absence of small pores and/or when an excess quantity of soluble salts is present. This examination illustrates the sensitivity of water composition to temperature. Figure 2-8 gives the predicted salinity in the waste package as a function of radial distance and at several time periods.

Water chemistry in the waste package is anticipated to be highly variable in space and time with important controls imposed by the temperature gradient.

## 2.7 FUTURE DIRECTIONS

The present model has shown that the environment on the waste package surface or the wasteforms, once the container is penetrated, can be highly saline. However, this prediction depends on the assumption of what solute is left behind upon evaporation of groundwater. It also assumes that the incoming water contains some solutes. Further investigation must be conducted on the effect of incoming water composition on the chemistry of the evaporated solution. Additionally, the brine solution is formed on the "boiler scale" on the waste package surface. This brine solution has to diffuse through the scale layer to reach the waste package surface. The kinetics of this process needs to be determined.

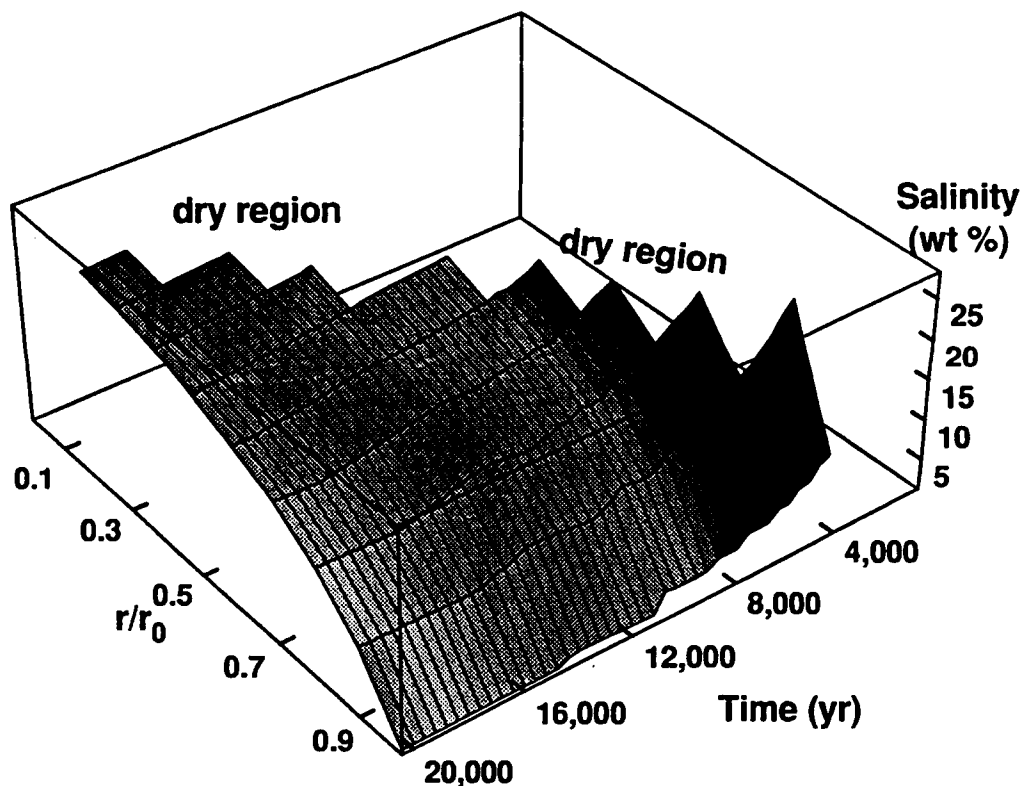


Figure 2-8. Predicted salinity on the surface of the waste package as a function of time and radial distance from the center of the waste package

## 3 CONTAINMENT MODELS

### 3.1 OVERALL APPROACH

The second step in the Corrosion Based Design Approach, as outlined in Section 1, is the material definition. The waste package conceptual design thus far has been assumed to consist of a single-wall container made of a corrosion-resistant alloy such as type 304L stainless steel or alloy 825, a Ni-Fe-Cr-Mo alloy. The following sections will review corrosion parameters for these two alloys to be used as input in containment models. The effect of an outer corrosion-allowance material in a bimetallic design on the inner corrosion-resistant material will also be discussed briefly. Parameters for alternate candidate materials such as alloy C-4 will be the subject of future progress reports.

The third step in the process is the failure mode and submode definitions. Staehle (1991) uses the potential-pH (or Pourbaix) diagrams for determining the regimes of various corrosion processes. While this approach has proven powerful under some circumstances, the limitations of this approach include the inability to consider kinetic aspects in a thermodynamic framework, the assumption that the corrosion behavior is determined by the potential-pH behavior of a single component of an alloy, and the lack of consideration of the influence of other environmental factors such as chloride. Several alternate approaches are available to determine the mode and submode of failure of a given material.

- The potential-time diagram can be used to compare the variation of corrosion potential to critical potentials for various corrosion processes as functions of time. This approach is explained in greater detail in the following sections. Other environmental factors, such as pH and chloride, are considered in the time variations of these potentials.
- Log activity [metal ion-chloride diagrams (Mohr and McNeil, 1992)] has been used in predicting the corrosion products of copper corrosion.
- For mechanical failures, fracture mechanism maps (Frost and Ashby, 1982; Ashby, 1992) can be used to locate various failure modes for a given type of material. However, fracture maps, at present, only yield a broad delineation of failure modes and quantitative extrapolations within a failure mode field are still tenuous. Also, fracture mechanism maps do not consider localized stress/strain fields such as those in the vicinity of cracks or defects.

#### 3.1.1 The Approach for Corrosion-Resistant Metallic Materials

The overall approach to predicting the mode of corrosion in the EBSPAC program is shown in Figure 3-1. While such an approach is tailored for corrosion-resistant or passive metallic materials, such as stainless steels, they can be applied to corrosion-allowance-type metallic materials with suitable modifications. During the dry period when the only anticipated corrosion mode is oxidation due to dry air or steam, the corrosion rate is anticipated to be quite low. Experimental data on candidate container materials in vapor or steam (Farmer et al., 1991) indicate corrosion rates in the range of 0.03–1  $\mu\text{m}/\text{yr}$ . Once aqueous conditions prevail at the container surface, a corrosion potential is established that is a function of environmental conditions, container material, and surface conditions. As shown in Figure 3-1, the corrosion potential is anticipated to be high initially due to a combination of oxygen in the solution and radiolysis products (if present). The latter become negligible for thick-walled containers. However, over the course of time, the corrosion potential may decrease due to reduction in concentration of

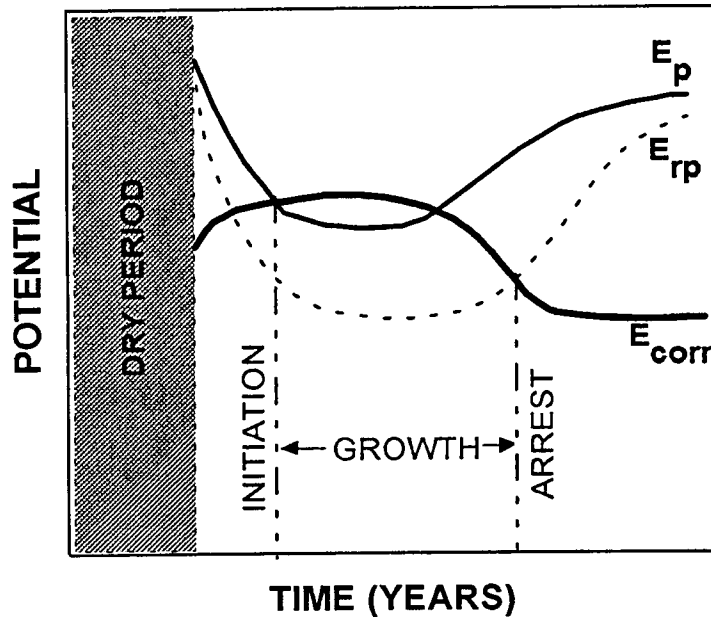


Figure 3-1. Overall approach to predicting corrosion failure modes (in this case, localized corrosion) of a corrosion-resistant alloy

radiolysis products and formation of a thick-scale layer which may result in a lower steady-state concentration of oxygen at the metal surface. On the other hand, factors that contribute to an increase in corrosion potentials include lowering of passive current density of the container material and lowering of temperature which results in increased solubility of oxygen in the solution. Another factor that affects the corrosion potential is the galvanic contact between various metallic materials in a multi-barrier design. Also shown in Figure 3-1 are the critical potentials for pitting. If the corrosion potential (or applied potential in the case of accelerated corrosion tests) exceeds the pit initiation potential,  $E_p$ , then pits initiate and start to grow. If the corrosion potential is less than the  $E_p$ , then the metal (assuming it is a passive alloy such as stainless steel) corrodes at a rate corresponding to the passive current density. Once initiated, the pits grow rapidly, but they cease growing if the corrosion potential becomes less than the repassivation potential,  $E_{rp}$ . The use of critical potentials has been generally shown to be valid for both pitting and crevice corrosion (Szklaarska-Smialowska, 1986; Staehle, 1991), although the issue of a single potential versus multiple potential for these different modes of corrosion is still being debated. The use of critical potentials, especially repassivation potential for crevice corrosion, for predicting the occurrence of stress corrosion cracking needs further research (Cragolino and Sridhar, 1992). Other corrosion phenomena such as hydrogen embrittlement and intergranular corrosion are also functions of potential, although a critical potential has not been established for these processes. In the following discussions, the corrosion potentials and critical potentials for localized corrosion are examined in greater detail.

### 3.1.2 Approach for Corrosion-Allowance Type Metallic Alloys

The approach outlined previously for passive alloys needs to be modified for other materials that are considered to be nonpassive or corrosion-allowance materials. Whether a material is classified as corrosion-resistant or corrosion-allowance type depends upon the environmental conditions. For example, copper which has been classified as a corrosion-allowance-type material exhibits a passive behavior at high temperatures and in the presence of high bicarbonate ion concentrations or high pH (Cragolino and Sridhar, 1991). In such a case, localized corrosion can be initiated above a critical potential, and the concepts outlined in the previous section apply to these materials (Sridhar et al., 1993; Nakayama and Akashi, 1993a). Under conditions of active corrosion (uniform corrosion), the corrosion rate is a continuous function of the corrosion potential. In such cases, the corrosion rate can be calculated using a Butler-Volmer formulation for both the anodic and cathodic processes considering transport related changes in surface concentrations and ohmic potential drops.

It can be seen from these discussions that modeling of corrosion and critical potentials is an important first step in assessing the corrosion performance of metallic container materials in aqueous environments.

## 3.2 CORROSION POTENTIAL

All aqueous corrosion processes are dependent on the corrosion potential of the metal exposed to a particular environment under consideration. The modeling of corrosion potential is considered to be the backbone of the performance assessment of metallic containers (Walton and Sagar, 1988; Macdonald and Urquidi-Macdonald, 1990; Marsh et al., 1987). The corrosion potential is defined as the potential at which the current due to all the cathodic processes is equal to the current due to all the anodic processes including the electrochemical dissolution of the metal.

$$\sum_{j=1}^n I_{a,j} - \sum_{k=1}^m I_{c,k} = 0 \quad (3-1)$$

where  $I_{a,j}$  refer to the anodic (oxidation) currents including that of the metal dissolution (called the corrosion current,  $I_{corr}$ ) and  $I_{c,k}$  refer to the cathodic (reduction) currents. If the anodic and cathodic processes occur uniformly throughout the surface of interest, then Eq. (3-1) can be written in terms of appropriate current densities. However, once extensive localized corrosion occurs, this assumption is no longer valid, and the areas of active corrosion and passive corrosion must be considered. Similarly, if a bimetallic container is used wherein the outer container is assumed to develop through-wall defects, then the areas of the outer container and the exposed inner container must be considered. In the following sections, uniform distribution of cathodic and anodic areas is assumed for simplicity. The corrosion potential of a given metal will vary with time depending on a number of factors such as temperature, environment composition, radiolysis, transport processes near the metal-environment interface, and photoelectrochemical processes in the passive film.

Calculation of the corrosion potential as a function of time has been made by Walton and Sagar (1988) for carbon-steel in a saturated environment for the Basalt Waste Isolation Project (BWIP). Calculation of the corrosion potentials for a variety of austenitic stainless steels and Cu-base alloys in an

unsaturated environment for the Yucca Mountain repository site was made by Macdonald and Urquidi-Macdonald (1990). The approaches used in both these models are essentially the same with differences introduced by the differences in the materials and environments.

The dependence of the anodic and cathodic current densities on potential is determined by the rate-determining step of the overall process. If the rate-determining step is charge transfer on an active, unfiled surface, then the net current density on the metal is given by a Butler-Volmer-type equation (Vetter, 1967).

$$i_j = i_{0j} \left[ \exp \left( \frac{\alpha_j z_j F}{RT} \eta_j \right) - \exp \left( - \frac{(1-\alpha_j) z_j F}{RT} \eta_j \right) \right] \quad (3-2)$$

where

- $i_{0j}$  = exchange current density for the  $j^{\text{th}}$  reaction
- $\eta_j$  =  $E_j - E_{eqj}$  is the overpotential
- $F$  = Faraday constant
- $\alpha_j$  = charge transfer coefficient
- $R$  = gas constant
- $T$  = temperature in °K
- $z_j$  = number of electrons involved in the process per mole

The exchange current density is given by:

$$i_{0j} = k_{+j} C_{rj} \exp \left( \frac{z\alpha_j F}{RT} E_{eqj} \right) = k_{-j} C_{oj} \exp \left( - \frac{z(1-\alpha_j)F}{RT} E_{eqj} \right) \quad (3-3)$$

where

- $k_{+j}$  and  $k_{-j}$  = the anodic (oxidation) and cathodic (reduction) reaction rate constants, respectively
- $C_{rj}$  and  $C_{oj}$  = concentrations of reduced and oxidized species, respectively
- $E_{eqj}$  = the equilibrium potential for a given partial electrochemical reaction given by the Nernst equation:

$$E_{eqj} = E_{0j} + \frac{RT}{zF} \sum_{i=1}^n \nu_i \ln a_i \quad (3-4)$$

where  $E_{0j}$  is the standard potential (equilibrium potential where the reaction species are in their standard states),  $a_i$  are the activities, and the stoichiometric coefficients,  $\nu_i$ , are positive for oxidized species and negative for the reduced species. It must be noted that the reaction rate constants in Eq. (3-3) are

dependent on the assumed reference potential (Vetter, 1967). Typically, the values of exchange current density are used directly from experimental measurements without recourse to Eq. (3-3). It must be emphasized that Eq. (3-2) is strictly valid only when charge transfer process is the rate-determining step. It does not consider transport process as the rate-determining step. At potentials sufficiently cathodic to the equilibrium potential,  $|\eta| > RT/zF$ , and the first term in Eq. (3-2) vanishes ( $\eta$  is negative) and Eq. (3-2) has the form of a Tafel relationship ( $\eta = a - b \log i$ ).

At the other extreme in many electrochemical corrosion processes is the case where transport of reacting species to or away from the electrode (container) surface is the rate-determining step. In a pure diffusion limited case, the current density corresponding to the partial reaction is controlled by diffusion. This represents an equilibrium situation because the charge transfer processes are assumed to be sufficiently fast to have attained equilibrium (Vetter, 1967). In other words, the Nernst equation [Eq. (3-4)] can be used to calculate the potential with an important difference: the surface concentration of species (outside the diffuse double layer) involved in the calculation of potential is determined by the diffusion current density. If the surface concentrations of species are termed  $c_j$  and the equilibrium (bulk) concentrations are  $C_j^0$ , the overpotential due to a purely diffusion controlled process is given by (Vetter, 1967):

$$E_{\text{diff}} - E_{\text{eq}} = \frac{RT}{zF} \sum \nu_j \ln \left( \frac{c_j}{C_j^0} \right) \quad (3-5)$$

where  $\nu_j$  are the stoichiometric coefficients and  $z$  is the net electron transfer. The concentrations are used instead of activities for simplicity. The concentrations,  $c_j$ , at the metal-electrolyte interface are determined by transport given by (Walton and Sagar, 1988):

$$\tau R_d \frac{dc_j}{dt} = \nabla \left[ \tau D \nabla c_j + \frac{z_j D_j F}{RT} c_j \nabla \phi_s + \tau D_j \nabla c_j - \nu c_j \right] + R_i \quad (3-6)$$

where

- $R_d$  = retardation factor
- $c_j$  = concentration of species
- $D$  = coefficient of hydrodynamic dispersion
- $D_j$  = molecular diffusion coefficient
- $\nu$  = Darcy velocity
- $\tau$  = porosity
- $R_i$  = reaction terms including radiolysis
- $\phi_s$  = potential in solution

As the electrode is polarized away from the equilibrium potential, the current-voltage relationship is represented initially by Eq. (3-2) (charge transfer process). However, at high polarization potentials, the current density assumes a limiting value dictated by transport and reaction controlled

processes [Eq. (3-5)]. The overall current-potential relationship for any of the cathodic processes can then be represented as (Vetter, 1967):

$$i = i_0 \left[ \frac{c_r}{C_r^0} \exp \left( \frac{\alpha z F}{RT} \eta \right) - \frac{c_o}{C_o^0} \exp \left( - \frac{(1-\alpha) z F}{RT} \eta \right) \right] \quad (3-7)$$

where

$c_r$  and  $c_o$  = the surface concentrations of reduced and oxidized species, respectively  
 $C_r^0$  and  $C_o^0$  = the equilibrium (bulk) concentrations

If a cathodic reaction of the  $m^{\text{th}}$  species, such as oxygen reduction, is such that the  $|\eta| > RT/zF$ , then the above equation can be written as

$$i_m = -i_{0^m} \left[ \frac{c_s^m}{C_{\text{bulk}}^m} \exp \left( - \frac{(1-\alpha) z_m F}{RT} \eta \right) \right] \quad (3-8)$$

The surface concentrations are determined by Eq. (3-6). If molecular diffusion is assumed to be the only transport mechanism and a steady-state diffusion condition is also assumed in the diffusion layer, then the surface concentration of reducing species can be written as

$$J_m = -4FD_m \tau \phi \frac{(C_{\text{bulk}}^m - c_s^m)}{\delta} \quad (3-9)$$

where

$J_m$  = flux of the  $m^{\text{th}}$  species  
 $D_m$  = diffusivity  
 $\tau$  = tortuosity  
 $\phi$  = porosity  
 $\delta$  = thickness of the diffusion layer (e.g., scale)  
 $C_{\text{bulk}}$  and  $c_s$  = bulk and surface concentrations of the species, respectively.

Assuming steady-state conditions at the metal-electrolyte interface, the current density of the reduction reaction of the  $m^{\text{th}}$  species must equal its diffusion flux. Combining Eqs. (3-8) and (3-9), the cathodic current density for the  $m^{\text{th}}$  species can be written as

$$i_m = -i_o^m \frac{\exp\left(-\frac{z_m \beta F \eta}{RT}\right)}{\left[1 + \frac{i_o^m \delta \exp\left(-\frac{z_m \beta F \eta}{RT}\right)}{C_{\text{bulk}}^m 4FD_m \tau \phi}\right]} \quad (3-10)$$

where  $\beta = 1 - \alpha$ . For oxygen reduction reaction, the bulk concentration is related to the partial pressure through Henry's law. For hydrogen evolution reaction, the bulk concentration of the  $H^+$  is related to the pH.

In order to calculate the corrosion potential, the anodic polarization behavior of the container metal is needed. It is difficult to represent the total active-passive-transpassive behavior of a metal mathematically, and, hence, it is generally assumed that the sum of the relevant cathodic reactions intersect the anodic polarization curve of the metal either in the active or the passive regime (Walton and Sagar, 1988). In the passive regime, the anodic current is essentially potential independent, given by the passive current,  $I_p$ . In such a simplified case, the corrosion potential can be calculated by summing all the cathodic currents to equal  $I_p$  [Eq. (3-1)], assuming that no other anodic processes other than dissolution occur. A sample calculation assuming oxygen reduction reaction and hydrogen evolution reaction for the cathodic processes and passive current density for the anodic process is shown in Table 3-1 and Figure 3-2.

**Table 3-1. Parameters used to calculate the kinetics of cathodic reactions and corrosion potentials shown in Figure 3-2. For all cases:  $T=95\text{ }^\circ\text{C}$ ;  $\text{pH}=8$ ;  $i_0(H^+) = 1 \times 10^{-4}\text{ A/m}^2$ ;  $i_{\text{pass}} = 1 \times 10^{-3}\text{ A/m}^2$ . Activation energies for exchange current densities for oxygen and hydrogen reactions were 100 and 40 KJ/mol, respectively.**

Parameters	Parameters Corresponding to Calculations Shown in Figure 3-2			
	(a)	(b)	(c)	(d)
$\delta\text{ (m)}$	$1 \times 10^{-3}$	$1 \times 10^{-3}$	$1 \times 10^{-3}$	$1 \times 10^{-3}$
$\tau \cdot \phi$	0.15	0.15	0.15	0.005
$\beta_{\text{ox}}$	0.75	0.25	0.25	0.75
$i_0(O_2)\text{ at }25\text{ }^\circ\text{C, (A/m}^2\text{)}$	$1 \times 10^{-8}$	$1 \times 10^{-8}$	$1 \times 10^{-6}$	$1 \times 10^{-8}$

The major limitation of the present corrosion potential models is the lack of availability of kinetic parameters for the various cathodic reactions. Macdonald and Urquidi-Macdonald (1990), while acknowledging uncertainties, were forced to use values of exchange current density on the basis of a

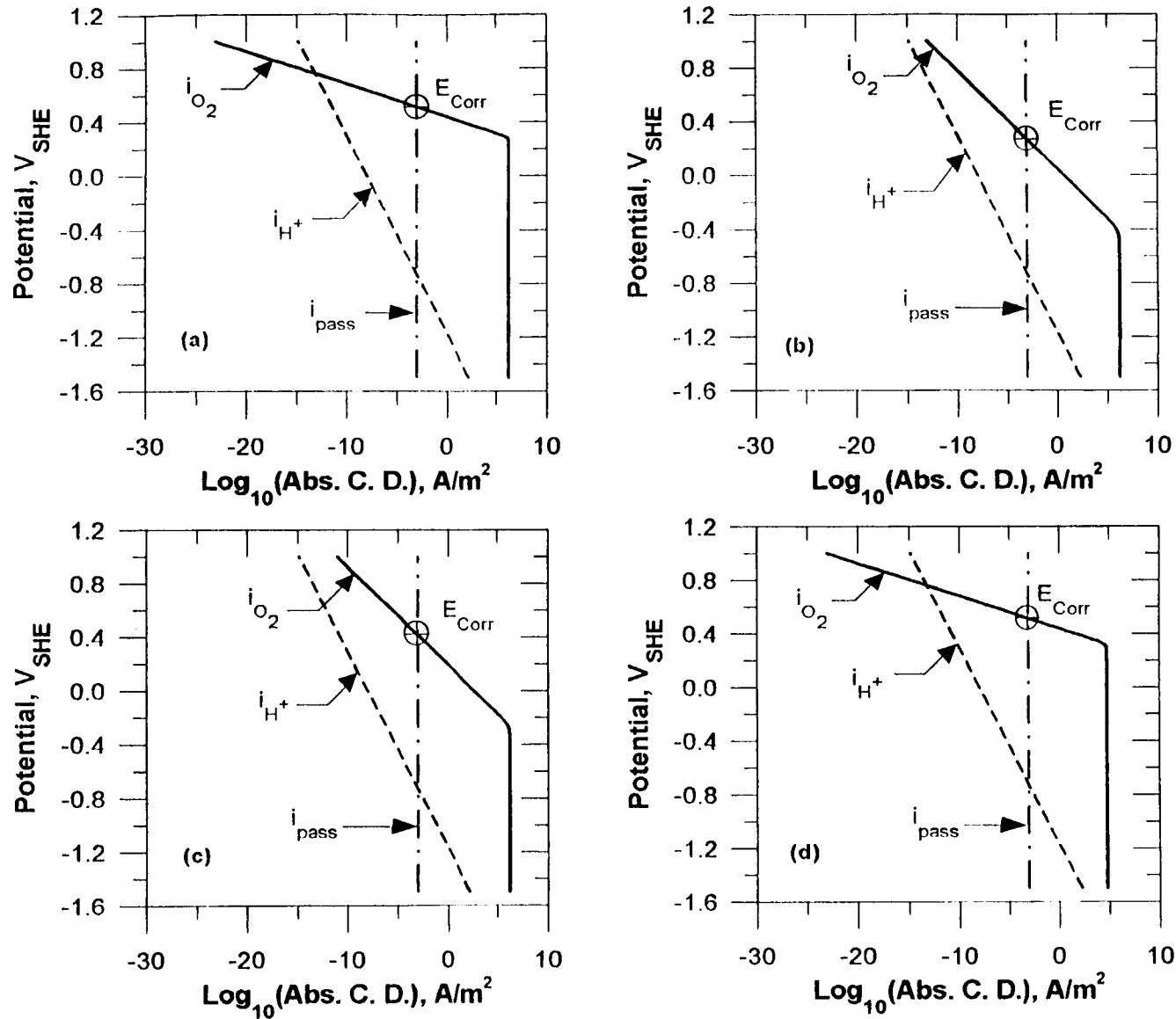


Figure 3-2. A sample calculation of the corrosion potential using oxygen reduction and hydrogen evolution as cathodic processes and passive current as the anodic process

general classification into slow, fast, and intermediate reactions. However, these values are extremely sensitive to the substrate and solution compositions. For example, the exchange current density for oxygen reduction reaction used by them was  $10^{-12}$  A/cm<sup>2</sup>. In a review of the oxygen electrode, Will (1976) suggests that the exchange current density can range from  $10^{-22}$  A/cm<sup>2</sup> for gold to  $10^{-5}$  A/cm<sup>2</sup> for palladium. Damjanovic (1969) lists the exchange current density of oxygen reduction on gold as  $10^{-9}$  A/cm<sup>2</sup> and on Pt as  $10^{-11}$  A/cm<sup>2</sup>. The exchange current densities on passive-film-forming materials have not been determined. Similar uncertainties accompany the other important reduction reaction, that of H<sub>2</sub>O<sub>2</sub>. The tremendous dependence of the kinetics of these reduction reactions on substrate can be seen in the effect of these oxidized species on the corrosion potentials of Pt and alloy 825 (Sridhar et al., 1993). Aeration increased the corrosion potential of alloy 825 by 247 mV, whereas it increased that of Pt by 648 mV. In contrast, the addition of H<sub>2</sub>O<sub>2</sub> increased the corrosion potential of alloy 825 by 663 mV, but that of Pt by 557 mV. The catalytic decomposition of H<sub>2</sub>O<sub>2</sub> on Pt and transition metals is also a factor in the overall reduction kinetics.

Another limitation is the lack of systematic data on the change in the passive current density with time of exposure. In particular, Macdonald and Urquidi-Macdonald (1990) calculate the time-average passive current density of all the alloys from the weight-loss data in long-term exposure tests. First, this is not mechanistically justified for Cu-based alloys because, under some environmental conditions relevant to the Yucca Mountain repository site, they exhibit active behavior. Second, it does not take into consideration the changes in the electronic properties of the film as a function of time. For example, Gorse et al. (1992) showed that aging the film under dry conditions can produce significant changes in the corrosion and pitting potentials of stainless steels. Recent experiments at the CNWRA (Dunn et al., 1993) have shown a decrease in passive current density due to thermal aging.

### 3.3 LOCALIZED CORROSION MODELS

Localized corrosion is considered to be one of the important failure modes determining the performance of high-level waste (HLW) container materials, especially those alloys that corrode at a low uniform corrosion rate (passive alloys). The importance of localized corrosion can be recognized when one compares the corrosion rate of a passive alloy (approximately 1  $\mu\text{m}/\text{yr}$  as uniform wall thinning) with that of an alloy undergoing active pitting (approximately 1,000 to 10,000  $\mu\text{m}/\text{yr}$  as a growing pit). In industrial structures, crevice corrosion is more commonly encountered than pitting. Indeed, in experimental investigations of pitting, precautions have to be taken to avoid crevice corrosion. However, crevices may act to provide a severe micro-environment within which either active general corrosion (total destabilization of a passive film) or pitting may take place. Additionally, the same type of mass-transport controlled governing equations can be written for a pit as for a crevice. For these reasons, the various approaches used to model crevice/pit initiation, growth, and repassivation are reviewed in this report.

It must be noted that two types of extrapolations from short-term data are needed for long-term prediction of the performance of the containers. The first, and most often discussed, is the temporal extrapolation. The second is the spatial extrapolation from small laboratory and prototype scale to several tens of thousands of containers. This latter aspect is not discussed in the present report. The Monte Carlo technique is being used in predicting the distribution of container failures by considering distributions of environmental conditions, corrosion potentials, and critical potential. Extreme value probabilistic methods have been used to examine localized corrosion of pipelines. The applicability of these techniques to the prediction of HLW containers will be examined in future reports.

### 3.3.1 Update to TWITCH

A computer code for generalized mass transport coupled with chemical reaction for the prediction of pitting and crevice corrosion initiation was developed in prior EBSPAC efforts. This chapter documents FY93 refinement of the TWITCH and MARIANA codes (Walton and Kalandros, 1992a, 1992b) and documents the application of the code to simulate pitting corrosion of copper.

Crevice corrosion is one of the predominant forms of localized corrosion limiting the service life of engineered structures. One method for improving the understanding and prediction of crevice corrosion is through the use of mathematical models. Mathematical models can be used to assist the interpretation and understanding of experimental results, particularly the relationship between the bulk solution electrolyte composition and the electrochemistry inside the localized corrosion cavity.

The model presented in this work differs from previously published models (Sharland, 1992; Watson and Postlethwaite, 1990) by: (i) incorporating improved treatment of activity coefficients in the transport and reaction equations, (ii) being general in format with reactions and aqueous species specified at run time rather than hard wired into the code, and (iii) allowing for both multiple cathodic and anodic reactions at the metal/solution interface. The model is capable of simulating processes such as crevice corrosion initiation, propagation rate of crevices (i.e., localized corrosion rate), and crevice repassivation as a function of external electrolyte composition and potential. The model is also capable of simulating pitting corrosion in situations where a one-dimensional approximation is appropriate. Examples are deep pits, very shallow pits, and pits where a restrictive cap is present at the mouth.

#### 3.3.1.1 Governing Equations

##### Mass Transport and Dissolution

The model considers mass transport by diffusion and electromigration. The flux equation for diffusion and electromigration of aqueous species is (Bockris and Reddy, 1977):

$$N_i = -\frac{D_i C_i}{RT} \nabla \bar{\mu}_i = -\frac{D_i C_i}{RT} \nabla (z_i F \phi_s + \mu_i) \quad (3-11)$$

where

- $N_i$  = flux of species  $i$
- $D_i$  = diffusion coefficient of species  $i$
- $C_i$  = concentration of species  $i$
- $z_i$  = charge of ionic species  $i$
- $\bar{\mu}_i$  = electrochemical potential of species  $i$
- $\mu_i$  = chemical potential of species  $i$
- $R$  = gas law constant
- $T$  = absolute temperature
- $F$  = Faraday constant

$\phi_s$  = electrostatic potential in solution

The chemical potential is given by

$$\mu_i = \mu_i^0 + RT \ln (a_i) \quad (3-12)$$

where  $\mu_i^0$  is the standard chemical potential of species  $i$  and the activity of each aqueous species is given by

$$a_i = C_i \gamma_i \quad (3-13)$$

where  $\gamma_i$  is the activity coefficient of species  $i$ .

Equation (3-11) can be expanded using Eqs. (3-12) and (3-13) giving

$$N_i = -\frac{z_i D_i F}{RT} C_i \nabla \phi_s - \frac{D_i}{\gamma_i} (\gamma_i \nabla C_i + C_i \nabla \gamma_i) \quad (3-14)$$

The flux of ions results in a current in the solution

$$i_s = F \sum_i z_i N_i \quad (3-15)$$

where

$i_s$  = net current density in the solution at any point in the crevice solution.

Combining Eqs. (3-14) and (3-15) and solving for the electrostatic potential in solution yields

$$\nabla \phi_s = \frac{-\left[ i_s + \sum_i \frac{z_i F D_i}{\gamma_i} (\gamma_i \nabla C_i + C_i \nabla \gamma_i) \right]}{\kappa} \quad (3-16)$$

where

$$\kappa = F^2 \sum_i \frac{z_i^2 D_i}{RT} C_i \quad (3-17)$$

A similar substitution to eliminate the potential from the transport equations is given by Newman (1991).

In order to specify the current in solution for a particular problem, one must consider conservation of charge and either electroneutrality or Poisson's equation for the potential. In the case of electroneutrality, there can be no storage of charge or capacitance in the solution. For one-dimensional geometry with a no-flux boundary at one end of the model domains, the current at any point assuming no charge buildup at any point is

$$i_s = \frac{1}{A} \int_x^L i_e P dx \quad (3-18)$$

where

- $i_e$  = current density at the metal-electrolyte interface
- $P$  = metal covered perimeter ( $2\pi r$  for a pit,  $2w$  for a crevice)
- $A$  = cross sectional area of crevice or pit ( $\pi r^2$  for a pit,  $wg$  for a crevice)
- $x$  = position in the crevice measured from the mouth
- $L$  = length of the crevice
- $r$  = pit radius
- $g$  = crevice gap
- $w$  = crevice width (assumed as one unit of length with  $w > g$ )

Both  $i_e$  and  $i_s$  can be functions of  $x$ . In Eq. (3-18), two surfaces of the crevice are assumed to be corroding. This simulates the crevice between two metals. For one-sided crevices, this will be divided by 2. Substituting Eq. (3-18) into Eq. (3-16) gives an expression for the potential gradient at any point in the crevice as a function of solution composition, gradients in activity coefficients, concentration gradients, and the current density across the metal-electrolyte interface. The potential at any point can be obtained by integration of Eq. (3-16) from the mouth, where a fixed potential is assumed, to the desired position in the crevice. In situations where the reactions at the metal-electrolyte interface are assumed to be potential dependent, the potential appears in both equations requiring numerical iteration for a solution. The iteration is performed by relaxation and occurs at each time step for each computational node.

The current density at the metal-electrolyte interface,  $i_e$ , is generally a function of the potential, temperature, and concentrations of the aqueous species present.

$$i_e = f(E, T, C_1, C_2, \dots, C_n) \quad (3-19)$$

The potential,  $E$ , is defined as the potential of the metal relative to the potential in solution:

$$E = \phi_m - \phi_s \quad (3-20)$$

where  $\phi_m$  is the potential of the metal. A constant anodic current density relatively independent of potential over a wide potential range can be assumed for the special case of a passivated metal. In addition to driving the current in solution, these reactions define the flux of ions at the metal-electrolyte interface.

$$\begin{aligned} \bar{N}_i &= \frac{\alpha_i i_e}{z_i F} \\ \sum_i \alpha_i &= 1 \end{aligned} \quad (3-21)$$

where

$$\begin{aligned} \bar{N}_i &= \text{flux of species } i \text{ into solution at the metal-electrolyte interface} \\ \alpha_i &= \text{a weighing factor indicating the relative rate of production of species } i \end{aligned}$$

By definition,  $\bar{N}_i$  points in a direction perpendicular to the plane representing the metal-electrolyte interface. The weighing factor,  $\alpha_i$ , can be based on alloy composition, assuming that congruent dissolution occurs, or can be modified to consider selective dissolution of a certain alloying element.

Assuming the flux at the metal-electrolyte interface is averaged over the crevice, the material balance at any point is given by

$$\frac{\partial C_i}{\partial t} = -\nabla \cdot N_i + \frac{P}{A} \bar{N}_i + R_i \quad (3-22)$$

where

$$\begin{aligned} R_i &= \text{rate at which species } i \text{ is produced through chemical reactions per unit volume in solution} \\ P &= \text{metal perimeter} \\ A &= \text{cross sectional area of crevice cavity} \\ C_i &= \text{concentration of species } i \text{ in aqueous solution} \end{aligned}$$

Since the equation for the flux in solution contains the concentration multiplied by the gradient in potential (i.e., two unknowns), the governing equations are inherently nonlinear, even without consideration of chemical reactions.

## Reactions in Crevice Solution

The chemical reaction equations in the crevice solution are solved for equilibrium by stoichiometric Gibbs free energy minimization (Smith, 1983). The Gibbs free energy of formation of a system is given by

$$G = \sum_i n_i \mu_i = \sum_i n_i (\mu_i^0 + RT \ln a_i) \quad (3-23)$$

where

$$\begin{aligned} G &= \text{Gibbs free energy} \\ n_i &= \text{moles of } i \text{ in 1 kg of water} \end{aligned}$$

The moles of a particular species  $i$  in the system can be related to the reaction progress variable:

$$n_i = n_i^0 + \sum_r \nu_{i,r} \xi_r \quad (3-24)$$

where

$$\begin{aligned} n_i^0 &= \text{moles of } i \text{ in 1 kg of water at initial time} \\ \nu_{i,r} &= \text{stoichiometric coefficient of species } i \text{ in reaction } r \\ \xi_r &= \text{reaction progress variable for reaction } r \end{aligned}$$

This states that the number of moles of species  $i$  present is equal to the number of moles originally present plus the number of moles produced or lost through multiple chemical reactions. The reaction progress variable for any reaction is unconstrained and can be either positive or negative. The activity of solids is assumed to be unity if the solid is present, and zero otherwise.

Minimization of Gibbs free energy is accomplished by taking the derivative of  $G$  with respect to each reaction progress variable and setting the result equal to zero:

$$\frac{\partial G}{\partial \xi_r} = \sum_i \frac{\partial G}{\partial n_i} \frac{\partial n_i}{\partial \xi_r} = \sum_i \mu_i \nu_{i,r} = \sum_i \nu_{i,r} (\mu_i^0 + RT \ln a_i) = 0 \quad (3-25)$$

Solving each resulting equation for the reaction progress variable yields the extent of each reaction which, in turn, yields the equilibrium concentration of each species. The equations are solved using Newton-Raphson method, which requires the Jacobian. The derivatives for the Jacobian are obtained analytically by computing the second derivative of  $G$  with respect to the various reaction progress variables. The basis for solution of the equations is 1 kg of water, thus  $n_i \equiv C_i$ .

## Calculation of Activity Coefficients

Three options are currently available in TWITCH for determining activity coefficients: (i) assume ideal solution (activity coefficients equal 1), (ii) calculate using the B-dot Debye-Hückel equation, and (iii) calculate using the Davies equation. The B-dot Debye-Hückel equation is given by (Helgeson, 1969):

$$\log(\gamma_i) = -Az_i^2 \frac{\sqrt{I}}{1 + a_i^0 B \sqrt{I}} + \dot{B}I \quad (3-26)$$

where

- $A$  = coefficient of Debye-Hückel limiting law =  $1.82 \times 10^6 (\epsilon T^{-3/2})$
- $I$  = ionic strength =  $0.5 \sum z_i^2 C_i$
- $C_i$  = concentration of aqueous species  $i$  in molal units
- $B$  = Debye-Hückel parameter =  $0.3 (\epsilon T)^{-1/2}$
- $a_i^0$  = ion size parameter for species  $i$
- $\dot{B}$  = B-dot parameter
- $\epsilon$  = dielectric constant

The Davies equation (Stumm and Morgan, 1981) is similar to the B-dot equation with  $a_i^0 B = 1$  and  $\dot{B} = 0.3$ . The Debye-Hückel and B-dot parameters are calculated as functions of temperature using correlations valid over the range 0 to 250 °C. Uncharged species, water, and solids are assumed to have activity coefficients of 1. An example of the adequacy of the approximations provided by the activity coefficient expressions can be obtained by comparison with experimental data.

Figure 3-3 demonstrates how the activity coefficient of calcium chloride varies with concentration. The vertical axis denotes the base 10 logarithm of the activity coefficient, and the horizontal axis denotes the molal concentration of calcium chloride. The dotted line represents experimental data collected by Staples and Nuttal (1977). The dashed line represents the Davies equation; the solid line is the B-dot equation.

At low molal concentrations, both equations accurately predict the activity coefficient. At higher concentrations, the Davies equation deviates markedly. Interestingly, the B-dot equation diverges less at high ionic strengths, underpredicting the experimental data as ionic strength increases. Alternate, more accurate approaches to modeling concentrated solutions (Pitzer, 1991) can be used but are numerically difficult to incorporate directly into the present code.

## Numerical Solution

The flux of aqueous species across each nodal interface is calculated using Eq. (3-14) after replacing all the concentration and activity coefficient derivatives with finite difference approximations.

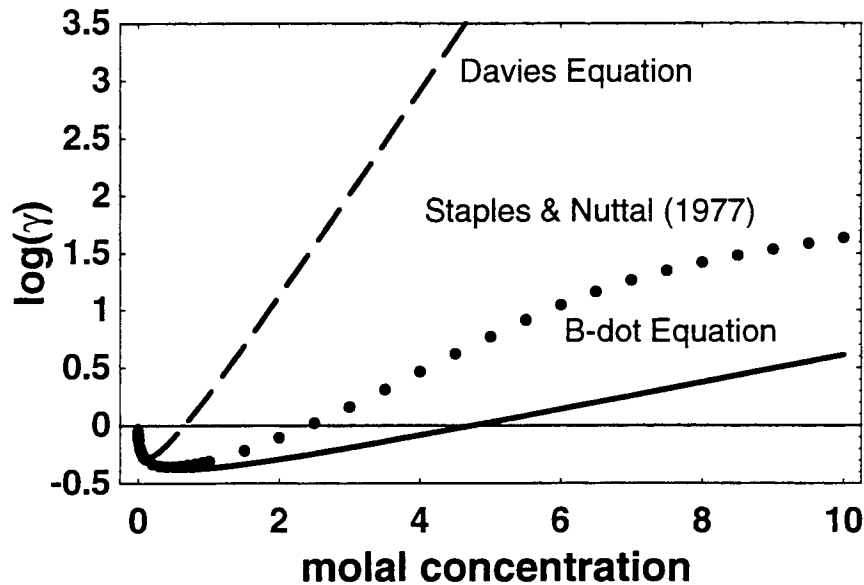


Figure 3-3. Comparison of calculated activity coefficients for calcium chloride with experimental data

The mass transport part of Eq. (3-22) is thereby converted to a series of ordinary differential equations

$$\frac{dC_i}{dt} = \frac{(A^{in} N_i^{in} - A^{out} N_i^{out})}{V} + \frac{A_s \bar{N}_i}{V} \quad (3-27)$$

where

- $V$  = volume of aqueous solution at the node
- $A$  = cross sectional area of corrosion cavity at nodal interface
- $N_i$  = flux of each ion in solution at nodal interface
- $A_s$  = metal surface area at each node
- $\bar{N}_i$  = flux of ion at metal-electrolyte interface inside node
- in, out* = nodal interface in the negative and positive  $x$  directions, respectively

The flux of each ion at the metal-electrolyte interface  $\bar{N}_i$  is estimated based upon the current density at the node. Equation (3-27) is written for every aqueous species at every node. Boundary conditions are specified as no flux at the base and fixed concentration at the mouth. The interface between nodes is defined to be at the midpoint between adjacent nodes, allowing for variable node spacing as specified by the user. Cross sectional area, metal surface area, and volume are calculated at each node based upon

user input of nodal spacing and crevice gap (or pit radius). When the crevice gap ( $g$ ) or pit radius ( $r$ ) are nonuniform,  $A_s$ ,  $A$ , and  $V$  are estimated using linear interpolation of the three-dimensional shape between nodes.

Equation (3-18) is discretized as

$$i_s = \frac{1}{A} \sum_i^n i_e A_s \quad (3-28)$$

with the summation going from each calculational node ( $i$ ) to the base of the corrosion cavity.

The interfacial concentration of each species is usually estimated by averaging concentrations at adjacent nodes. However, when high potential gradients are present, the central differencing scheme can become unstable. An effective Peclet number for the system can be defined as

$$Pe \equiv \frac{\left( \frac{z_i F D_i V \phi_s}{RT} \right)}{\left( \frac{D_i}{\Delta x} \right)} = \frac{\Delta x z_i F \nabla \phi_s}{RT} \quad (3-29)$$

If the absolute value of the Peclet number is greater than two, an upwinding scheme is used. In the case where  $z_i \Delta \phi_s > 0$ , the interfacial concentration is assumed to be equal to the concentration at the next higher node. When  $z_i \Delta \phi_s < 0$ , the concentration at the lower node is used. The assumption involved with upwinding is that, when electromigration is strong, relative to diffusion, the best estimate of concentration at the nodal interface is the concentration at the up-gradient node.

The upwinding scheme is only first-order accurate, whereas the central difference method is second-order accurate. Thus, some accuracy is sacrificed to obtain increased stability. Refinement of the grid can be used to eliminate the upwinding and gain increased accuracy. As with any numerical code, adequacy of the discretization can be checked by continual refinement of the grid until the answers no longer change significantly. Smaller nodal spacings are recommended at locations where concentration and potential gradients are greatest. In the case of corrosion problems, this will usually be near the mouth.

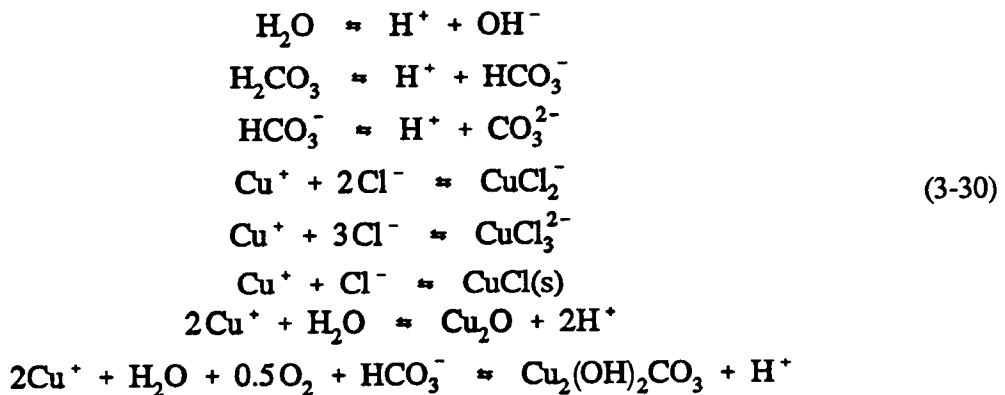
The equations are integrated in time using one of three specified ordinary differential equation (ODE) solvers with monitored accuracy and step-size control. If the desired accuracy is not achieved, then the step size is reduced automatically. The three solvers are an Adams method (Hindmarsh, 1983); the Bulirsch-Stoer method (Press et al., 1986); and the fifth-order Runge-Kutta method (Press et al., 1986).

The assumption is made that the characteristic times of chemical reactions in aqueous solution are much shorter than those of the mass transport or corrosion processes. Thus, the aqueous solution is assumed to be at equilibrium. For hydrolysis and aqueous complex reactions, this is typically an excellent assumption. For heterogeneous precipitation/dissolution reactions, this is merely a convenient approximation made necessary by the absence of detailed kinetic data. In order to keep the code general, there is no built-in database. Instead, the required thermodynamic and transport data are read from an input deck. Reactions are input in the form of a stoichiometric matrix. Only reactions passed in the matrix are considered and all homogeneous reactions are solved to equilibrium. Heterogeneous reactions are subject to mass balance and kinetic constraints and may not reach equilibrium. For example, if all the mass of a particular solid is depleted, the reaction is automatically removed from consideration.

Given the local equilibrium assumption, the equations governing mass transport and corrosion may be decoupled from those governing equilibrium reactions in the aqueous solution. At the end of each time step, the equilibrium assumption is applied by calling the equilibrium solver. The term  $R_i$  in Eq. (3-22) is thus not considered.

### 3.3.1.2 Application of TWITCH to Modeling Copper Pitting

In order to continue improving the TWITCH code, a number of simulations have been performed on a variety of localized corrosion problems. This section documents the work on modeling pitting corrosion of copper. The primary goal of the copper pitting modeling was to compare predicted secondary mineral formation in actual and modeled pits. The chemical reactions in Eq. (3-30) and species were considered.



The initial and boundary conditions are given in Table 3-2. These are values after equilibration of the input values. The potential-independent anodic current density is assumed to be  $10^{-6}$  A/cm<sup>2</sup>. Copper is assumed to dissolve as  $\text{Cu}^+$ . The pit shape is shown in Figure 3-4. In order to simulate the corrosion product formation, 21 finite difference nodes were used with 15 species and 8 reactions. The narrowing at the mouth was done to simulate the effect of a partially porous cap of cuprite and malachite forming at the mouth of a hemispherical pit. The hemispherical pit was modeled as a V shape at the bottom with a narrowing at the mouth.

Figures 3-5 to 3-8 give some of the ion concentrations as a function of depth in the pit. Oxygen, carbonate, bicarbonate, and carbonic acid levels drop off precipitously just inside the mouth as a result

of malachite precipitation. At the high boundary concentrations assumed, chloride concentrations are relatively flat inside the pit (not shown). Dissolved copper and hydrogen ion increase with depth in the pit. The potential drop in the pit is shown in Figure 3-8. Potential drop is about 30 mV and depends heavily on boundary concentrations of chloride.

The amount of solids precipitated (per liter of crevice volume) is shown in Figure 3-9. Malachite precipitates just inside the mouth where oxygen and bicarbonate anion moving into the pit by diffusion and electromigration meet and react with dissolved copper cations transporting out of the pit by diffusion and electromigration. This results in a sharp reaction front, visible in the distributions of all three ions. A little further inside the pit, but still near the mouth, Cuprite begins to precipitate. Cuprite precipitation occurs throughout the rest of the pit but is greatest near the mouth and at the base. At the very bottom of the it, Nantokite precipitates as a salt film.

**Table 3-2. Initial and boundary conditions for species used in copper pit model**

Species	Boundary Condition	Initial Condition
H <sup>+</sup>	$3.5 \times 10^{-4}$	$1.7 \times 10^{-7}$
H <sub>2</sub> CO <sub>3</sub> *	$3.1 \times 10^{-5}$	$8.9 \times 10^{-6}$
HCO <sub>3</sub> <sup>-</sup>	$3.7 \times 10^{-8}$	$2.2 \times 10^{-5}$
CO <sub>3</sub> <sup>2-</sup>	$5.0 \times 10^{-15}$	$6.2 \times 10^{-9}$
Na <sup>+</sup>	$1.2 \times 10^{-4}$	$1.2 \times 10^{-4}$
Cl <sup>-</sup>	$4.7 \times 10^{-4}$	$9.9 \times 10^{-5}$
Cu <sup>+</sup>	$9.2 \times 10^{-7}$	$3.0 \times 10^{-20}$
O <sub>2</sub> (aq)	$1.0 \times 10^{-55}$	$1.0 \times 10^{-5}$
CuCl(s)	$2.5 \times 10^{-5}$	0
Cu <sub>2</sub> O	$1.9 \times 10^{-4}$	0
Malachite	0	0
CuCl <sub>2</sub> <sup>-</sup>	$1.3 \times 10^{-8}$	$1.9 \times 10^{-23}$
CuCl <sub>3</sub> <sup>2-</sup>	$4.2 \times 10^{-11}$	$1.3 \times 10^{-26}$

### 3.3.1.3 Future Developments

One of the major limitations of many of the crevice corrosion models for stainless steel is their inability to predict a critical potential for pitting/crevice corrosion, unless rather artificial current-potential relationships are introduced. For example, Galvele (1976) was able to predict a critical pitting potential by assuming that the electrochemical response of the metal inside the pit can be represented by a Tafel-type relationship. Pickering (1991) assumed that a significant active-passive peak exists inside a crevice such that ohmic potential drop from the mouth to the inside of the pit shifts the potential from the passive to active regime. However, experimental findings indicate that neither a Tafel-type behavior nor a significant active-passive peak is observed unless the environment becomes sufficiently acidic and high in chloride concentration (Sridhar et al., 1992). Hence, prior to active pit/crevice initiation, most of the metal exhibits a potential-independent current density. A similar shortcoming exists in the present version of TWITCH. An approach to predicting a critical potential is to assume that the crevice surfaces consist of a variety of ridges and that the gap can assume very low values in a small region and relatively large values in other areas. Thus, crevice corrosion can initiate in the regions with small gaps relatively rapidly, but requires a potential sufficiently large for this small active crevice corrosion front to propagate into larger gap regions. Such varying gaps can be modeled in TWITCH. Another approach, suggested

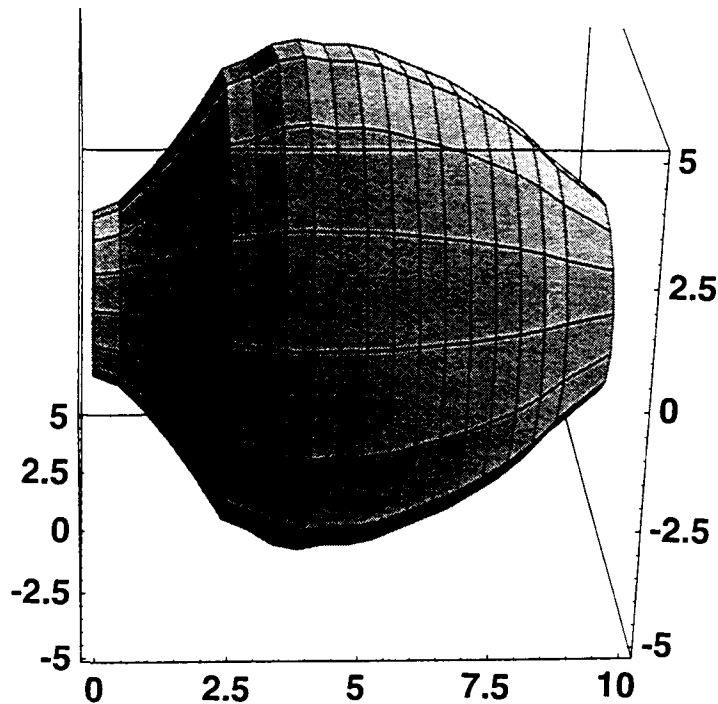


Figure 3-4. Geometry of copper pit assumed in modeling. Narrowing at the mouth was imposed to simulate mass transport limitations caused by a cap of corrosion products. Total pit depth was assumed to be 10 mm.

by Alkire and Lott (1989), assumes that crevice corrosion initiates not by acidification but by the formation of a critical concentration of thiosulfate from the dissolution of manganese sulfide (MnS) inclusions in the crevice. The electrochemical dissolution of MnS occurs by an active process thus involving a potential-dependent current density. However, this model is not applicable to electroslag remelted alloys, such as alloy 825, which do not have significant amounts of MnS.

Recent experiments in crevices of alloy 825 and type 304L stainless steel (Sridhar and Dunn, 1993) have indicated that, in both these cases, a decrease in pH occurs only after a certain anodic potential is applied externally (or an external oxidant such as  $H_2O_2$ ) is supplied. Furthermore, the current increase always preceded changes in crevice chemistry. It is possible that crevice corrosion initiates at very small areas where the gap is small and then spreads laterally if the external potential is large enough. In such a case, the changes in local chemistry may not be large enough to be detectable before crevice corrosion spreads over a wider area. Such a sequence of events can be simulated by TWITCH by the appropriate use of crevice gap variation. This is important to demonstrate, through the use of a model, that in practical crevices, a critical potential can exist.

### 3.4 CRITICAL POTENTIALS

The following sections discuss the literature on various types of localized corrosion models. The PA codes such as SOTEC and SCCEX, at present, use only the empirical models.

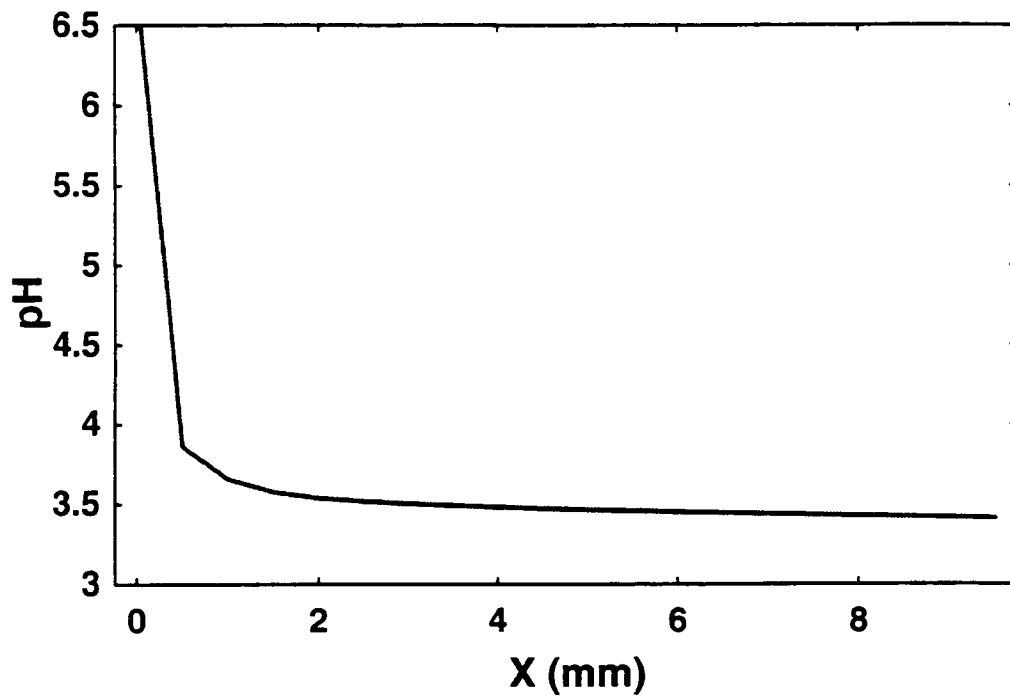


Figure 3-5. pH in copper pit

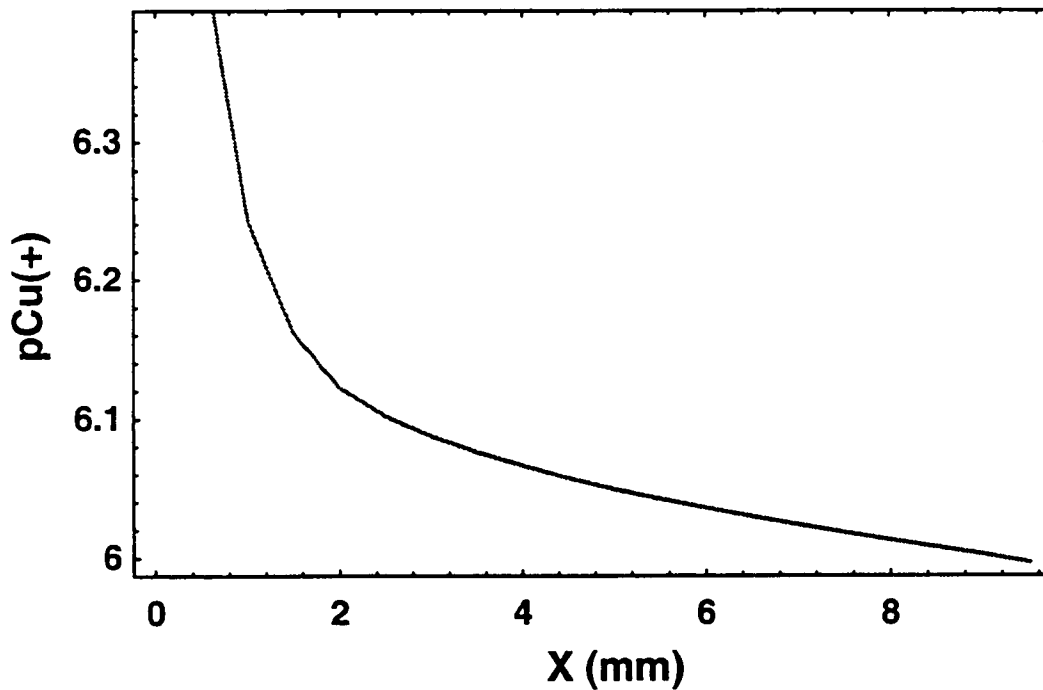


Figure 3-6. Negative log [cuprous ion concentration] as a function of depth in pit

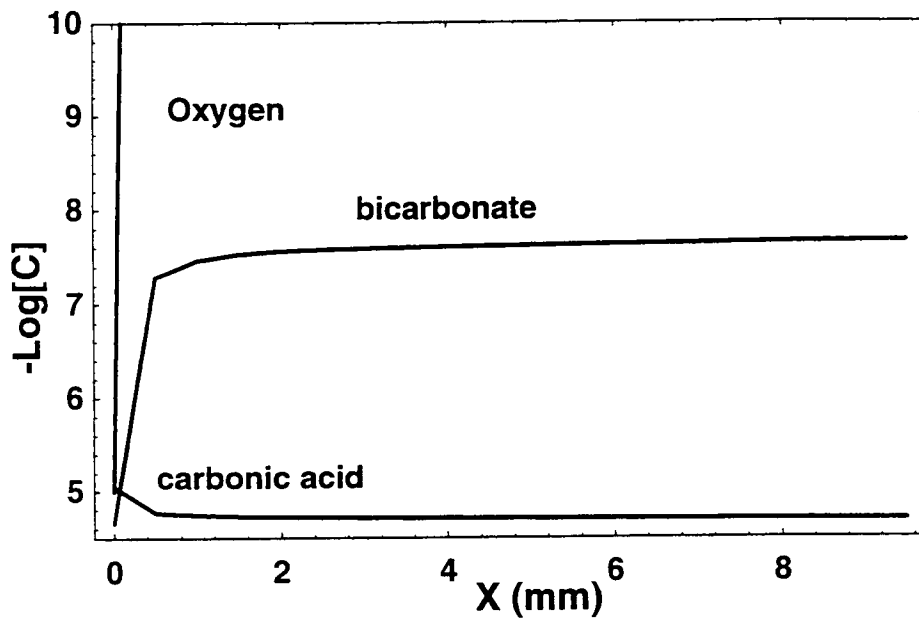


Figure 3-7. Bicarbonate, dissolved carbon dioxide plus carbonic acid, and dissolved oxygen inside the pit. Concentrations drop precipitously near the mouth where malachite precipitation occurs.

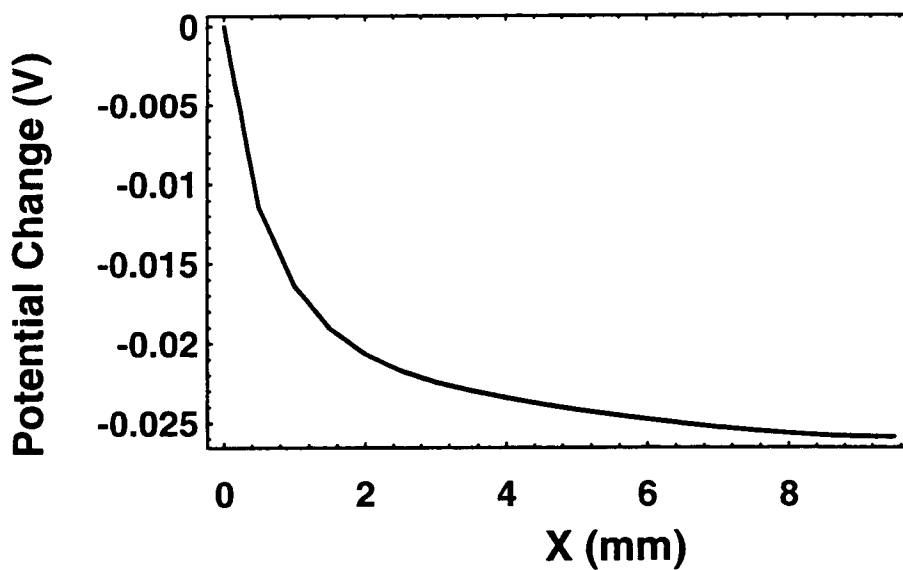


Figure 3-8. Potential drop in copper pit

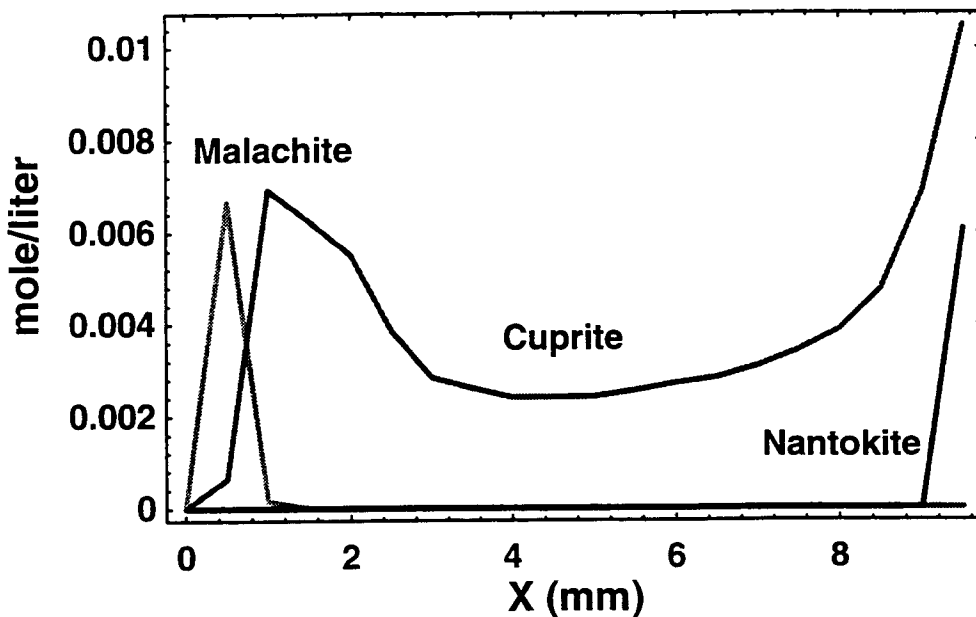


Figure 3-9. Precipitation of solids in copper pit in moles/liter of crevice

### 3.4.1 Stochastic Models

Many experimental findings have indicated that pit initiation is a stochastic process (Shibata, 1983; Shibata and Takeyama, 1977, 1981; Shibata and Takamiya, 1986; Williams et al., 1985a, 1985b; Mola et al., 1990). This means that statistical distributions describe the critical pit initiation potential and the pit initiation time at any given potential. Shibata and Takeyama (1977) proposed a model for pitting potential based initially on the assumption of a pit generation rate,  $\lambda$ , independent of time, but dependent on applied potential. However, their model was really a curve fitting approach using an exponential distribution to fit their experimental data of pit initiation times (survival probability) at various applied potentials. Based on their data, they found that the pit generation rate had three values depending on the survival time. At short survival times,  $\lambda$  was proportional to  $(E - E_{crit})$ , where  $E$  is the applied potential and  $E_{crit}$  is a critical potential below which no pit initiation events were observed within the experimental time scale. At intermediate and long survival times (it must be emphasized that these experiments were only conducted up to a total time of 70 sec), the pit generation rate was exponentially dependent on potential. The assumption of an exponential distribution of survival probability was not fully explained and a more general Weibull distribution could have fit the data just as well without the need to introduce three pit generation rates. Shibata and Takeyama (1981) modified their original approach to include a pit generation rate,  $\lambda$ , and a repassivation rate,  $\mu$ , but retained the exponential distribution. Again based on experimental data, they suggested that  $\lambda$  increased exponentially with applied potential, while  $\mu$  was independent of applied potential. Together these two parameters defined the observed pitting potential,  $E_p$ , and its observed dependence on potential scan rate. Shibata and Takamiya (1986) showed that  $\lambda$

decreased with a decrease in chloride concentration, but the effect of chloride concentration on  $\mu$  was relatively small. Williams et al. (1985a, 1985b) developed a stochastic model for pit initiation based on their earlier investigations of the electrocrystallization process. They assumed that small, random fluctuations in current density or concentration of species ( $H^+$ ,  $Cl^-$ ) at the metal-electrolyte interface can cause nucleation of metastable pits. These fluctuations were assumed to occur over a scale corresponding to the surface roughness of the metallic surface. These metastable pits do not all survive—some repassivate. However, the metastable pits that survived beyond a critical age,  $\tau_c$ , were assumed to result in stable pits that can then grow. Based on these assumptions, they derived the probability,  $P(t)$ , that no stable pits form at any given time,  $t$

$$\ln [P(t)] = -\lambda a(t - \tau_c) \exp(-\mu \tau_c) \quad (3-31)$$

where

- $\lambda$  = frequency of nucleation of metastable pits per unit area (different from that of Shibata's)
- $\mu$  = probability of repassivation
- $\tau_c$  = critical age beyond which the metastable pits become stable pits
- $a$  = specimen area

Henshall (1992) essentially used the same approach, but with a Monte-Carlo technique, to predict the evolution of stable pits on type 304 stainless steel. Williams et al. (1985b) also provided a mechanistic rationale for their stochastic theory. They considered pit nucleation events to be related to the creation of micro-crevice cells between the protuberances on the surface of the metal. They hypothesized that, while the passive current density is small on an average, there can be wide fluctuations within the very small areas corresponding to the surface roughness that can cause formation of a highly acidic micro-environment and initiate active corrosion in these small areas. These fluctuations in local current densities were assumed to decrease with a decrease in applied potential, and, hence, the presence of a critical pitting potential was rationalized. More recently, Stewart and Williams (1992) suggested that the stochastic event in the pit initiation process on commercial austenitic stainless steels is the supply of sulfur from the dissolved MnS inclusions to the micropit surrounding the inclusion, and, therefore, the rate of generation of stable pits depends on the size and distribution of sulfide inclusions. The similarity of these arguments to crevice corrosion discussed in the previous section is obvious.

Unfortunately, for predictive purposes, one is still left with a need to assume values for a critical potential below which no nucleation of metastable pits takes place and a critical age beyond which these pits become stable. More importantly, the pit generation rate and repassivation probability can be derived only from experimental measurements over time scales much smaller than the required time periods for containment. There seems to be no fundamentally justifiable scheme by which  $\lambda$  and  $\mu$ , derived from short-term laboratory experiments (1,000 sec or less) in concentrated chloride solutions, can be extrapolated to long time periods in predicted repository environments. From the perspective of long-term prediction and design for long-term performance, one then has to resort to deterministic models that attempt to predict the critical pitting potentials. However, it must be noted that deterministic models can be used to derive distribution of pit initiation times or potentials by assuming distributed values of more fundamental parameters (Macdonald and Urquidi-Macdonald, 1992a).

### 3.4.2 Deterministic Mechanistic Models

Mechanisms of pitting corrosion have been investigated since the 1920s and are continuing to evolve. Many of the older models have been attempts to provide qualitative explanations of observed phenomenology. Some of the models, at least in the form they were originally proposed, have been discarded in light of new data. The reader is referred to other sources for more information (Szklańska-Smiałowska, 1986). However, the current mechanistic theories can be divided into two major categories: (i) those that assume that pitting is initiated in a passive film by the creation and movement of defects (Okada, 1984; Lin et al., 1981), and (ii) those that assume that microscopic defects, such as inclusions, exist prior to the initiation of pits and these defects modify the local environment such that the passive film is destabilized, either by a critical concentration of  $H^+$  (Galvele, 1976, 1981; Gravano and Galvele, 1984) or by a critical combination of  $Cl^-$  and thiosulfate (Alkire and Lott, 1989). The latter two models are applicable to pitting repassivation also. However, destabilization of passive films by a critical concentration of anionic species implies that a more fundamental process is responsible for the destabilization. Hence, the metal chloride nuclei model by Okada (1984) and the point defect model by Lin et al. (1981) are still of interest from this perspective. The latter is of particular interest because it appears to be useful in predicting not only the effects of environmental variables, but also the role of alloying elements. For example, in Lin et al. (1981) the critical pitting potential is derived from the consideration of the effect of chloride ions on the movement of cationic species in the passive film. The fundamental assumption of the model is that the passive film growth takes place by the transport of anionic species from the solution-passive film interface inward to the metal and cationic species in the opposite direction. Movement of cationic species away from the metal-passive film interface towards the solution phase generates point defects in the form of cation vacancies in the film-metal interface. Under ideal circumstances, the cation vacancies will diffuse into the metal and be absorbed. However, when the rate of movement of cations away from the metal is unequal to the rate of movement of cation vacancies into the metal, concentration of cation vacancies build up at the metal-film interface which, upon attaining a critical size, become pit nuclei. The role of chloride was seen as enhancing the transport of cations away from the metal-film interface to the solution-film interface. Based on this hypothesis, Lin et al. (1981) derived the relationship between the critical potential for pit nucleation and bulk chloride concentration as

$$E_p = \frac{4.606RT}{\chi F \alpha} \log \frac{J_m}{J^0 u^{-\chi/2}} - \frac{2.303RT}{\alpha F} \log a_{Cl^-} \quad (3-32)$$

where

- $\chi$  = charge of the cation
- $F$  = Faraday constant
- $\alpha$  = charge transfer coefficient
- $J_m$  = rate of submergence of the cation vacancies into the metal
- $J^0$  = migrational flux of cations
- $u$  = pre-exponential term associated with the chloride-oxygen vacancy at the solution-film interface
- $T$  = temperature
- $a_{Cl^-}$  = activity of chloride ion in the solution

It can be seen from Eq. (3-32) that this model can explain the typical dependence of pitting potential on chloride concentration.

Additionally, in a more recent paper (Urquidi-Macdonald and Macdonald, 1987), the distributed values of pitting potential and incubation time were derived using the point defect model. This was derived by assuming that there is a distribution of defects within the passive film such that the diffusivity of cations is distributed. However, this need not be the only factor in the model that may be assumed to be distributed. Hence, the point defect model should be examined in detail in terms of the effect of temperature and chloride concentration on the distribution of pitting potential and incubation time.

The pit repassivation potential,  $E_{rp}$ , is typically not as variable as the pit initiation potential. However, because there has long been a controversy as to the existence of a minimum repassivation potential, not much effort has been placed in modeling repassivation potential. Recently, there has been an increased interest in pitting repassivation potential (Nakayama and Akashi, 1993b; Sridhar and Cragolino, 1992; Thompson and Syrett, 1992) in terms of utilizing it as a lower-bound parameter for life prediction. Tsujikawa et al. (1987) modeled some of their experimental results on repassivation potentials of pits and crevices and suggested that the repassivation potential is related to the effect of external potential on solution composition inside the pits or crevices. However, their model cannot be used to directly obtain repassivation potentials. Nevertheless, this will be a useful concept to explore using a more rigorous transport treatment such as that available in TWITCH.

### 3.4.3 Empirical Models

For PA calculations, detailed models discussed previously are not suitable. Empirically obtained critical potentials are used in such cases. These critical potentials exhibit a complex dependence on various environmental factors. The relationships of the critical potentials to material and environmental factors are called empirical models. As part of the EBSPAC activities, these empirical models from the literature and CNWRA experimental programs are reviewed and collated. In the SCCEX code, the environmental factors calculated in Section 2.4 and 2.5 are input into the empirical equations discussed in this section.

The effect of various anionic species on the localized corrosion resistance of alloy 825 and type 316L stainless steel has been examined using statistical experimental designs (Sridhar et al., 1993; Thompson et al., 1992). These results suggested that chloride is the predominant factor in determining the localized corrosion resistance of these alloys. The following equations represent the dependence of the  $E_p$  and  $E_{rp}$  on anionic concentrations (Sridhar et al., 1993).

$$(LCI)_{316L} = 364.12 + 320.2(X_{Cl}) \quad (3-33)$$

$$\begin{aligned} (LCI)_{825} = & 95.5 + 84.5(X_{Cl}) - 84.5(X_{NO_3}) - 87.0(X_{Cl} \cdot X_{NO_3}) \\ & - 10.2(X_F) + 9.4(X_T \cdot X_F) - 8.1(X_T \cdot X_{NO_3}) \\ & - 7.0(X_{Cl} \cdot X_T \cdot X_{NO_3}) \end{aligned} \quad (3-34)$$

where

$$LCI = \frac{(E_p - E_{rp}) \cdot 100}{E_p} \cdot \text{Visual Rating} \quad (3-35)$$

and

$$X_A = \frac{2(A - A_{avg})}{(A_{max} - A_{min})} \quad (3-36)$$

While this approach can indicate the complex effects of environmental factors without considerable experimental effort, the essential utility of these empirical models is the prioritizing of the factors most important to localized corrosion. The limitations of the approach include the validity of Eqs. (3-33) and (3-34) only within the ranges of factors examined and the assumption of linearity. In the case of temperature, for example, it has been shown that the  $E_p$  shows a sigmoidal relationship (Brigham, 1974) with a steep dependence only at an intermediate temperature range. In the case of chloride concentration, a logarithmic dependence has been shown to be valid (Szklarska-Smialowska, 1986). Hence, the dependence of  $E_p$  on chloride concentration and temperature was examined in greater detail. More specifically, the general dependence of  $E_p$ ,  $E_{rp}$ , and  $E_{rc}$  were considered to be of the general form:

$$E_{crit} = A(t) + B(t) \times \log(\text{Cl}) \quad (3-37)$$

where the constants  $A(t)$  and  $B(t)$  were considered as linear functions of temperature and  $t$  is the temperature in degrees Celsius. While this does not take into consideration the complex temperature dependence indicated by Brigham (1974), it is satisfied by most experimental findings when considered over a limited temperature regime.

The details of the experimental correlations are shown in Appendix A. For alloy 825, the following parameters were found.

For  $E_p$

$$A(t) = 200\text{mV} (t \geq 50^\circ\text{C}) ; B(t) = -120 \text{ mV/decade} (t \geq 50^\circ\text{C}) \quad (3-38)$$

For  $E_{rp}$

$$A(t) = 346.5 - 6.7(t^\circ\text{C}) ; B(t) = 76.3 - 1.9(t^\circ\text{C}) \quad (3-39)$$

For types 304/304L stainless steel, the following relationships were found.

For  $E_p$

$$A(t) = 187.4 - 3.7(t^\circ C) ; B(t) = -76 + 0.06(t^\circ C) \quad (3-40)$$

For  $E_{rp}$

$$A(t) = -172.4 - 2.4(t^\circ C) ; B(t) = -80.1 + 0.35(t^\circ C) \quad (3-41)$$

For alloy C-22/C-276/C-4, pitting did not occur even at high applied potentials and in NaCl solutions up to 4 M in concentration (Sridhar et al., 1993; Lukezich and Ahluwalia, 1992). It must be noted that some of the  $E_p$  and  $E_{rp}$  values reported in the literature for these alloys must be viewed with suspicion if they are not accompanied by reports of visual observations. In these types of alloys, one can observe hysteresis in the cyclic polarization curve without observing pitting/crevice corrosion (Sridhar et al., 1993). Pitting in alloy C-4 has been reported in brines containing  $MgCl_2$  (approximately 8 M  $Cl^-$  and pH of 4.9) at 90 °C under gamma radiation (Smialos et al., 1990). Hence, the effect of high concentrations of Cl and long-term tests on the performance of these alloys needs further examination. Other Ni-Cr-Mo alloys, such as alloys C-276, 59, and C-22, while lacking the high-temperature stability of alloy C-4, generally exhibit superior resistance to localized corrosion (Heubner and Köhler, 1992; Hodge and Ahluwalia, 1993).

### 3.5 STRESS CORROSION CRACKING MODELS

Stress corrosion cracking (SCC) is one of the most insidious forms of failure that may affect the long-term performance of metallic containers for HLW disposal. The term defines a phenomenon by which many ductile metals and alloys fail as a result of the initiation and propagation of cracks under the concurrent action of a tensile stress (applied or residual) and a specific corrosive environment that could be gaseous or liquid. The environments of most interest in the case of HLW disposal are aqueous and can be condensed layers of moisture or bulk solutions, both containing salts of aggressive anions. These aqueous environments arise from modifications of groundwater through reactions with minerals, coupled to evaporation and concentration processes, as discussed in Section 2.

There are two reasons that make SCC a particularly insidious phenomenon. One is that SCC occurs in metals and alloys that are extremely resistant to uniform corrosion in the same environment as a result of the formation of a film on the metal surface that slows down the corrosion rate by several orders of magnitude. These films may be passivating layers, tarnish films, or dealloyed layers. The second reason is that SCC can occur at stresses that may be far lower than those required for macroscopic yielding, often as a result of residual stresses. Cracks, which are initiated by the specific action of the corrodent at the metal solution/interface, can propagate through the material with velocities ranging from  $10^{-12}$  to  $10^{-3}$  m/s, depending primarily upon the alloy/environment system as well as on other environmental, mechanical, and metallurgical variables. These velocities are significantly lower than the rates of crack propagation associated with brittle failure of high-strength, low-toughness materials, which are of the order of several thousand meters per second, corresponding to the propagation rate of elastic waves in solid materials. However, when stress corrosion cracks have propagated to a depth at which the remaining load-bearing section of the material reaches its fracture stress in air, the material fails by

normal overload fracture, usually by microvoid coalescence in the case of ductile alloys, such as those selected as candidate container materials.

The following sections review the literature of mechanistic and empirical models for SCC. Only certain aspects of the empirical models (crack growth rate equations) are used in PA codes such as SCCEX.

### 3.5.1 Mechanistic Models

Many attempts have been made to develop a mechanistic understanding of stress corrosion cracking in terms of a theory based on scientifically accepted principles followed by appropriate mathematical modeling. From experimental observation of the effect of the main variables affecting the initiation and propagation of cracks, such as the nature and concentration of the chemical species present in the environment, either as active cracking promoters ( $C_A$ ) (e.g.,  $\text{Cl}^-$  for austenitic stainless steels or  $\text{CO}_3^{2-}/\text{HCO}_3^-$  for ferritic steels) or as cracking inhibitors ( $C_{\text{Inh}}$ ) (e.g.,  $\text{CrO}_4^{2-}$  for the caustic cracking of stainless steels), potential ( $E$ ), temperature ( $T$ ), pH, stress ( $\sigma$ ), etc., it is expected that quantitative measurements of the failure time,  $t_f$ , can be expressed by simple functional relationships between these variables.

$$t_f = f(C_A, C_{\text{Inh}}, T, E, \text{pH}, \sigma, \dots) \quad (3-42)$$

Similar expressions, in turn, can be developed for predicting failure times when those variables are modified through mathematical modeling from basic electrochemical and mechanical principles. As noted in the previous section, SCC proceeds through an initiation stage followed by a propagation step, and, therefore

$$t_f = t_i + t_p \quad (3-43)$$

where

- $t_f$  = total failure time
- $t_i$  = initiation or induction time
- $t_p$  = crack propagation time

In many cases of SCC failures, there is indirect evidence that the initiation stage is the dominant term in the lifetime of the component. However, the initiation stage has not been extensively investigated, mainly due to the experimental difficulties involved in the detection of a crack nucleus prior to noticeable growth. Therefore, very limited attempts have been made to model crack initiation. Using a linear-elastic fracture mechanics (LEFM) approach, Hagn (1984) has evaluated a critical threshold crack size,  $a_{\text{th}}$ , for both SCC and corrosion fatigue (CF) as

$$a_{th} = \frac{1}{\pi} \left( \frac{\Delta K_{th}}{Y \Delta \sigma_0} \right)^2 \quad (3-44)$$

where

- $\Delta K_{th}$  = threshold stress intensity factor range  
 $\Delta \sigma_0$  = alternating tensile stress  
 $Y$  = a geometrical coefficient given by the following expression

$$Y = \left[ \frac{1.13 - 0.07 \left( \frac{a}{c} \right)}{1 + 1.47 \left( \frac{a}{c} \right)^{1.64}} \right]^{1/2} \quad (3-45)$$

where  $a$  and  $c$  are the major and minor axes of the half elliptical pit which is assumed to be the crack nucleus. However, the limitations of Eq. (3-44) for predicting the size of the crack at the beginning of the propagation step should be noted, because it is based on an experimental determination of  $\Delta K_{th}$  under cyclic stresses. This value generally depends on the stress intensity ratio,  $R = K_{min}/K_{max}$ , the mean stress intensity factor,  $K_m$ , and the frequency. Additional assumptions are required to derive an induction or initiation time for SCC from  $a_{th}$ . Hagn (1984) also noted that Eq. (3-44) is applicable to values of  $a_{th}$  greater than 80  $\mu\text{m}$ . This threshold crack size, however, is almost an order of magnitude larger than the minimum depth usually reported in the literature for actively growing cracks. Finally, no consideration of the electrochemical factors involved in the initiation of SCC are included in Eq. (3-44).

Another attempt of modeling the initiation stage of SCC has been done by Ranjan and Buck (1985) and Buck and Ranjan (1986). Using a crack-tip opening displacement (CTOD) model based on LEFM concepts, combined with simple electrochemical considerations by assuming the anodic process under activation control, they expressed the initiation or incubation time as

$$t_i = \left[ \frac{K_{Isc}^2}{\pi B (\sigma^2 - \sigma_0^2)} \right] \exp \left( \frac{-\beta F (E - E_{corr})}{RT} \right) \quad (3-46)$$

where

- $K_{Isc}$  = threshold stress intensity for stress corrosion cracking  
 $\sigma$  = applied stress  
 $\sigma_0$  = stress necessary to close the crack nucleus

- $\beta$  = transfer coefficient for the anodic reaction  
 $E$  = potential  
 $E_{\text{corr}}$  = corrosion potential,

whereas  $B$  is given by the following equation

$$B = \left( \frac{M}{zF\rho} \right) i_{\text{corr}} \quad (3-47)$$

where

- $M$  = atomic weight  
 $\rho$  = density  
 $i_{\text{corr}}$  = corrosion current density

This model was applied to the SCC of  $\alpha$ -brass in oxygenated ammoniacal solutions. Although the model provides an analytical relationship between  $t_i$  and both mechanical ( $\sigma$ ) and electrochemical ( $E$ ) variables, significant discrepancies were reported (Buck and Ranjan, 1986) between the values of  $B$  and  $\beta$  calculated from the current density versus potential plots and those calculated from the measured values of  $t_i$  using Eqs. (3-46) and (3-47).

Contrary to what happens regarding crack initiation, many mechanistic models have been proposed for crack propagation. As noted many times (Parkins, 1972, 1990; Jones and Ricker, 1992), it is unlikely that a single mechanism for SCC exists. The proposed mechanisms can be classified into two basic groups. One includes those in which crack growth is stimulated by the anodic process, whereas the second one is determined by cathodic processes. In the second group, hydrogen embrittlement is the predominant failure process for a wide range of relatively high-strength materials, including steels, aluminum-base, and titanium-base alloys. No further consideration will be given to hydrogen embrittlement because it is not considered to be an important failure process for the current candidate container materials (Sridhar et al., 1991), with the possible exception of titanium alloys and some specific steels.

This review of SCC models will be confined to anodic-induced processes. From models that were essentially qualitative in nature, some mathematical models have evolved in recent years. Three of these models will be analyzed in some detail. There are the slip-dissolution model, the film-induced cleavage model, and the surface mobility model.

### 3.5.1.1 Slip-Dissolution Model

The slip-dissolution model is probably one of the most quoted models to explain the SCC behavior of ductile alloys. In its most simple expression, which has been termed an electrochemical knife by Beck (1974), the crack velocity is simply derived from Faraday's laws according to an expression similar to Eq. (3-47), in which

$$v = \left( \frac{M}{zF\rho} \right) i_{\text{tip}} \quad (3-48)$$

where  $i_{\text{tip}}$  indicates the current density at the crack tip which is assumed to be a bare metal. The high aspect ratio of the crack is preserved because the crack walls are assumed to be almost instantaneously repassivated by the formation of a protective film, and the role of stress is merely to open the crack sides allowing the solution to reach the crack tip. Many methods for measuring transient currents on bare surfaces, including scratching, scraping, fast straining, fast fracture, etc., have been used to determine  $i_{\text{tip}}$  (Beck, 1977; Newman, 1987). However, controversy exists about the simulation of the environment present at the crack tip, the correction for the potential drops expected in fast transients, and the approximations involved in the calculation of the reactive area (Turnbull and Psaila-Dombrowski, 1992). Nevertheless, for a variety of alloy/environment systems, a proportional relationship between crack velocity and current density, according to Eq. (3-48), was presented by Lacombe and Parkins (1977), summarizing experimental results obtained by several authors.

Many attempts were made to modify Eq. (3-48), by considering separately the electrochemical and mechanical factors operating at the crack tip that may determine the value of the crack velocity. Whereas continuous anodic dissolution is implicitly assumed in Eq. (3-48), several authors (Forty and Humble, 1963; McEvily and Bond, 1965; Vermilyea, 1972, 1977; Scully, 1975; Newman, 1981) and more recently Ford (1979, 1983) suggested a discontinuous anodic process caused by film formation, rupture of the film by slip-step emergence, dissolution at slip-steps, and reformation of the film in a repetitive sequence. It is beyond the scope of this review to provide a detailed analysis of the differences between these models. Expressions recently presented by Ford and Andresen (1992) illustrate more clearly the role of the electrochemical and mechanical factors. They assumed that at the crack tip, the metal dissolution rate on a bare surface,  $i_{\text{tip}}$ , can be maintained for a time,  $\tau_0$ , before the current density decreases because of the film formation. Such current density decay, corresponding to a repassivation process under potentiostatic conditions is expressed as

$$i_t = i_{\text{tip}} \left( \frac{t}{\tau_0} \right)^{-n} \quad (3-49)$$

If the metal is stressed, the strain in the growing film will increase with time. Once the strain exceeds the fracture strain of the film,  $\epsilon_f$ , the dissolution/repassivation process described by Eq. (3-49) will repeat itself. The periodicity of this event,  $\tau_f$ , is defined by the ratio  $\epsilon_f/\dot{\epsilon}_{\text{tip}}$ , where  $\dot{\epsilon}_{\text{tip}}$  is the strain rate at the crack tip. Therefore, if  $\tau_f > \tau_0$ ,

$$v = \left( \frac{M}{zF\rho} \right) \frac{Q_f}{\tau_f} \quad (3-50)$$

where  $Q_f$  is the oxidation charge density passed between film rupture events. By integrating the differential expression corresponding to Eq. (3-49),  $Q_f$  can be obtained and replaced in Eq. (3-50) resulting in

$$v = \left( \frac{M}{zF\rho} \right) \left( \frac{i_{\text{tip}}}{1-n} \right) \left( \frac{\tau_0 \dot{\epsilon}_{\text{tip}}}{\epsilon_f} \right)^n \quad (3-51)$$

which will be reduced to Eq. (3-48) for the limiting case in which  $\tau_f$  is less than  $\tau_o$ , meaning that the crack tip is maintained as a bare surface.

Although  $i_{\text{tip}}$ ,  $\tau_o$ ,  $n$ , and  $\epsilon_f$  can be independently determined by electrochemical techniques using straining electrodes, in several cases the predicted values do not correspond with the experimentally measured crack growth rates. Therefore, Eq. (3-51) has been reformulated (Ford, 1983; Ford and Andresen, 1992) as

$$v = A(\dot{\epsilon}_{\text{tip}})^n \quad (3-52)$$

where  $A$  and  $n$  are constants depending on certain properties of the material and the environment at the crack tip. On the basis of extensive experimental work conducted on sensitized type 304 stainless steel in oxygenated water systems typical of the environments prevailing in BWRs, Ford and Andresen (1987) suggested the following expressions for  $A$  and  $n$ .

$$A(\text{cm/s}) = 7.8 \times 10^{-3} n^{3.6} \quad (3-53)$$

$$n = \left\{ \frac{e^{f(\kappa)}}{[e^{f(\kappa)} + e^{g(E_{\text{corr}})}]} \right\}^{h(\text{EPR})} \quad (3-54)$$

where  $f$ ,  $g$ , and  $h$  are parameters depending on the following variables:

- $E_{\text{corr}}$  = corrosion potential at the mouth of the crack in  $\text{mV}_{\text{SHE}}$
- $\kappa$  = room temperature conductivity of the bulk solution in  $\mu\text{S/cm}$
- EPR = degree of grain boundary sensitization as measured by the Electrochemical Potentiokinetic Reactivation (EPR) technique in  $\text{C/cm}^2$

However, one of the main limitations in the application of Eq. (3-52) is that  $\dot{\epsilon}_{\text{tip}}$  cannot be directly measured. Several authors (Lidbury, 1984; Parkins, 1987; Ford, 1990) have developed or

reviewed empirical or theoretical formulations of  $\dot{\epsilon}_{\text{tip}}$  in terms of macroscopic stress or strain variables. Considerable uncertainty exists regarding the validity of these formulations. The empirical relationships used by Ford (1990) for type 304 stainless steel are

$$\dot{\epsilon}_{\text{tip}}(s^{-1}) = 4.1 \times 10^{-4} K^4 \quad (3-55)$$

for constant loading where the stress intensity factor,  $K$ , is expressed in  $\text{MPa} \cdot \text{m}^{1/2}$ , and

$$\dot{\epsilon}_{\text{tip}}(s^{-1}) = 10 \dot{\epsilon}_{\text{app}} \quad (3-56)$$

for constant applied strain rate,  $\dot{\epsilon}_{\text{app}}$  in  $s^{-1}$ . However, in a previous publication, Ford and Andresen (1987) suggested, instead of 10, values of 1 and 5 as coefficients in Eq. (3-56) for transgranular stress corrosion cracking (TGSCC) and intergranular stress corrosion cracking (IGSCC), respectively.

Although the slip-dissolution model was initially applied to the TGSCC of austenitic stainless steel in hot, acidic chloride solutions, it is increasingly viewed as primarily associated with IGSCC. However, Ford and Andresen (1988) have extended the application of the model to a variety of alloy systems including pressure vessel steels (ASTM A533/A508), austenitic stainless steels (304/316L), and nickel-base alloys (600/182) in high-temperature ( $\sim 300$  °C) aqueous environments. For this purpose, empirical correlations have been developed on the basis of a combination of laboratory experimental results and field observations. Using a simplified expression of the stress intensity factor,  $K$ , given by

$$K = Y\sigma(\pi a)^{1/2} \quad (3-57)$$

where  $Y$  is a geometric factor and  $a$  is the crack size, the dependence of  $a$  with time is given by

$$a(t) = \left\{ a_i^{(1-2n)} + 7.8 \times 10^{-3} n^{3.6} (1-2n) [C\pi^2(Y\sigma)^4]^{n_i} t \right\}^{(1-2n)} \quad (3-58)$$

From the analysis of the extensive work conducted by Ford and Andresen (1988), it can be concluded that most of the final expressions for calculating crack growth rates and crack depth require the input of field data in order to adjust several of the parameters included in the model. This is particularly true in the case of the parameter  $n$  as expressed in Eq. (3-54).

Macdonald and Urquidi-Macdonald (1991, 1992b) have questioned the electrochemical basis of the slip-dissolution model as formulated by Ford and Andresen, by stating that the model does not account for the conservation of charge. By coupling the cathodic reactions occurring on the passive surfaces with the metal dissolution at the crack tip, they claimed that the control of the crack growth rate may switch from the crack internal environment to the external environment, depending upon the increase

in the resistivity of the solution and the kinetics of the reduction reaction. However, apart from this, Macdonald and Urquidi-Macdonald (1991, 1992b) also assumed that slip-dissolution is the basic mechanism for crack advance.

In the Macdonald and Urquidi-Macdonald model (1992b), the crack growth rate is calculated also with an expression based on Faraday laws

$$v = \left( \frac{M}{zF\rho} \right) \left( \frac{I_0}{2A_{\text{crack}}} \right) \quad (3-59)$$

where

$A_{\text{crack}}$  = area of the crack mouth  
 $I_0$  = current averaged over the slip dissolution/repassivation cycle as given by:

$$I_0 = 2i_0^0 A_{\text{tip}} \left( \frac{\tau_0}{\tau_f} \right)^{1/2} \exp \left[ - \frac{(\phi_s^L - \phi_s^0)}{b_a} \right] \quad (3-60)$$

where

$i_0^0$  = standard exchange current density for the dissolution reaction  
 $A_{\text{tip}}$  = crack tip area  
 $\tau_0$  = a constant derived from the repassivation transient  
 $\tau_f$  = time of cyclical fracture of the passive film at the crack tip  
 $\phi_s^L$  = potential in solution adjacent to the crack tip  
 $\phi_s^0$  = standard potential  
 $b_a$  = Tafel's constant

The same problems, described above for the definition of the crack tip strain rate, are also encountered in this model. In particular, no threshold value for  $K$  below which SCC does not occur can be defined and crack growth rate seems to increase almost continuously with  $K$  up to relatively high  $K$  values ( $\sim 50 \text{ MPa} \cdot \text{m}^{1/2}$ ) without exhibiting the characteristic plateau.

### 3.5.1.2 Film-Induced Cleavage Model

The high crack growth rates observed in certain cases of TGSCC, which cannot be explained in terms of bare-surface current densities, as well as the apparent discontinuous crack advance events, which are observed as distinctive crack arrest markings on fracture surfaces, are difficult to reconcile with a model based on slip dissolution. This led to the postulation of environmentally induced cleavage as an alternative crack advance mechanism (Pugh, 1985).

Sieradzki and Newman (1985) have developed the concept that cracks initiated in brittle, thin films formed by anodic reaction at the crack tip could propagate by cleavage over distances of a few microns in the ductile substrate. It is beyond the scope of this review to provide a detailed discussion of the electrochemical and mechanical factors involved in the development of this model. Turnbull (1993) has critically reviewed most of the experimental evidences for and against this model. Atomistic calculations and computer simulations have been presented in support of the model. However, few attempts have been made towards establishing quantitative expressions for crack propagation rate.

Parkins (1990) considered the time interval between the repetitive events of film growth and crack jumping (essentially, the time to grow the film since the jump is assumed to be almost instantaneous) as that required to reach the critical strain for crack initiation in the film,  $\epsilon_c$ . This time is strain-rate dependent and equal to  $\epsilon_c/\dot{\epsilon}$ . Therefore, the crack velocity is defined as

$$v = (l + j) \frac{\dot{\epsilon}}{\epsilon_c} \quad (3-61)$$

where

- $l$  = film thickness
- $j$  = jump distance in the cleavage event.

In contrast, Cole et al. (1988) expressed the crack growth rate as

$$v = \left( \frac{M}{zF\rho} \right) \frac{Q_\tau}{\tau} \quad (3-62)$$

where  $Q_\tau$  is the anodic charge density passed during the interval,  $\tau$ , between successive cleavage events (calculated from the spacing between arrest markings divided by the crack velocity). The main limitation of both Eqs. (3-61) and 3-(62) is that they cannot be used for predicting crack growth rates because parameters only accessible through fractographic or metallographic observation of failed specimens are required. It is difficult to conceive that the size of the cleavage step is not influenced by modifications in mechanical conditions, such as stress or strain.

### 3.5.1.3 Surface Mobility Model

The surface mobility model developed by Galvele (1987) is not specific to anodic cracking processes but is claimed to be applicable to SCC, liquid metal embrittlement, and hydrogen embrittlement of nonhydride-forming metals. The crack propagation results from the capture of vacancies by the stressed lattice at the tip of the crack, as depicted schematically in Figure 3-10. The rate-controlling step is the rate of movement of excess ad-atoms and, in turn, vacancies along the surface of the crack; the role of the environment is to change the surface self-diffusivity of the metal or alloy. The mechanism predicts that SCC should be observed on tensile-stressed metals at temperatures below  $0.5 T_m$  ( $T_m$  is the melting point of the metal in °K), under environmental conditions that promote high surface mobility. In

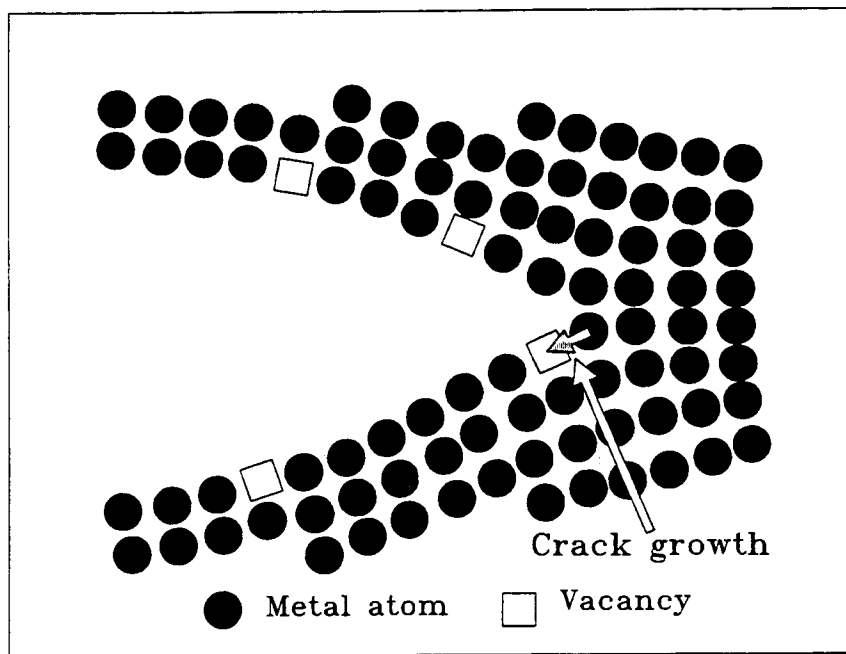


**Figure 3-10.** The capture of a vacancy by the stressed tip of the crack is the elementary step for crack propagation in the surface-mobility SCC mechanism (Galvele, 1987)

particular, this can occur when a contaminant that enhances surface diffusion is chemi-adsorbed on a metal surface. According to Galvele (1992), the environment also assures a free supply of vacancies to the metal surface by selective dissolution of the alloy or by film growth processes dominated by movement of cation vacancies.

In this model, crack velocity for SCC based on anodic processes is given by

$$v = \left( \frac{D_s}{L} \right) \left[ \exp \left( \frac{\sigma a^3}{kT} \right) - 1 \right] \quad (3-63)$$

where

- $D_s$  = coefficient of surface self-diffusion
- $L$  = diffusion path of the ad-atoms or vacancies (typically  $10^{-8}$  m)
- $\sigma$  = maximum stress at the crack tip
- $a$  = atomic distance
- $k$  = Boltzmann constant
- $T$  = absolute temperature

With the exception of a few specific cases, the value of  $D_s$  is not readily measurable but can be estimated by using the following expression

$$D_s = 7.4 \times 10^{-2} \exp\left(\frac{-30T_m}{RT}\right) + 1.4 \times 10^{-6} \exp\left(\frac{-13T_m}{RT}\right) \quad (3-64)$$

where  $T_m$  is the melting point of the surface-adsorbed impurity.

This model is highly controversial, and Turnbull (1993) has raised objections to the use of thermodynamically based equations for the calculations of vacancy concentrations, as well as some of the approximations used by Galvele. Nevertheless, the model has been applied by Galvele and coworkers to the prediction of crack velocity for several alloy/environment systems with reasonable success (Bianchi and Galvele, 1987; Duffó et al., 1988; Duffó and Galvele, 1988, 1990; Galvele, 1990).

### 3.5.2 Empirical Models

The application of LFM concepts to the study of SCC, pioneered by Brown (1968), led to the possibility of establishing quantitative, although empirical, relationships between crack velocity and the effective tensile stress acting at the crack tip, as defined by the stress intensity factor,  $K$ . In most of the cases of SCC, the relative movement of the two crack surfaces corresponds to the opening mode (Mode I). The associated  $K$  is then defined as  $K_I$ , according to expressions similar to Eq. (3-57), in which  $Y$  is a parameter that depends on the specimen and crack geometries, and the loading configuration. For the simple case of a through-thickness crack of length,  $2a$ , located in the center of a large plate subject to a uniform tensile stress,  $Y$  becomes equal to 1.

An important observation is that many alloy/environment systems exhibit the dependence between the logarithm of crack velocity and  $K_I$  depicted schematically in Figure 3-11. This simplified curve consists of three parts: (i) a stress-dependent part at low stress intensities (Stage I), (ii) a nearly stress-independent part at intermediate stress intensities (Stage II), and (iii) another stress-dependent part at high stress intensities (Stage III). This last stage precedes the fast failure that occurs at the critical stress intensity,  $K_{Ic}$ , at which crack velocities are in the range of a thousand meters per second. This parameter, commonly termed fracture toughness, is an intrinsic material property. On the other hand, subcritical crack growth occurs in Stage I at a rate that usually increases exponentially with  $K_I$ , above the threshold stress intensity for SCC,  $K_{Isc}$ , which is an environmental-dependent parameter. Hence, the crack velocity in Stage I can be expressed as

$$v_I = v_o \exp [c_1(K_I - K_{Isc})] \quad (3-65)$$

where  $v_o$  is the minimum crack velocity that can be measured, corresponding to  $K_{Isc}$ . Values of  $c_1$  ranging from 0.5 to 3  $[\text{MPa} \cdot \text{m}^{1/2}]^{-1}$  were reported by Speidel (1971) for aluminum alloys in aqueous solutions. For steels and stainless steel,  $c_1$  values are probably close to the upper limit of that range.

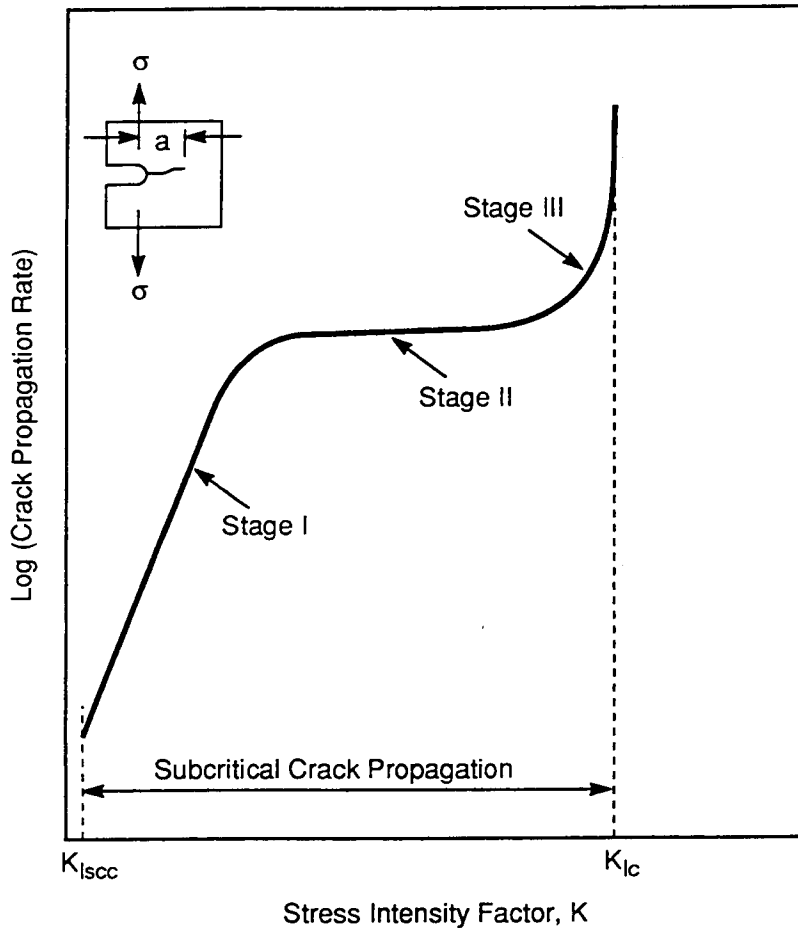


Figure 3-11. Schematic of crack velocity versus stress intensity showing the three stages of crack propagation

Although the dependence represented in Eq. (3-65) is frequently reported in the literature, it is difficult to obtain accurate velocity data in Stage I. Speidel (1971) indicated that the dependence could also be expressed in terms of  $K_I^2$ . Recently, Jones and Simonen (1993) have suggested that a Paris-type relationship, as observed under cyclic loading, could also be applicable to Stage I growth. Therefore, crack velocity can be expressed as

$$v = c_1^* K_I^m \quad (3-66)$$

where  $c_1^* = v_o / K_{Isc}^m$ , using the same symbols as in Eq. (3-65). Jones and Simonen (1993) reviewed data obtained by many authors for a variety of materials and experimental conditions and found that  $m$  varied from values as low as 2 for brass to up to 24 for stainless steels, with most of the values for steels above 5.

As noted earlier,  $K_{Isc}$  is defined as a threshold or minimum stress intensity below which an existing crack will not grow. Despite the strong dependence of crack velocity on  $K_I$ , Speidel (1971) suggested the adoption of a conventional limit of  $10^{-9}$  or  $10^{-10}$  m/s for the definition of  $K_{Isc}$ . In more

recent work, in which SCC of a variety of Fe-Cr-Ni alloys was investigated in concentrated chloride solutions at boiling temperatures, a minimum velocity,  $v_o$ , of  $3 \times 10^{-11}$  m/s was adopted for the determination of  $K_{Isc}$  (Speidel, 1981). However,  $v_o$  can be reduced to values lower than  $3 \times 10^{-13}$  m/s by using improved techniques for measuring crack extension, which are able to detect a crack advance of about 10  $\mu\text{m}$ , and extended testing times (at least 1 yr). On the basis of these concepts, the validity of  $K_{Isc}$  as a bounding parameter for performance should be assessed through an appropriate combination of experimental and modeling work. As previously reviewed (Cragolino and Sridhar, 1992),  $K_{Isc}$  values ranging from approximately 8 to 20  $\text{MPa} \cdot \text{m}^{1/2}$  have been observed for types 304, 304L, 316, and other similar austenitic stainless steels in chloride-containing solutions at temperatures ranging from 80 to 130 °C. As expected, the values in the lower end of that range are observed with both increasing temperatures and chloride concentration.

The crack velocities measured in Stage II range from  $10^{-11}$  to  $10^{-6}$  m/s for a variety of alloys in aqueous solutions, depending also on metallurgical and environmental conditions. Speidel (1971) has suggested empirical expressions for the crack growth rate in Stage II that require further evaluation. The effect of the concentration of aggressive anions can be expressed as

$$v_{II} = v_{II}(0) + c_2 C_A^n \quad (3-67)$$

where

- $v_{II}$  = plateau crack growth rate
- $v_{II}(0)$  = crack growth rate at very low concentrations of the aggressive anion
- $c_2$  = a constant
- $C_A$  = concentration of the aggressive anion
- $n$  = exponent ranging from 0.33 to 1

The effect of temperature on crack growth rate is given by

$$v_{II} = v_{II}^o \exp(-E_a/RT) \quad (3-68)$$

where  $E_a$  is the apparent activation energy. For certain alloy/environment systems (e.g., aluminum-base and titanium-base alloys in chloride-containing solutions), it has been observed (Speidel, 1971; Blackburn et al., 1972) that  $E_a$  ranges from 18 to 23 kJ/mole. This range of values seems to indicate that the crack growth in Stage II is mainly controlled by diffusional processes in aqueous solutions for which typical values for several electrolytes (e.g., NaCl, CaCl<sub>2</sub>, HCl, and NaOH) are approximately 10 to 12 kJ/mole (Oelkers and Helgeson, 1988). However, Russell and Tromans (1979) found for cold-worked-type 316 stainless steel in hot, concentrated MgCl<sub>2</sub> solutions,  $E_a$  values ranging from  $63 \pm 2$  to  $67 \pm 2$  kJ/mole with increasing cold work from 25 to 50 percent. These higher values suggest that the rate-controlling steps in stainless steels seem to be dominated by chemisorption or kinetic effects, including electrochemical dissolution and repassivation.

The crack growth rate in Stage I is also dependent on temperature. Speidel (1971) has suggested the following expression for the crack velocity.

$$v_I = v_I^o \exp [(-E_a + c_3 K_I)/RT] \quad (3-69)$$

where  $c_3$  is a constant. The value of  $E_a$  in Stage I for aluminum alloys in chloride solutions is approximately 110 kJ/mole (Speidel, 1971), which is almost an order of magnitude larger than that for Stage II. A similar value was reported for a titanium alloy in 10 M HCl solution (Feeny and Blackburn, 1971).

Once a crack is initiated, propagation, even at velocities in the lowest end of the range measured in Stage II, will lead to failure of containers within the containment period, unless a crack arrest mechanism can be postulated. It can be concluded that any attempt to use an empirical model for predicting the occurrence of SCC as a failure process should rest on predicting the environmental and electrochemical conditions that would avoid crack initiation or would lead to crack arrest.

It is now clearly recognized that  $K_{Isc}$ , as well as crack growth rates in Stage I and II, are affected by the electrode potential. Eremias and Marichev (1980) demonstrated that an increase in potential of about 350 mV, with respect to the open-circuit potential, decreases  $K_{Isc}$  from 12 to 2 MPa · m<sup>1/2</sup> for an austenitic stainless steel in boiling, concentrated LiCl solution. A cathodic overpotential of 50 mV, on the other hand, increased  $K_{Isc}$  up to 16 MPa · m<sup>1/2</sup>. Concurrently, this effect of potential resulted in a pronounced increase of  $v_I$  (more than an order of magnitude) under an anodic overpotential of 50 mV. Russell and Tromans (1979) did not observe an effect of potential on the plateau crack velocity (Stage II) for type 316 stainless steel in hot, concentrated MgCl<sub>2</sub> solution. However, the application of a potential 50 mV lower than the corrosion potential lead to crack arrest.

The existence of a critical potential for TGSCC in austenitic stainless steel in hot, concentrated chloride solutions, below which crack initiation does not occur, has been reported since the 1960s as reviewed by Cragnolino and Sridhar (1992). The importance of Russell and Tromans' (1979) observation is that a propagating crack can be arrested if the potential is lowered below the critical potential. As discussed in detail previously (Cragnolino and Sridhar, 1992), the existence of a critical potential for SCC makes justifiable an approach based on the use of this potential as a bounding parameter for evaluating the SCC resistance of a container material. In addition, Tsujikawa and coworkers (Tsujikawa et al., 1985; Tamaki et al., 1990) have shown that the critical potential for SCC coincides with the repassivation potential for crevice corrosion for type 316 stainless steel in hot, dilute chloride solutions. On the basis of this concept, the approach for predicting the environmental conditions for the occurrence of SCC becomes similar to that described for localized corrosion. In the case of SCC, another constraint to be considered arises from the use of  $K_{Isc}$  as an additional bounding parameter. As discussed previously, this parameter is, in turn, influenced by the environmental conditions and the potential.

### 3.5.3 Future Directions

As part of the program for the design of the waste package, the DOE has reviewed some of the models for SCC proposed in the literature (Farmer et al., 1991). Although it is emphasized that initiation

models are more important than propagation models for the time scales of interest to repository design, most of the models examined refer to propagation. For the case of stainless steels, or in general the group of Fe-Ni-Cr-Mo alloys that includes alloy 825, it is concluded that the main limitation to apply the Ford and Andresen model is the lack of appropriate correlations between crack growth rate and crack tip strain rate under conditions relevant to the repository environment. Some of the concepts regarding crack initiation are similar to those described in Section 3.5.1. No consideration is given, however, to the concept of a critical potential.

In the development of EBS-PAC, on the contrary, the main emphasis will be placed on the evaluation of the critical potential concept. The concept will be extended to other container materials through suitable combination of modeling and experimental work. A quantitative evaluation of data available for stainless steel and some nickel-base alloys will be made initially to establish empirical correlations between critical potentials and environmental variables, such as chloride concentration and temperature. This will be followed by evaluation of the coincidence between critical potential for SCC and repassivation potential for crevice corrosion. If this approach is valid, further analysis and modeling of the conditions for SCC will be simplified. A particular effort will be made for improving the modeling of the environmental conditions related to crack initiation in terms of the repassivation for crevice corrosion. This could result in a mechanistic understanding of the critical potential for SCC.

## **3.6 MECHANICAL FAILURE MODELS**

In assessing the integrity of a waste package over its performance period, the potential mechanical failure models have to be considered. These models, in general, represent the structural response of the waste package to the various mechanical loads that may be imposed in the repository system. The loads are the direct result of tectonic movements, seismic activity, and local collapse of rock material due to thermal and hydrologic conditions of the repository. The resulting action of these loads provides both static and dynamic forces on the waste package. The FY93 focus of the mechanical failure models has been to develop simple analytical expressions to represent the types of failure. To develop these analytical expressions, simplifying assumptions for describing the geometry of the waste package and the loading conditions have been made. Three mechanical failure models were developed. These are buckling, yielding, and fracture. These models are included in the SCCEX code.

### **3.6.1 Buckling Failure Model**

Buckling is a phenomenon where the stability of the geometry of a structural component is compromised by the action of external compressive components of loads. Analytical expressions for buckling are only available for a limited number of simple geometries and loading conditions (Roark and Young, 1975). Typically, expressions for buckling of beams, plates, and simple shells with point or pressure loadings are available. The loads are assumed to be statically applied. To develop a buckling analysis for a specific waste package design with multiple loading conditions, a numerical analysis scheme (e.g., a finite element analysis) may be required.

For the current application, a case of a single waste package represented by a metal cylinder, placed vertically in an oversized borehole, is considered. Under the normal condition of the cylindrical waste package in an unsaturated environment, it is not subject to any lithostatic or hydrostatic loads. The major load assumed here is that caused by a seismic load. It is assumed that the consequence of this seismic load is for the waste package to strike the wall of the borehole and the shell to buckle locally.

To represent this model, a buckling expression from Roark and Young (1975) for a pressure-loaded, curved shell was modified and used. The pressure load was calculated as a pseudostatic load resulting from the dynamic action of the waste package against the borehole wall. Assuming a complete transfer of energy as a result of the impact, the total force acting on the shell is equal to the product of the mass of the waste package, including its contents, and the acceleration from the ground seismic motion. To obtain the pressure loading on the cylinder, the total force was distributed over the area of contact between the cylinder and the borehole wall. For the current analysis it is assumed that 10 percent of the circumference of the cylindrical waste package is in contact during impact with the borehole wall.

A key parameter in determining the buckling stability of a cylindrical shell is its thickness. In a waste package, a reduction of the thickness of the waste package with time can be anticipated due to corrosion processes. An expression for a buckling model, described below, has been developed in terms of the time-dependent thickness.

$$R_B = \frac{99Et_R^3\pi}{60r^2(1 - \nu^2)} \quad (3-70)$$

where

- $R_B$  = residual buckling load capacity for the waste package
- $E$  = Young's Modulus
- $\nu$  = Poisson's ratio
- $r$  = inner radius of the waste package
- $t_R$  = remaining thickness at any given time after accounting for corrosion of the waste package

It should be noted that the constants in the expression are based on the initial thickness-to-radius ratio of the waste package being 1:10. Also, as a conservative measure, a factor of safety of 2 or 3 can be included in the expression to evaluate the sensitivity of a waste package failure to a buckling-type failure. The wall thickness assumed here is that of the container and the wasteforms, and associated support systems are assumed not to contribute to buckling resistance. This is a conservative assumption.

### 3.6.2 Yield Failure Model

Structural components are designed using strength of materials principles. In the designs, the stress and deformation levels in the structural materials are limited and maintained within elastic regions for most loading conditions. However, there may be cases when loads are exceeded and will result in failures caused by excessive deformations. In the case of the waste package, it is anticipated that the wall thickness will reduce with time due to corrosion. As a result, the waste packages may experience yield failures due to wall thinning. The model used here is simple. It is assumed that the material will fail once the yield strength of the material is reached. The residual yield capacity ( $R_y$ ) of the waste package is given by

$$R_Y = R_{YO} \frac{A_R}{A} = R_{YO} \frac{t_R}{t} \quad (3-71)$$

where

- $R_{YO}$  = yield strength of the material
- $A$  = initial cross section area of the solid part of the cylinder
- $A_R$  = remaining cross section area of the solid part of the cylinder
- $t$  = initial thickness of the cylinder
- $t_R$  = remaining thickness of the cylinder after corrosion

A factor of safety can also be incorporated into the expression above to permit conservative calculations. Typically, a factor of 2 or 3 is used in analyses.

### 3.6.3 Fracture Failure Model

In the fabrication of structural components, there are several defects introduced in the various materials. These defects may be a result of the processing of the material, welding techniques, or poor workmanship. The detection of these defects also poses problems, such as the limitations of the detection capability of an inspection technique. However, the materials have an inherent capacity to resist further cracking. This capacity is defined as the fracture toughness ( $K_{Ic}$ ) of the material. In a fracture model, a relationship is developed among the applied stress, the flaw or defect size, and the toughness of the material (Rolfe and Barsom, 1977). Here, a flaw tip stress concentration is described in terms of a square root relationship for a defined flaw size and a net section applied stress. The model for fracture of a surface flaw in a cylinder, oriented along the circumferential direction and placed on the outer surface is expressed as

$$R_F = \frac{K_{Ic}}{Y(\pi a)^{0.5}} \quad (3-72)$$

where

- $Y$  = geometry factor
- $a$  = crack depth or the depth of a corroded pit
- $K_{Ic}$  = fracture toughness
- $R_F$  = permissible external stress

A factor of safety (2 or 3) may be used for this failure model to account for added conservatism.

## 4 RELEASE RATE MODELS

As stated in 10 CFR 60.113(a)(1)(ii)(B), the annual release rate of any radionuclide from the EBS shall not exceed  $10^{-5}$  part of its total inventory in the repository calculated at the end of 1,000 yrs. The same stipulation applies to the total release rate. The most commonly used approach to the calculation of this release rate has been in terms of various transport models with either fixed boundary conditions at the wasteform surfaces in terms of a solubility limit concentration or by coupling the transport equations to a reaction rate at the wasteform surfaces (McGrail and Engel, 1993; Pigford et al., 1990).

### 4.1 CURRENT CONCEPTUAL MODELS

Because of the difficulty in simulating every process and barrier or potential barrier to radionuclide release, PA models typically take credit for only a subset of the controlling barriers and processes. The resulting PA code and analysis attempts to bound the actual performance of the system. An important corollary to the bounding approach is that omission of phenomena from the calculations results in a pessimistic (conservative) estimation of performance. This section discusses several different alternatives for estimation of radionuclide release rate. The alternatives are not mutually exclusive and could be used in combination.

#### 4.1.1 Mass Transport Analysis

The most commonly used approach to release rate is mass transport-limited release (McGrail and Engel, 1993; Pigford et al., 1990; Johnson and LeNeveu, 1993). Dissolution/alteration of the wasteform (spent fuel or glass) results in release of radionuclides into the water in the waste package. The concentration of low solubility radionuclides within the failed waste container is controlled by the solubility of secondary mineral phases or solid solutions. The concentration of high solubility radionuclides within the failed waste container is controlled by a combination of wasteform alteration or dissolution rate, mass transport rate away from the waste package, and radioactive decay. This inner boundary condition is used in mass transport due to advection and diffusion of the radionuclides from the failed waste container into the surrounding rock. The mass transport step depends heavily upon the transport properties of the failed container materials (pit size, etc.), packing material, and surrounding host rock as well as hydraulic gradients and water availability in the repository horizon.

The mass transport approach is appealing because: (i) solubility is a thermodynamic property and (ii) mass transport, particularly diffusion dominated mass transport, is well understood and can be predicted or bounded with high confidence. The reliance on thermodynamics and transport properties has made the mass transport approach the standard for release rate calculations.

Key areas of uncertainty in mass transport analysis of release rates are estimates of wasteform dissolution/alteration rate, radionuclide solubility, and transport properties. Current applications of transport analysis assume that the waste package environment is homogeneous, allowing one solubility limit (for each element) and one spent fuel alteration rate to apply to the entire waste package. In water-saturated, anaerobic repositories, this key assumption is likely to be defensible. However, as discussed in previous sections, the chemical environment inside a failed waste container at Yucca Mountain is likely to be highly variable in time and space. If the chemical environment is as heterogeneous as predicted and sensitive to difficult-to-predict properties of the system, then the mass transport analysis, assuming single solubility limit as currently implemented, needs re-examination.

In theory, mass transport analysis can be modified to consider spatial and temporal variability of chemical environments inside the failed waste container. The inside of the container can be described as a series of finite difference or finite element nodes, each with a different value for temperature, salinity, solubility, wastefrom alteration rate, and radionuclide concentration. This requires detailed data on (i) speciation and solubility of radionuclides and major ions over a range of solutions from dilute to saturated brines of variable composition and, (ii) detailed prediction of temperature and transport properties inside the failed (and presumably partially collapsed) container. Obtaining the data for a detailed release model including spatial and temporal heterogeneity in an aqueous chemical environment is a difficult task. For example, data on radionuclide speciation at 25 °C in dilute solutions is incomplete. Extension to high temperatures and a wide range of brines is a large effort. Accurate prediction of transport properties inside the failed waste container requires detailed understanding of system geometry during corrosion and buckling of the container, cladding, and spent fuel. Geometry is likely to change in a complex manner during failure. Detailed and accurate predictions during this period are difficult.

#### **4.1.2 Elevation of Temperature Above Boiling Point of Water**

In this concept, older fuel and high thermal loading are used to "dry out" the repository in the vicinity of the waste packages for an extended period of time, generally longer than 10,000 yrs. The period where the waste package temperature is above the local boiling point of water is assumed to be free of corrosion and leaching.

The high thermal loading strategy is appealing because temperatures can be predicted with high accuracy. There are several disadvantages. Higher temperatures may be associated with greater physical and chemical changes to the mountain. These changes may be difficult to predict. The assumption that temperatures in excess of the boiling point will prevent water from contacting corrosion is problematic since, in concentrated solutions, free water can be present well in excess of the boiling point of water.

#### **4.1.3 Gradient Reversal**

In addition to drying out the system, thermal loading causes a circulatory system to be set up whereby liquid water flows towards the waste package and water vapor diffuses and flows away from the waste container. This flow system effectively traps water-transported radionuclides inside the waste package. Reversal of the flow system requires that the supply of liquid water (e.g., from fracture flow) reaching the waste package exceed the rate of evaporation. The time period for reversal of flow can be calculated based upon temperature history and postulated flow (drip) rates. This method of containment is less sensitive to the influence of concentrated solutions in maintaining waste on the waste container.

#### **4.1.4 Container Corrosion**

Radionuclide release cannot occur until the waste container has corroded. If a container lifetime in excess of 10,000 yrs can be demonstrated, then most quantitative performance measures for the repository can be met with a single barrier. The 10,000+ yr container is an appealing concept, especially in combination with other barriers, thereby leading to a redundant demonstration of containment.

## 4.1.5 Release Controlling Phenomena Currently Included in SCCEX Code

All of the above models have been implemented in EBS-PAC with varying degrees of detail. This provides an opportunity to compare the predictions, data requirements, and assumptions of each of the alternative methods for PA relative to the release rate standard. Evaluation of multiple methods for demonstration of release rate limits provides a broad foundation for regulatory analysis. The release models have been implemented in the SCCEX computer code, and the preliminary results from the simulations will be presented in a subsequent report.

## 4.2 RADIONUCLIDE RELEASE SIMULATIONS

In order to illustrate the effects of various factors on radionuclide release rate, a set of simulations were performed. The simulations represent a parametric study of the effects of thermal loading on the waste package environment and release rate. The model for the evolution of the environment is the same as that used to model the environment change on the container surface as described in Sections 2.4 and 2.5. The assumptions for five different scenarios are given in Table 4-1. The simulations assume a single waste package in the middle of a set of

Table 4-1. Parameters used for calculating temperature profile of an assemblage of waste packages

Scenario	Initial Thermal Load	Spent Fuel per Waste Package
a	$5.93 \times 10^8 \text{ J/yr/m}^2$	2.3 t
b	$4.44 \times 10^8 \text{ J/yr/m}^2$	2.3 t
c	$3.33 \times 10^8 \text{ J/yr/m}^2$	2.3 t
d	$3.33 \times 10^8 \text{ J/yr/m}^2$	1 t
e	$3.33 \times 10^8 \text{ J/yr/m}^2$	4 t

equally spaced waste packages. The repository is assumed to be square. Waste package spacing is calculated as the spacing to give the input overall thermal loading based upon total waste loading, waste loading per waste package, and initial age at emplacement. A total of 70,000 metric tons of 60 percent PWR fuel at 33,000 MWd/MTU burnup and 40 percent BWR fuel at 27,500 MWd/MTU burnup, with an initial age at emplacement of 15 yrs, is assumed (DOE, 1993c). Data that are identical for all simulations are given in Table 4-2. Total simulation time is 15,000 yrs after emplacement. The water is assumed to drip directly on the waste container at a constant rate without consideration of hydrothermal umbrella effects. Corrosion of the waste container was assumed to occur rapidly by localized corrosion at the time of initial container wetting. This assumption was made to eliminate variable container lifetime as a factor between the simulations. A separate study is being performed to examine container lifetime issues and will be reported subsequently. Figure 4-1 gives the predicted temperature of the waste container surface over a 15,000-yr period. The temperature simulation is based upon conduction-only heat transfer. Heat transfer near the waste container should be conduction dominated after the first several hundred years which are omitted from the plot. Depending upon overall thermal loading, temperature eventually drops below the local boiling point of pure water ( $\sim 97^\circ\text{C}$ ). Figure 4-2 gives predicted wetting of the container.

The simplified evaporation model assumes that water evaporation rate is proportional to the amount of the container surface that is wetted. Overall evaporation rates are thus a result of wetted area,

salinity, temperature, and temperature gradients in the rock near the container. In these simulations, wetting of the container surface occurs at about the same time for scenarios "a" and "b" in Table 4-1, independent of total thermal loading. Wetting of the container is delayed for scenario "a" representing the hotter repository. If it is assumed that first generation of leachate occurs after the entire surface is wetted, time of first liquid leachate generation extends out to 5,000+ yrs and is proportional to thermal loading. Predicted salinity of the water is given in Figure 4-3. In each scenario, the lowering of vapor pressure by high solute concentration is predicted to have a critical role in maintaining water on the container surface. Although not illustrated in a figure, dripping water is also anticipated to deposit a scale layer on the container surface. Figures 4-4 through 4-6 give the same sequence of illustrations for scenarios "c," "d,"

and "e." This set of scenarios examines the importance of the amount of waste put in a waste package at a constant overall thermal loading. The amount of waste per container is at least as important as overall thermal loading strategy in influencing waste package performance. The importance of individual waste container loading is related to the temperature gradients near the waste container. Higher temperature gradients near the container enhance evaporation of any water reaching the container thereby slowing the first time of leachate generation. Comparison of Figures 4-2 and 4-5 shows that the time of leachate generation for scenario "e" is slightly longer than for scenario "a," despite the much lower container temperature for scenario "e." In this example, the temperature gradients near the waste container were controlled by changing the amount of waste per container. In a repository design, the temperature gradients near the waste container could also be controlled by use of packing material with lower thermal conductivity than the rock. For example, crushed rock packing would create higher temperature gradients as well as form a capillary barrier to liquid flow near the container.

A point of interest is the long lag time between initial wetting of the container surface and time of first leachate generation. It is assumed in these calculations that complete wetting of the container surface is needed before the water runs off from the container surface. Prior to full wetting of the container, evaporation rates exceed drip rates, precluding formation of liquid leachate. As long as potential evaporation exceeds water supply, liquid advection of water is always towards the waste package. The flow towards the waste package means that even diffusional releases would have to be

**Table 4-2. Common parameters used for simulating radionuclide release rate from waste packages**

Parameter	Assumed Value
Container length	4 m
Container radius	0.33 m
Packing thickness	0.01 m
Rock thermal conductivity	$5.68 \times 10^7$ J/yr/m/K
Packing thermal conductivity	$3.79 \times 10^7$ J/yr/m/K
Density $\times$ heat capacity for rock	$2.4 \times 10^6$ J/m <sup>3</sup> /K
Tortuosity for rock and packing	0.12
Porosity of rock and packing	0.10
Water drip rate	$10^{-3}$ m <sup>3</sup> /yr
Salt content of dripping water	0.0613 kg/m <sup>3</sup>
Scale content of dripping water	0.2121 kg/m <sup>3</sup>
Wasteform alteration rate	$10^{-3}$ /yr
Radioactive decay constant	$10^{-6}$ /yr

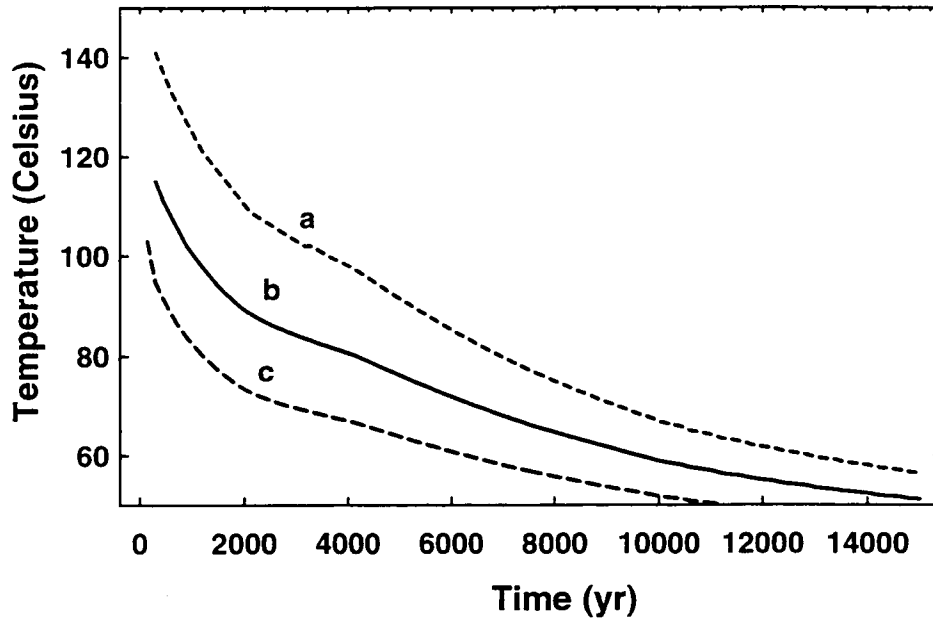


Figure 4-1. Waste container temperature based on heat conduction for scenarios a, b, and c

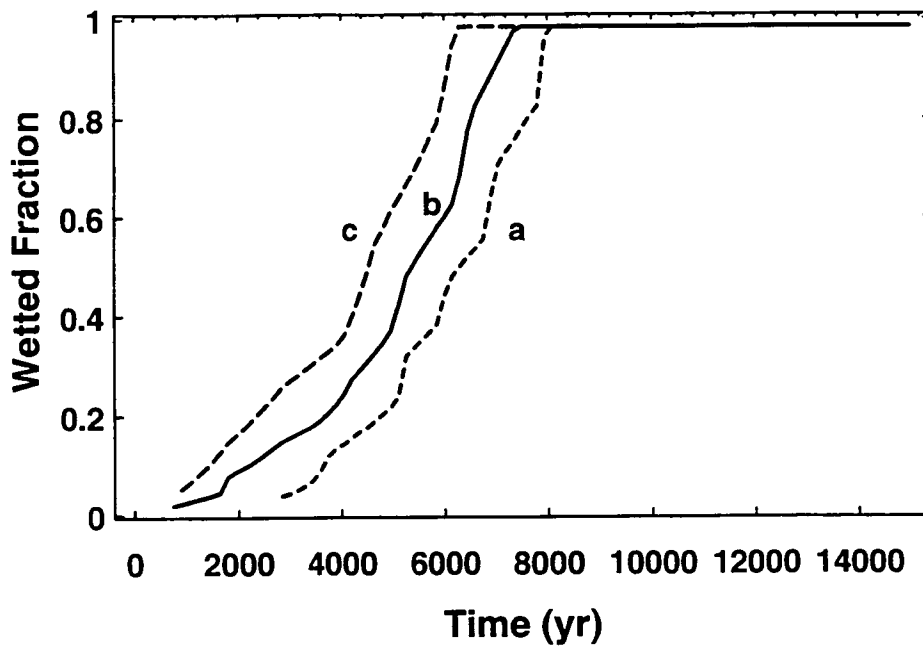


Figure 4-2. Water coverage of container surface for scenarios a, b, and c

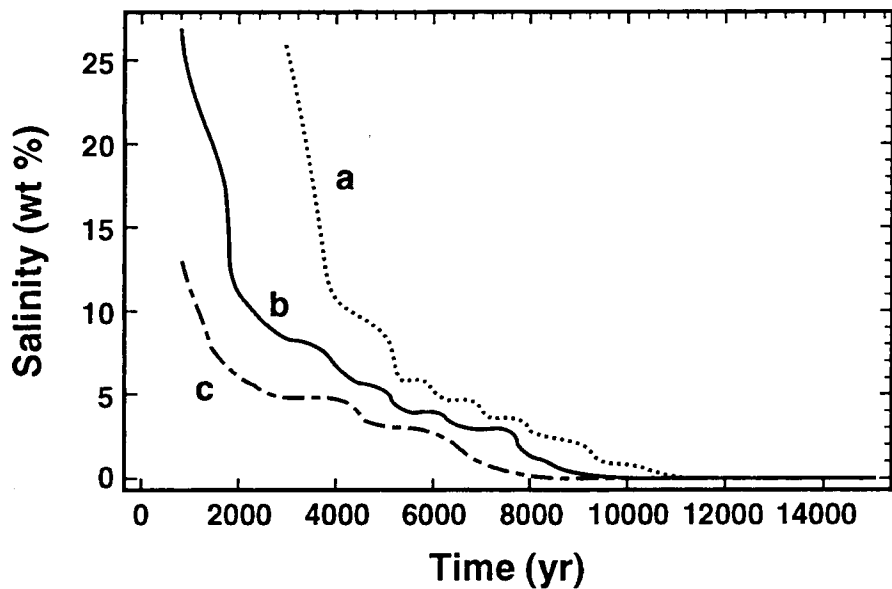


Figure 4-3. Predicted salinity for scenarios a, b, and c

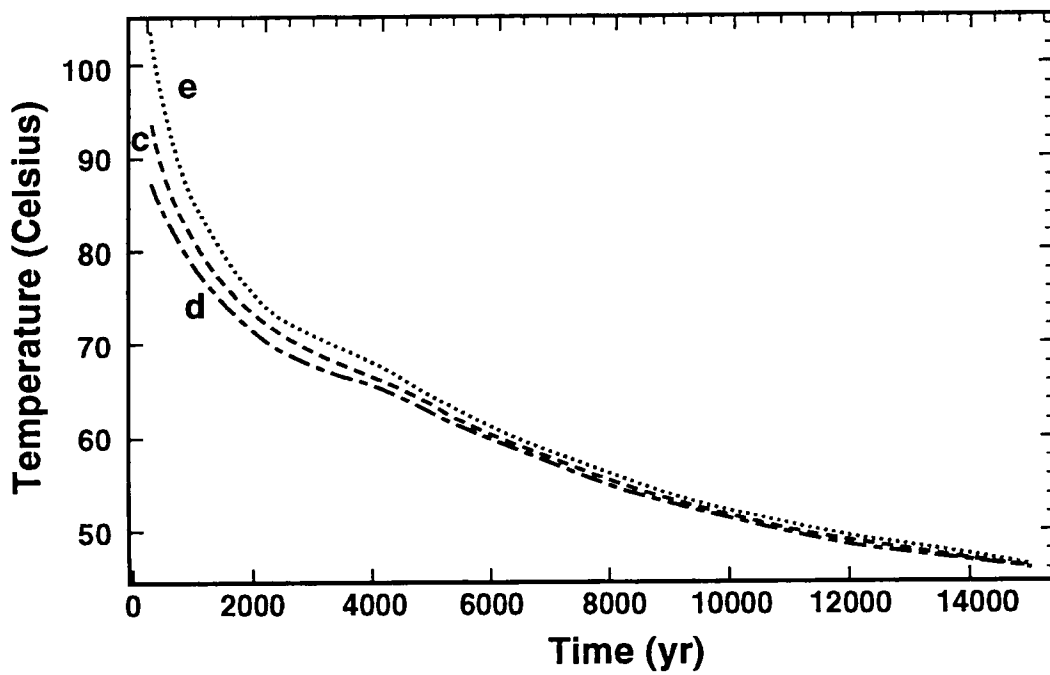


Figure 4-4. Waste container temperature based on heat conduction for scenarios c, d, and e

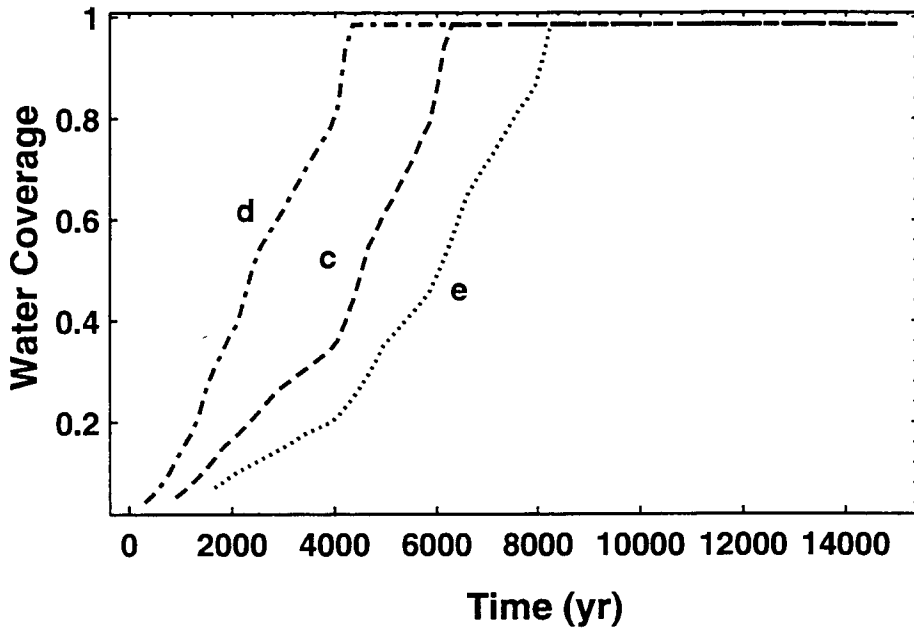


Figure 4-5. Water coverage of container surface for scenarios c, d, and e

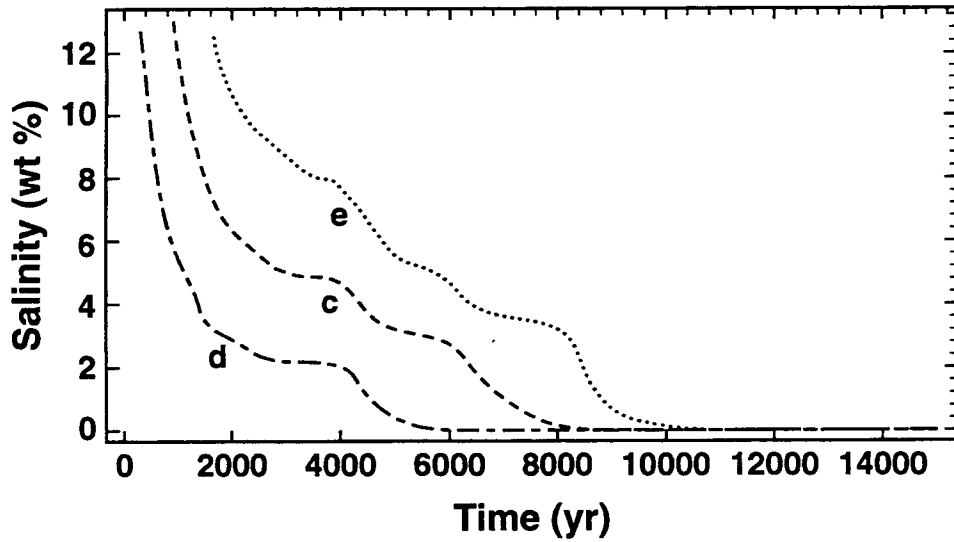


Figure 4-6. Predicted salinity for scenarios c, d, and e

sufficiently rapid to overcome the flow rates. In this concept, release of dissolved radionuclides is unlikely as long as potential evaporation rates are high. However, this time lag can be considerably shorter if the whole container surface does not need to be wetted before leachate runs off.

The long lag period between wetting and liquid leachate generation has other implications for the nature of releases. Because of salinity-related lowering of vapor pressure, small amounts of liquid water, probably present as films, may be available for container corrosion and wastefrom alteration several thousand years prior to the time of leachate generation. In the case of highly soluble radionuclides (e.g., iodine, technetium), the situation promotes pulse release of radionuclides when dripping water reaches an individual container. While it is unlikely that the pulse releases will migrate far from the waste package, this could cause difficulties with meeting release rate requirements.

### 4.3 ELECTROCHEMICAL DISSOLUTION MODEL

For highly soluble radionuclides, the dissolution rate of the spent fuel is important in predicting release rates. The electrical impedance of the  $UO_2$  matrix is likely to play as important a role as its structural and microchemical characteristics in determining its dissolution behavior for many reasons.

- The electrical conductivity of non-stoichiometric  $UO_{2+x}$  changes by several orders of magnitude as one proceeds from stoichiometric  $UO_2$  to higher oxidation states (Sunder and Shoesmith, 1991, and associated references). For example, Aronson et al. (1961) have shown that the specific electrical conductivity of  $UO_{2+x}$  can be obtained from

$$\sigma = \frac{3.8 \times 10^6}{T} (2x)(1-2x) e^{\left(\frac{-0.3}{kT}\right)} \quad (4-1)$$

where,  $0.001 \leq x \leq 0.23$ ,  $\sigma$  is the specific conductivity in  $(\text{ohm} \cdot \text{cm})^{-1}$ , and  $k$  is the Boltzmann's constant in  $\text{eV}/^\circ\text{K}$ . It is interesting to note that the electrical conductivity of  $UO_{2.028}$  calculated from the above equation at  $100^\circ\text{C}$  (assuming that the equation is valid at this temperature) is  $0.05 (\text{ohm} \cdot \text{cm})^{-1}$ , in comparison to that of an insulator such as Alumina which is  $10^{-11} (\text{ohm} \cdot \text{cm})^{-1}$  and that of a conductor such as copper which is  $6 \times 10^5 (\text{ohm} \cdot \text{cm})^{-1}$ . From approximately  $UO_{2.06}$  to  $UO_{2.25}$ , the material is a p-type semiconductor and the oxygen occupies interstitial positions in a fluorite structure. At higher oxidation states up to about  $UO_{2.66}$ , the compound is an n-type semiconductor with the crystal structure changing from fluorite to a layered type structure (Shoesmith and Sunder, 1991). Beyond this point, the solubility of the oxide increases and various uranyl compounds are formed depending upon the environmental conditions. Because of the semiconductive nature of the oxide (the band gap of 2 eV is higher than that of Si but lower than  $\text{Cu}_2\text{O}$ ), the dissolution of  $UO_{2+x}$  is photosensitive.

- In spent fuel as well as in many naturally occurring uraninite, the oxide is doped with many impurities of different valences resulting in either excess electrons (n-type semiconductor) or holes (p-type semiconductor) (Hocking et al., 1992). Thus, a comparison of the corrosion behavior of natural uraninite with pure  $UO_2$  and spent fuel under oxidizing conditions must recognize these fundamental changes in the electronic properties of these materials as well

as in the structural and microchemical properties. Secondly, at various ranges of oxidation states, a p-type conductor, which may be expected to support dissolution, and an n-type semiconductor, which may be expected to support reduction reactions, can coexist, causing selective dissolution of certain phases.

- Reactor irradiation can result in the doping of  $\text{UO}_{2+x}$  lattice with impurities and secondary phases of metallic character (Manaktala, 1993). In such cases, not only can these phases corrode preferentially, but they can also act as cathodic sites for oxygen reduction-promoting anodic dissolution of  $\text{UO}_{2+x}$ .

Sunder and Shoesmith (1991) have demonstrated that beyond about  $-100 \text{ mV}_{\text{SCE}}$ , electrochemical processes dominate the dissolution behavior. While the exact cutoff potential is debatable (for example, test duration may play a role), the relevance of their finding to an oxidizing environment such as Yucca Mountain is obvious. For the case of  $\text{UO}_{2+x}$ , Shoesmith and Sunder (1991) estimate that chemical dissolution plays a dominant role only for very low values of  $x$  (i.e., stoichiometric  $\text{UO}_2$ ) and under highly reducing conditions ( $\text{O}_2$  concentration less than  $10^{-5} \text{ M}$  and no radiolysis products). Unfortunately, it is difficult to estimate the true chemical dissolution rate of  $\text{UO}_2$  because of the difficulty of maintaining stoichiometry upon exposure. Based on analogy with the dissolution rate of  $\text{NiO}$ , they estimate the chemical dissolution rate of  $\text{UO}_2$  under reducing conditions to be approximately  $2 \times 10^{-10} \text{ gm/d/cm}^2$ . Bruno et al. (1991) calculated a leaching rate of  $\text{UO}_{2+x}$  under reducing conditions (hydrogen purge, Pd catalyst) of  $4.4 \times 10^{-9} \text{ gm/d/cm}^2$  using a flow-through system.

For the case of a purely chemical dissolution, the source term can be estimated based on some form of coupled surface reaction-transport model. For example, Murphy et al. (Murphy, Oelkers, and Lichtner, 1989) describe a one-component, unidimensional system under steady state by:

$$-\phi D_i \rho \left( \frac{\partial m_i}{\partial x} \right)_r = k_r \beta_r \left( 1 - \frac{m_{i,s} \gamma_i}{K_r} \right) \quad (4-2)$$

where

- $m_i$  = molality of the  $i^{\text{th}}$  aqueous species
- $D_i$  = effective diffusion coefficient
- $\phi$  = porosity
- $x$  = distance
- $k_r$  = reaction rate constant for the dissolution of the  $i^{\text{th}}$  species
- $K_r$  = equilibrium constant for the reversible analog of the dissolution reaction
- $m_{i,s}$  = molality of the aqueous species at the surface
- $\beta$  = ratio of surface area for the dissolution reaction to the surface area perpendicular to the concentration gradient
- $\gamma_i$  = activity coefficient of the  $i^{\text{th}}$  species
- $\rho$  = density of the solution

This is essentially equivalent to that proposed by Garisto and Garisto (1988) where the equilibrium constant  $K_r$  is given in terms of solubility. The reaction rate constant is an empirically derived parameter that is dependent upon temperature for a given dissolution reaction. Unfortunately, an explicit dependance upon redox condition cannot be used in this formulation since the chemical dissolution reactions will vary with redox potential and empirically derived rate constants must be used for each dissolution reaction. More importantly, the reaction rate of an electroactive surface depends on the corrosion potential rather than on the environmental  $E_h$ . As demonstrated by Needes et al. (1975), the leaching rate of  $UO_{2+x}$  in a carbonate-bicarbonate solution was greater in the presence of various redox couples in the order  $Fe(CN)_6^{3-} > H_2O_2 > Cu(NH_3)_4^{2+} > O_2$ , whereas the environmental  $E_h$  was found to vary in the order  $H_2O_2 > O_2 > Fe(CN)_6^{3-} > Cu(NH_3)_4^{2+}$ . This is because the kinetics of these redox couples on the surface must also be considered and are notoriously slow for oxygen.

An equivalent form for the reaction flux on the right-hand side of Eq. (4-2) exists for an electrochemical reaction (Vetter, 1967) in the form of the Butler-Volmer equation, with the rate constant for dissolution depending explicitly upon both temperature and potential. This is shown in Eq. (4-3) for the dissolution of  $UO_{2+x}$ . Equation (4-3) can be written for all the species taking part in redox reactions such as oxygen and hydrogen peroxide.

$$i = k_+ \cdot c_r \cdot e^{\left(\frac{\alpha z F}{RT} E\right)} - k_- \cdot c_o \cdot e^{-\left(\frac{(1-\alpha) z F}{RT} E\right)} \quad (4-3)$$

where

- $i$  = total current density equivalent to the net flux that is the sum of dissolution flux ( $UO_2 \rightarrow UO_2^{2+}$ ) and reduction flux ( $UO_2^{2+} \rightarrow UO_2$ )
- $k_+, k_-$  = reaction rate constants for these processes which are characteristics of the surface condition and electronic states of the spent fuel
- $c_r, c_o$  = concentrations of the reduced species and the oxidized species, respectively
- $E$  = potential
- $F$  = Faraday constant
- $z$  = charge
- $\alpha$  = transfer coefficient which is in the range of 0.3 to 0.5

As discussed in Section 3, under natural conditions, the net current must be equal to zero and the solution of this set of equations similar to Eq. (4-3) will yield the corrosion potential,  $E_{corr}$ . This then can be used to obtain the surface dissolution rate from Eq. (4-3). Of course, the electrochemical approach does not eliminate the necessity to use empirically generated parameters (such as  $k_+$  and  $k_-$ ), but does create an explicit and logical method to include the effect of changing redox potentials. More importantly, the electrochemical approach considers the *corrosion potential* to be more relevant to spent fuel dissolution than environmental  $E_h$ , which is arrived at by equilibrium considerations of dissolved species. This is exemplified by the results of Needes et al. (1975) who showed that the dissolution rate of  $UO_2$  in a variety of oxidizing environments compared very well with the corrosion rates under applied potentials when the potentials corresponded to the corrosion potentials in these environments.

An electrochemical approach to experimental studies also reveals some of the causes of the observed discrepancies in literature on spent fuel dissolution. For example, Gray et al. (1992) studied the dissolution rate of spent fuel (after removing grain boundary radionuclides) in a flow loop as a function of total carbonate concentration and found that the dependence was weak. Others (Grambow, 1989) have found a greater dependence of dissolution rate with total carbonate concentration. It is possible that these seeming differences may be related to the different regimes of corrosion potential under which these tests were conducted (none of these tests measured corrosion potential). This is illustrated in Figure 4-7 (Sunder and Shoesmith, 1991). In this figure, it can be seen that under reducing conditions (low-corrosion potentials), the dissolution rate did not depend on several environmental species, whereas at higher potentials when  $U^{VI}$  species were released, the complexing effects of carbonate result in a higher dissolution rate.

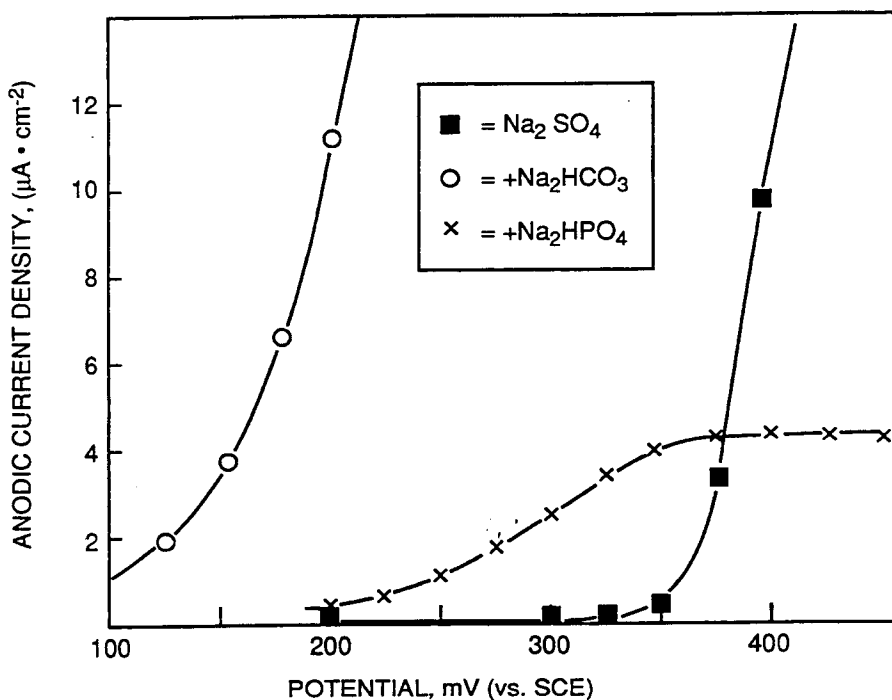
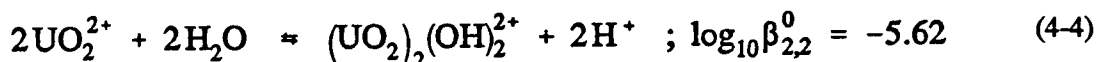
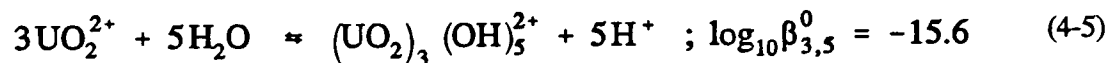


Figure 4-7. Steady state dissolution current of unirradiated  $UO_2$  as a function of applied potential and environmental species. ■ — 0.1 M  $Na_2SO_4$ ; ○ — 0.1 M  $NaHCO_3$ ; X — 0.1 M  $Na_2HPO_4$  (Sunder and Shoesmith, 1991)

Another factor that is important in the study of the dissolution rate of spent fuel is the local chemistry. Just as in the case of metal containers, the chemistry of local areas such as fuel-cladding interface and cracks in the fuel can be significantly different from that of the bulk. In analogy with metals where the hydrolysis of  $Cr^{3+}$  results in acidic conditions inside crevices, the hydrolysis of  $UO_2^{2+}$  to dihydroxide can occur by the following reaction (Wanner and Forest, 1992):



More recently, Choppin and Mathur (1991) indicated that the hydrolysis of U(VI) to polymeric hydroxide complexes becomes dominant at concentrations of U(VI) exceeding about  $10^{-6}$  M. They suggested that the hydrolysis equilibrium:



In the latter case, for a  $\text{UO}_2^{2+}$  concentration of  $10^{-6}$  M in a crevice, the crevice pH can decrease to roughly 5. The solubility of corrosion products such as Schoepite ( $\text{UO}_3 \cdot 2\text{H}_2\text{O}$ ) increases with a decrease in pH. Hence, further investigation of the crevice corrosion of  $\text{UO}_2$  is warranted.

## 5 SUMMARY

The performance assessment of the EBS is examined using the corrosion-based design approach suggested by Staehle (1991). Of greatest importance to the EBS performance is the phase and composition of the environment contacting the container. Unfortunately, for the partially saturated environment at the Yucca Mountain repository horizon, the definition of the environment is attended by great uncertainties both in regard to conceptual models and parameters. In Section 2, a conceptual model is presented that assumes that liquid water drips onto the waste packages through fractures in the rock from a condensed layer near the top of the repository. Based on this assumption, the evolution of the chemistry of the environment due to evaporation is calculated. It is suggested that the evaporation would result in the precipitation of insoluble silicates (boiler scale) on the waste packages, but also would result in the concentration of the aqueous environment on top of this scale. This concentration of the aqueous environment, in its saturated condition, can lead to a vapor pressure depression and migration of water towards the container. This migration of water, in turn, can lead to retention of a highly saline water film on top of the boiler scale on the waste packages well above the nominal boiling point of water. This model is included in the current version of the SCCEX code. The uncertainties in this conceptual model include the range of chemistries of the incoming water drips, the rate of dripping, the rate of infiltration of meteoric water, the heterogeneities in the host rock and backfill, the orientation of waste packages, and the heterogeneities in the waste package thermal load. A more rigorous consideration of the chemical changes due to evaporation also needs to be included in the model.

The second step in the EBS performance assessment process is the definition of the waste package materials. Currently, there is a diversity of alternate conceptual designs ranging from single, thin-wall containers in vertical boreholes with air-gap to double-wall containers in horizontal drifts with backfill. It is argued that the approach used in the EBSPAC, SCCEX, and IPA programs can be adapted to a variety of designs with suitable modifications to the parameters considered. This adaptation can be done by creating a framework within which new failure modes can be included in a systematic manner as new designs are put forward. One such framework is the potential-pH diagram suggested by Staehle (1991). The framework considered in the EBSPAC program is the corrosion potential versus time diagram. This framework cannot evaluate purely mechanical failures, however, and other provisions, such as deformation and fracture mechanism maps, must be made for such failures (Ashby, 1992).

The calculation of corrosion potential of container materials under repository-relevant conditions is outlined in Section 3. A simple model assuming a steady-state molecular diffusion process coupled to a charge-transfer reaction at the surface of the waste package is used. Oxygen reduction and hydrogen ion reduction are considered to be the only cathodic processes coupled to a potential-independent anodic current. The effects of variation of various parameters related to the oxygen reduction kinetics are examined. This model is included in the current version of the SCCEX code. There is a dearth of kinetic data pertinent to not only oxygen-reduction, but also other redox processes related to radiolysis products. Hence, models such as the one described in Section 3 can serve to focus experimental investigations. The same approach can be used to calculate the corrosion potential of the inner container of a bimetallic structure. In this case, the galvanic effects due to the anodic polarization of the external corrosion-allowance type material must be included in the calculations. Such analyses of the effects of through-wall penetrations of various sizes on the outer container will be performed in future efforts of the EBSPAC program.

Localized corrosion is considered to be one of the most important failure modes of container materials. A detailed mechanistic model, TWITCH, for calculating the local environment in a crevice or a pit was developed. For the austenitic alloys, this model predicts a decrease in pH and an increase in chloride concentration, irrespective of the externally applied or corrosion potential. In reality, the crevice corrosion initiation depends on the external potential. Modifications to the model to predict this important relationship between crevice corrosion initiation and external potential have been suggested. The model was also exercised for copper and qualitatively predicts the corrosion products formed in pits on copper in the correct order. However, the assumptions made regarding the copper dissolution process must be examined further. Stochastic models of pitting were examined since these models are being adopted by the DOE for prediction of pitting probability of container materials. It is pointed out that the stochastic models assume a lower-bound critical potential and hence the dependence of critical potentials on environmental factors must be examined in greater detail. Empirical models of critical potentials were examined. Because of the current limitations of detailed mechanistic models, the dependence of the critical potentials on environmental factors has to be gleaned from experimental data. Data for alloy 825 and type 304L stainless steel were examined and included in the SCCEX code. Future areas of evaluation include the review of data pertinent to higher Ni-base alloys, such as alloy C-4, which are part of the alternate conceptual designs.

Models for SCC in which crack growth is stimulated by the anodic process were evaluated with a focus on the slip-dissolution model. While this model has enjoyed some success in predicting SCC behavior in many environments, these predictions have had a considerable element of experimental calibration. Uncertainties exist in these models in terms of accurate estimations of the crack-tip strain rate and bare-metal dissolution rate. Although many attempts have been made to calculate and measure these parameters, there is still a lack of consensus in the literature on the values of these parameters. From the point of view of long-term prediction, two alternative approaches can be used: (i) empirically developed crack growth rate relationships, one of which is included in the current version of the SCCEX code; and (ii) empirically developed critical potentials for SCC. Data regarding the former are reviewed briefly. However, since the minimum measurable crack growth rate is about  $10^{-11}$  m/sec (about a 40-yr life for a 0.5-in.-thick wall), it will be difficult to derive significant life once the crack growth process takes place. The critical potential concept is attractive because it can be used as a criterion to prevent crack growth. Further benefits can be derived if it can be shown to be related to the critical potentials for localized corrosion. However, there is little agreement regarding the existence of a critical potential for SCC and its relationship to other localized corrosion phenomena.

Models for purely mechanical failure were discussed briefly in Section 3. The buckling model makes the conservative assumption that the container is unreinforced by its internal contents and evaluates the thickness required to cause buckling given a set of external stresses. The time variation of thickness due to corrosion processes is considered. An alternative failure mechanism considered is the tensile fracture using the concepts of LEFM. The uncertainties in the utilization of LEFM concepts in predicting fracture failure include the validity of a single parameter such as K in characterizing the stress field around short cracks and the large plastic zone size arising in relatively ductile and high-toughness materials. These materials, such as alloy 825, preclude the use of plane-strain toughness values for container wall thicknesses of about 0.5 inch. For example, the fracture toughness of alloy 825 can be estimated to be at least  $110 \text{ MPa} \cdot \text{m}^{1/2}$  ( $100 \text{ Ksi} \cdot \text{in}^{1/2}$ ) based on data on similar single-phase Ni-base alloys such as alloy 625 (Walter and Chandler, 1973). For this toughness, if plane-strain conditions have to be valid, the thickness must be at least about 7 cm (2.8 in.). Nevertheless, these calculations, which are included in the current version of the SCCEX code, demonstrate the ability to combine corrosion models with mechanical failure models and to indicate the effect of initial defects present in the container.

A simple model for release rate of radionuclides from spent fuel based on the ingress and egress of water from the waste packages was presented. Without egress of water from the waste package boundaries, no transport of radionuclides can occur. However, the essential uncertainty in this calculation is the assumption that the waste packages have to be completely covered by a water film before egress of water from the waste packages to the surrounding rock medium can occur. The limitations of solubility-based transport models were discussed, followed by a review of the electrochemical dissolution model and its advantages and disadvantages. The prediction of spent-fuel dissolution rate, using the electrochemical model, involves the use of corrosion potential (a concept similar to that of the metallic containers) rather than environmental  $E_h$ , although the latter influences the former. As with the corrosion potential calculations of container metals, much uncertainty exists regarding the parameters governing the cathodic processes on spent fuel that dictates the corrosion potential. The local environment near the spent fuel, which can be influenced by the hydrolysis of U(VI) species, must be better understood as it can influence the solubility of U(VI) species resulting from oxidative dissolution.

## 6 REFERENCES

- Alkire, R.C., and S.E. Lott. 1989. The role of inclusions on initiation of crevice corrosion of stainless steel. II. Theoretical studies. *Journal of the Electrochemical Society* 136: 3256-3262.
- Ananthaswamy, J., and G. Atkinson. 1985. Thermodynamics of concentrated electrolyte mixtures. 5. A review of thermodynamic properties of aqueous calcium chloride in temperature range 273.15-373.15 °K. *Journal of Chemical and Engineering Data* 30: 120-128.
- Aronson, S., J.E. Rulli, and B.E. Schaner. 1961. Electrical properties on nonstoichiometric uranium dioxide. *Journal of Chemical Physics* 35: 1382-1388.
- Ashby, M.F. 1992. *Materials Selection in Mechanical Design*. Oxford, England: Pergamon Press.
- Beck, T.R. 1974. Reactions and kinetics of newly generated titanium surfaces and relevance to stress corrosion cracking. *Corrosion* 30: 408-414.
- Beck, T.R. 1977. Techniques for studying initial film formation on newly generated surfaces of passive metals. *Electrochemical Techniques for Corrosion*. R. Baboian, ed. Houston, TX: National Association of Corrosion Engineers: 27-34.
- Benton, H.A. 1993. Waste package development program. *DOE-NRC Technical Exchange on Substantially Complete Containment and Waste Package/Engineered Barrier System Design Concepts*. Washington, DC.
- Bianchi, G.L., and J.R. Galvele. 1987. Embrittlement of copper by the surface mobility mechanism. *Corrosion Science* 27: 631-635.
- Bird, R.B., W.E. Stewart, and E.N. Lightfoot. 1960. *Transport Phenomena*. New York, NY: John Wiley and Sons.
- Blackburn, M.J., W.H. Smyrl, and J.A. Feeney. 1972. Titanium alloys. *Stress-Corrosion Cracking in High Strength Steels and in Titanium and Aluminum Alloys*. B.F. Brown, ed. Washington, DC: Naval Research Laboratory: 245-363.
- Bockris, J.O'M., and M.D.N. Reddy. 1977. *Modern Electrochemistry*. New York, NY: Plenum Press.
- Brigham, R.J. 1974. Temperature as a crevice corrosion criterion. *Corrosion* 30: 396-399.
- Brown, B.F. 1968. The application of fracture mechanics to stress-corrosion cracking. *Metallurgical Reviews* 13: 171-183.
- Bruno, J., I. Casas, and I. Puigdomenech. 1991. The kinetics of dissolution of  $UO_2$  under reducing conditions and the influence of an oxidized surface layer ( $UO_{2+x}$ ): Application of a continuous flow-through reactor. *Geochimica et Cosmochimica Acta* 56: 647-658.

- Buck, O., and R. Ranjan. 1986. Evaluation of a crack-tip-opening-displacement model under stress-corrosion conditions. *Modeling Environmental Effects on Crack Growth Processes*. R.H. Jones and W.W. Gerberich, eds. Warrendale, PA: The Metallurgical Society: 209-223.
- Buscheck, T.A., and J.J. Nitao. 1992. The impact of thermal loading on repository performance at Yucca Mountain. *Third High-Level Radioactive Waste Management Conference*. La Grange Park, IL: American Nuclear Society: 1003-1017.
- Carslaw, H.S., and J.C. Jaeger. 1959. *Conduction of Heat in Solids*. Oxford: Oxford University Press.
- Choppin, G.R., and J.N. Mathur. 1991. Hydrolysis of Actinyl (VI) cations. *Radiochimica Acta* 52/53: 25-28.
- Cole, A.T., R.C. Newman, and K. Sieradzki. 1988. A comparison and evaluation of bare surface electrochemical techniques for the investigation of stress corrosion cracking in alpha brass. *Corrosion Science* 28: 109-118.
- Cragolino, G.A., and N. Sridhar. 1991. *A Review of Localized Corrosion of High-Level Nuclear Waste Container Materials—I*. CNWRA 91-004. San Antonio, TX: Center for Nuclear Waste Regulatory Analyses.
- Cragolino, G.A., and N. Sridhar. 1992. *A Review of Stress Corrosion Cracking of High-Level Nuclear Waste Container Materials—I*. CNWRA 92-021. San Antonio, TX: Center for Nuclear Waste Regulatory Analyses.
- Damjanovic, A. 1969. Mechanistic analysis of oxygen electrode reactions. *Modern Aspects of Electrochemistry*. J.O'M. Bockris and B.E. Conway, eds. New York, NY: Plenum Press. 5: 369-483.
- Doering, T.W. 1993. Robust waste package concept (multibarrier). *High Level Radioactive Waste Management*. La Grange Park, IL: American Nuclear Society: 1: 551-557.
- Duffó, G.S., and J.R. Galvele. 1988. SCC of silver alloys due to surface mobility. *Corrosion Science* 28: 207-210.
- Duffó, G.S., and J.R. Galvele. 1990. Surface mobility stress corrosion cracking mechanism in silver alloys. *Environment-Induced Cracking of Metals*. R. Gangloff and M.B. Ives, eds. Houston, TX: National Association of Corrosion Engineers: 261-264.
- Duffó, G.S., I.A. Maier, and J.R. Galvele. 1988. The influence of temperature on the susceptibility of type AISI 304 stainless steel to transgranular and intergranular stress corrosion cracking in LiCl solutions. *Corrosion Science* 28: 1003-1018.
- Dunn, D.S., N. Sridhar, G.A. Cragolino. 1993. The effect of surface conditions on the localized corrosion of a candidate high-level nuclear waste container material. *Twelfth International Corrosion Congress*. Houston, TX: National Association of Corrosion Engineers.

- Eremias, B., and V.V. Marichev. 1980. Electrochemical aspects of stress corrosion crack growth in austenitic stainless steel. *Corrosion Science* 20: 307-312.
- Farmer, J.C., G.E. Gdowski, R.D. McCright, and H.S. Ahluwalia. 1991. Corrosion models for performance assessment of high-level radioactive-waste containers. *Nuclear Engineering and Design* 129: 57-88.
- Feeney, J.A., and M.J. Blackburn. 1971. The status of stress corrosion cracking of titanium alloys in aqueous solutions. *Theory of Stress Corrosion Cracking in Alloys*. J.C. Scully, ed. Brussels, Belgium: North American Treaty Organization: 355-398.
- Ford, F.P. 1979. Relationship between mechanisms of environmental cracking and design criteria. *Proceedings of the Third International Conference on Mechanical Behavior of Materials*. K. Miller and R. Smith, eds. Oxford, U.K.: Pergamon Press: 1: 431-440.
- Ford, F.P. 1983. Stress corrosion cracking of iron-base alloys in aqueous environments. *Treatise on Materials Science and Technology. Vol. 25. Embrittlement of Engineering Alloys*. C.L. Briant and S.K. Banerji, eds. New York, NY: Academic Press: 235-274.
- Ford, F.P. 1990. The crack-tip system and its relevance to the prediction of cracking in aqueous environments. *Environment-Induced Cracking of Metals*. R.P. Gangloff and M.B. Ives, eds. Houston, TX: National Association of Corrosion Engineers: 139-165.
- Ford, F.P., and P.L. Andresen. 1987. The theoretical prediction of the effect of system variables on the cracking of stainless steel and its use in design. *CORROSION/87*. Paper No. 83. Houston, TX: National Association of Corrosion Engineers.
- Ford, F.P., and P.L. Andresen. 1988. Development and use of a predictive model of crack propagation in 304/304L, A533B/A508 and Inconel 600/182 alloys in 288 °C water. *Proceedings of the Third International Symposium on Environmental Degradation of Materials in Nuclear Power Systems-Water Reactors*. G.J. Theus and J.R. Weeks, eds. Warrendale, PA: The Metallurgical Society: 789-800.
- Ford, F.P., and P.L. Andresen. 1992. Electrochemical effects on environmentally-assisted cracking. *Parkins Symposium on Fundamental Aspects of Stress Corrosion Cracking*. S.M. Bruemmer, E.I. Meletis, R.H. Jones, W.W. Gerberich, F.P. Ford, and R.W. Staehle, eds. Warrendale, PA: The Minerals, Metals, and Materials Society: 43-67.
- Forty, A.J., and P. Humble. 1963. Influence of surface tarnish on the stress corrosion of brass. *Philosophical Magazine* 8: 247-253.
- Frost, H.J., and M.F. Ashby. 1982. Deformation mechanism maps. *The Plasticity and Creep of Metals and Ceramics*. Oxford, U.K.: Pergamon Press.
- Galvele, J.R. 1976. Transport processes and the mechanism of pitting of metals. *Journal of the Electrochemical Society* 123: 464-474.

- Galvele, J.R. 1981. Transport processes in passivity breakdown — II. Full hydrolysis of the metal ions. *Corrosion Science* 21: 551-579.
- Galvele, J.R. 1987. A stress corrosion cracking mechanism based on surface mobility. *Corrosion Science* 27: 1-33.
- Galvele, J.R. 1990. Surface mobility-stress corrosion cracking mechanism of steels for steam turbine rotors. *Corrosion Science* 30: 955-958.
- Galvele, J.R. 1992. Surface mobility mechanism of SCC. *Parkins Symposium on Fundamental Aspects of Stress Corrosion Cracking*. S.M. Bruemmer, E.I. Meletis, R.H. Jones, W.W. Gerberich, F.P. Ford, and R.W. Staehle, eds. Warrendale, PA: The Minerals, Metals, and Materials Society: 85-101.
- Garisto, N.C., and F. Garisto. 1988. *Mass Transport—Precipitation Coupling in Finite Systems*. AECL-9562. Whiteshell, Canada: Atomic Energy of Canada, Ltd.
- Garrels, R.M., and F.T. Mackenzie. 1966. Origin of the chemical compositions of some springs and lakes. *Advances in Chemistry Series* 67: 222-242.
- Gorse, D., J.C. Joud, and B. Baroux. 1992. The effect of ageing on passive films formed on stainless steels by annealing in hydrogen atmospheres. *Corrosion Science* 33: 1455-1478.
- Grambow, B. 1989. *Spent Fuel Dissolution and Oxidation, An Evaluation of Literature Data*. SKB Technical Report 89-13. Swedish Nuclear Fuel and Waste Management Co.
- Gravano, S.M., and J.R. Galvele. 1984. Transport processes in passivity breakdown — II. Full hydrolysis plus ion migration plus buffers. *Corrosion Science* 24: 517-534.
- Gray, W.J., H.R. Leider, and S.A. Steward. 1992. Parametric study of LWR spent fuel dissolution kinetics. *Journal of Nuclear Materials* 190: 46-52.
- Hagn, L. 1984. Lifetime prediction for parts in corrosive environments. *Corrosion in Power Generating Equipment*. M.O. Speidel and A. Atrens, eds. New York, NY: Plenum Press: 481-516.
- Helgeson, H.C. 1969. Thermodynamics of hydrothermal systems at elevated temperatures and pressures. *American Journal of Science* 729-804.
- Henshall, G.A. 1992. Stochastic models for predicting pitting corrosion damage of HLRW containers. *Proceedings of the Topical Meeting on Nuclear Waste Packaging, Focus '91*. La Grange Park, IL: American Nuclear Society, Inc. 225-232.
- Henshall, G.A., W.G. Halsey, W.L. Clarke, and R.D. McCright. 1993. *Modeling Pitting Corrosion Damage of High-Level Radioactive Waste Containers, With Emphasis on the Stochastic Approach*. UCRL-ID-111624. Livermore, CA: Lawrence Livermore National Laboratory.

- Heubner, U., and M. Köhler. 1992. Time-temperature precipitation and time-temperature sensitization behavior of highly corrosion resistant nickel-chromium-molybdenum alloys. *Werkstoffe und Korrosion* 43: 181-190.
- Hindmarsh, A.C. 1983. ODEpack, A systematized collection of ODE solvers. *Scientific Computing*. R.S. Stepelman et al., eds. Amsterdam, The Netherlands: North-Holland Publishing Co. 55-64.
- Hocking, W.H., D.W. Shoesmith, and J.S. Betteridge. 1992. Reactivity effects in the oxidative dissolution of UO<sub>2</sub> nuclear fuel. *Journal of Nuclear Materials* 190: 36-45.
- Hodge, F.G., and H.S. Ahluwalia. 1993. The influence of long-term low temperature aging on the performance of candidate high-nickel alloys for the nuclear waste repository. *12th International Corrosion Congress*. Houston, TX: National Association of Corrosion Engineers.
- Hyatt, M.V., and M.O. Speidel. 1972. High strength aluminum alloys. *Stress-Corrosion Cracking in High Strength Steels and in Titanium and Aluminum Alloys*. B.F. Brown, ed. Washington, DC: Naval Research Laboratory: 147-244.
- Johnson, L.H., and D.M. LeNeveu. 1993. Performance assessment of engineered barrier using the vault model. *Scientific Basis for Nuclear Waste Management XVI*. C.G. Interrante and R.T. Pabalan, eds. Pittsburgh, PA: Materials Research Society: 689-696.
- Jones, R.H., and R.E. Ricker. 1992. Mechanisms of stress-corrosion cracking. *Stress-Corrosion Cracking. Materials Performance and Evaluation*. R.H. Jones, ed. Materials Park, OH: ASM International: 1-40.
- Jones, R.H., and E.P. Simonen. 1993. Stage I stress corrosion cracking behavior. *Materials Science and Engineering A* 160: 127-136.
- Jury, W.A., W.R. Gardner, and W.H. Gardner. 1991. *Soil Physics*. New York, NY: John Wiley and Sons.
- Lacombe, P., and R.N. Parkins. 1977. Low strength steels — Session evaluation. *Stress Corrosion Cracking and Hydrogen Embrittlement of Iron Base Alloys*. R.W. Staehle, J. Hochmann, R.D. McCright, and J.E. Slater, eds. Houston, TX: National Association of Corrosion Engineers: 521-523.
- Lidbury, D.P.G. 1984. The estimation of crack tip strain rate parameters characterizing environment assisted crack growth data. *Embrittlement by the Localized Crack Environment*. R.P. Gangloff, ed. Warrendale, PA: The Metallurgical Society: 149-172.
- Lin, L.F., C.Y. Chao, and D.D. Macdonald. 1981. A point defect model for anodic passive films. *Journal of the Electrochemical Society* 128 (6): 1194-1198.
- Liu, C-T., and W.T. Lindsay. 1972. Thermodynamics of sodium chloride solutions at high temperatures. *Journal of Solution Chemistry* 1 (1): 45-69.

- Lukezich, S.J., and H.S. Ahluwalia. 1992. The corrosion performance of candidate high nickel alloys in simulated nuclear waste repository environments. *Nuclear Waste Packaging. Focus '91*. La Grange Park, IL: American Nuclear Society. 170-176.
- Macdonald, D.D., and M. Urquidi-Macdonald. 1990. Thin-layer mixed potential model for the corrosion of high-level waste canisters. *Corrosion* 46 (5): 380-390.
- Macdonald, D.D., and M. Urquidi-Macdonald. 1991. A coupled environment model for stress corrosion cracking in sensitized type 304 SS in LWR environments. *Corrosion Science* 32: 51-61.
- Macdonald, D.D., and M. Urquidi-Macdonald. 1992a. Corrosion damage function — Interface between corrosion science and engineering. *Corrosion* 48 (5): 354-367.
- Macdonald, D.D., and M. Urquidi-Macdonald. 1992b. An advanced coupled environment fracture model for predicting crack growth rate in LWR heat transport circuits. *Proceedings of the Fifth International Symposium on Environmental Degradation of Materials in Nuclear Power Systems—Water Reactors*. D. Cubicciotti and E.P. Simonen, eds. La Grange Park, IL: American Nuclear Society: 345-349.
- Manaktala, H.K. 1993. *Characteristics of Spent Nuclear Fuel and Cladding Relevant to High-Level Waste Source Term*. CNWRA 93-006. San Antonio, TX: Center for Nuclear Waste Regulatory Analyses.
- Marsh, G.P., K.J. Taylor, S.M. Sharland, and P.W. Tasker. 1987. An approach to evaluating the general and localized corrosion of carbon steel containers for nuclear waste disposal. *Scientific Basis for Nuclear Waste Management X*. Pittsburgh, PA: Materials Research Society. 84: 227-238.
- McEvily, A.J., and A.P. Bond. 1965. On the initiation and growth of stress corrosion crack in tarnished brass. *Journal of the Electrochemical Society* 112: 131-138.
- McGrail, B.P., and D.W. Engel. 1993. Coupled process modeling and waste package performance. *Scientific Basis for Nuclear Waste Management XVI*. C.G. Interrante and R.T. Pabalan, eds. Pittsburgh, PA: Materials Research Society. 294: 215-223.
- Mohr, D.W., and M.B. McNeil. 1992. Modified log-activity diagrams as a tool for modeling corrosion of nuclear waste container materials, with particular reference to copper. *Journal of Nuclear Materials* 190: 329-342.
- Mola, E.E., B. Melle, E.M. Rodriguez de Schiapparelli, J.L. Vincente, R.C. Salvarezza, and A.J. Arvia. 1990. Stochastic approach to pitting corrosion modeling. I. The case of quasi-hemispherical pits. *Journal of the Electrochemical Society* 137: 1384-1390.
- Murphy, W.M., E.H. Oelkers, and P.C. Lichtner. 1989. Surface reaction versus diffusion control of mineral dissolution and growth rates in geochemical processes. *Chemical Geology* 78: 357-380.

- Murphy, W.M. 1991. Geochemical modeling. *Report on Research Activities for Calendar Year 1990*. W.C. Patrick, ed. NUREG/CR-5817. CNWRA 90-01A. San Antonio, TX: Center for Nuclear Waste Regulatory Analyses: 2-24 to 2-41.
- Nakayama, G., and M. Akashi. 1993a. Critical conditions for initiation of localized corrosion of mild steels in contact with bentonite used in geological disposal packages of nuclear waste. *Scientific Basis for Nuclear Waste Management XVI*. C.G. Interrante and R.T. Pabalan, eds. Pittsburgh, PA: Materials Research Society. 294: 329-334.
- Nakayama, G., and M. Akashi. 1993b. Localized corrosion prediction for nuclear waste disposal container materials. *High-Level Radioactive Waste Management*. La Grange Park, IL: American Nuclear Society: 1761-1769.
- National Research Council. 1928. *International Critical Tables of Numerical Data, Physics, Chemistry and Technology*. Vol. III. New York, NY: McGraw-Hill.
- Needes, C.R.S., M.J. Nichol, and N.P. Finkelstein. 1975. Electrochemical model for the leaching of uranium dioxide: 2 — Alkaline carbonate media. *Leaching and Reduction in Hydrometallurgy*. A.R. Burkin, ed. London: Institute of Mining and Metallurgy.
- Newman, J.F. 1981. The stress corrosion of steel in sodium hydroxide solution: A film-rupture model. *Corrosion Science* 21: 487-503.
- Newman, R.C. 1987. Measurement and interpretation of electrochemical kinetics on bare metal surfaces. *Corrosion Chemistry within Pits, Crevices and Cracks*. A. Turnbull, ed. Teddington, U.K.: Her Majesty's Stationary Office: 317-356.
- Newman, J.S. 1991. *Electrochemical Systems*. Englewood Cliffs, NJ: Prentice Hall.
- Nitao, J.J. 1989. *V-TOUGH—An Enhanced Version of the TOUGH Code for the Thermal and Hydrologic Simulation of Large-Scale Problems in Nuclear Waste Isolation*. UCID-21954. Livermore, CA: Lawrence Livermore National Laboratory.
- Oelkers, E.H., and G.C. Helgeson. 1988. Calculation of the thermodynamic and transport properties of aqueous species at high pressures and temperatures: Aqueous tracer diffusion coefficients of ions to 1000 °C and 5 kb. *Geochimica et Cosmochimica Acta* 52: 63-85.
- Okada, T. 1984. Halide nuclei theory of pit initiation in passive metals. *Journal of the Electrochemical Society* 131 (2): 241-247.
- Parkins, R.N. 1972. Stress corrosion spectrum. *British Corrosion Journal* 7: 15-28.
- Parkins, R.N. 1987. Factors influencing stress corrosion crack growth kinetics. *CORROSION/87*. Paper No. 177. Houston, TX: National Association of Corrosion Engineers.
- Parkins, R.N. 1990. Stress corrosion cracking. *Environment-Induced Cracking of Metals*. R.P. Gangloff and M.B. Ives, eds. Houston, TX: National Association of Corrosion Engineers: 1-29.

- Patil, K., A.D. Tripathi, G. Pathak, and S.S. Kattl. 1991. Thermodynamic properties of aqueous electrolyte solutions. 2. *Journal of Chemical and Engineering Data* 36: 225-230.
- Patrick, W.C. 1986. *Spent Fuel Test — Climax: An Evaluation of the Technical Feasibility of Geologic Storage of Spent Nuclear Fuel in Granite*. UCRL-53702. Livermore, CA: Lawrence Livermore National Laboratory.
- Perry, R.H., and C.H. Chilton. 1973. *Chemical Engineer's Handbook*. Fifth Edition. New York, NY: McGraw-Hill.
- Peters, C.A., I.C. Yang, J.D. Higgins, and P.A. Burger. 1992. A preliminary study of the chemistry of pore water extracted from tuff by one-dimensional compression. *Water-Rock Interaction*. Kharaka and Maest, eds. 741-745.
- Pigford, T.H., P.L. Chambré, and W.W.-L. Lee. 1990. *A Review of Near-Field Mass Transfer in Geologic Disposal Systems*. LBL-27045. Berkeley, CA: Lawrence Berkeley Laboratory.
- Pitzer, K.S., ed. 1991. *Activity Coefficients in Electrolyte Solutions*. Second Edition. Boca Raton, FL: CRC Press.
- Press, W.H., P.F. Brian, S.A. Teukolsky, and W.T. Vetterling. 1986. *Numerical Recipes: The Art of Scientific Computing*. Cambridge: Cambridge University Press.
- Pruess, K., J.S.Y. Wang, and Y.W. Tsang. 1990. On thermohydrologic conditions near high-level nuclear wastes emplaced in partially saturated fractured tuff 1. Simulation studies with explicit consideration of fracture effects. *Water Resources Research* 26 (6): 1235-1248.
- Pruess, K., and Y. Tsang. 1993. Modeling of strongly heat-driven flow processes at a potential high-level nuclear waste repository at Yucca Mountain, Nevada. *High-Level Radioactive Waste Management*. La Grange Park, IL: American Nuclear Society: 568-575.
- Pugh, E.N. 1985. Progress towards understanding the stress corrosion problem. *Corrosion* 41: 517-526.
- Ranjan, R., and O. Buck. 1985. Predicting initiation of crack growth under stress corrosion cracking conditions. *Predictive Capabilities in Environmentally Assisted Cracking*. R. Rungta, ed. New York, NY: The American Society of Mechanical Engineers: PVP-Vol. 99: 79-89.
- Rard, J.A., and R.F. Platford. 1991. Experimental methods: Isopiestic. *Activity Coefficients of Electrolyte Solutions*. K. Pitzer, ed. Second Edition. Boca Raton, FL: CRC Press. 209-277.
- Reed, D.T. 1991. Progress in assessing the effect of ionizing radiation on the anticipated waste package environment at the Yucca Mountain potential repository site. *Proceedings of the Topical Meeting on Nuclear Waste Packaging, Focus '91*. La Grange Park, IL: American Nuclear Society. 58-67.
- Rimstidt, J., M.A. Williamson, and W.D. Newcomb. 1991. Element redistribution in Yucca Mountain radioactive waste repository produced by evaporation and condensation of water in a thermal

field. *Proceedings of the Topical Meeting on Nuclear Waste Packaging, Focus '91*. La Grange Park, IL: American Nuclear Society.

Roark, R.J., and W.C. Young. 1975. *Formulas for Stress and Strain*. New York, NY: McGraw-Hill.

Rolfe, S.T., and J.M. Barsom. 1977. *Fracture and Fatigue Control in Structures: Application of Fracture Mechanics*. Englewood Cliffs, NJ: Prentice-Hall, Inc.

Russell, A.J., and D. Tromans. 1979. A fracture mechanics study of stress corrosion cracking of type 316 austenitic steel. *Metallurgical Transactions A* 10: 1229-1238.

Scully, J.C. 1975. Stress corrosion crack propagation: A constant charge criterion. *Corrosion Science* 15: 207-224.

Sharland, S.M. 1992. A mathematical model of the initiation of crevice corrosion in metals. *Corrosion Science* 33: 183-201.

Shibata, T. 1983. Stochastic approach to the effect of alloying elements on the pitting resistance of ferritic stainless steels. *Transactions of Iron and Steel Institute of Japan* 23: 785-788.

Shibata, T., and H. Takamiya. 1986. Effect of pH and  $[Cl^-]$  on the stochastic process of pitting corrosion of Mo containing stainless steels. *Critical Issues in Reducing the Corrosion of Steels*. H. Leidheiser, Jr. and S. Haruyama, eds. Houston, TX: National Association of Corrosion Engineers: 17-27.

Shibata, T., and T. Takeyama. 1977. Stochastic theory of pitting. *Corrosion* 33: 243-251.

Shibata, T., and T. Takeyama. 1981. Death and birth stochastic process in pitting corrosion of 17Cr ferritic stainless steels. *Metallic Corrosion. Proceedings — 8th International Congress on Metallic Corrosion 1981*. Frankfurt am Main, Germany: DECHEMA. 1: 146-151.

Shoesmith, D.W., and S. Sunder. 1991. *An Electrochemistry Based Model for the Dissolution of  $UO_2$* . AECL-10488. Pinawa, Manitoba, Canada: Atomic Energy of Canada Limited.

Shoesmith, D.W., and S. Sunder. 1992. The prediction of nuclear fuel dissolution rates under waste disposal conditions. *Journal of Nuclear Materials* 190: 20-35.

Sieradzki, K., and R.C. Newman. 1985. Brittle behaviour of ductile metals during stress-corrosion cracking. *Philosophical Magazine A* 51: 95-132.

Smialos, E., W. Schwarzkopf, R. Köster, B. Fiehn, and G. Halm. 1990. *Corrosion Testing of Selected Packaging Materials for Disposal of High-Level Waste Glass in Rock Salt Formations*. KfK 4723. Karlsruhe, Germany: Kernforschungszentrum.

Speidel, M.O. 1971. Current understanding of stress corrosion crack growth in aluminum alloys. *Theory of Stress Corrosion Cracking in Alloys*. J.C. Scully, ed. Brussels, Belgium: North American Treaty Organization: 289-344.

- Speidel, M.O. 1981. Stress corrosion cracking of stainless steel in NaCl solution. *Metallurgical Transactions A* 12: 779-789.
- Sridhar, N., and G.A. Cragolino. 1992. Repassivation potentials for long-term life prediction of localized corrosion. *Scientific Basis for Nuclear Waste Management*. Pittsburgh, PA: Materials Research Society. To be published.
- Sridhar, N., and D.S. Dunn. 1993. The effects of surface chromium depletion on the localized corrosion alloy 825 high-level waste container material. Paper No. 138. *CORROSION/94*. Houston, TX: NACE International.
- Sridhar, N., B.E. Wilde, C. Manfredi, S. Kesavan, and C. Miller. 1991. *Hydrogen Absorption and Embrittlement of Candidate Container Materials*. CNWRA 91-008. San Antonio, TX: Center for Nuclear Waste Regulatory Analyses.
- Sridhar, N., G.A. Cragolino, and D.S. Dunn. 1993. *Experimental Investigations of Localized Corrosion of High-Level Waste Container Materials*. CNWRA 93-004. San Antonio, TX: Center for Nuclear Waste Regulatory Analyses.
- Staehle, R.W. 1991. Combining design and corrosion for predicting life. *Life Prediction of Corrodible Structures*. R.N. Parkins, ed. Houston, TX: National Association of Corrosion Engineers. To be published.
- Stewart, J., and D.E. Williams. 1992. The initiation of pitting corrosion on austenitic stainless steel: On the role and importance of sulfide inclusions. *Corrosion Science* 33 (3): 457-474.
- Stumm, W., and J.J. Morgan. 1981. *Aquatic Chemistry, an Introduction Emphasizing Chemical Equilibria in Natural Waters*. New York, NY: John Wiley and Sons.
- Sunder, S., and D.W. Shoesmith. 1991. *Chemistry of UO<sub>2</sub> Fuel Dissolution in Relation to the Disposal of Used Nuclear Fuel*. AECL-10395. Pinawa, Manitoba, Canada: Atomic Energy of Canada Limited.
- Szklarska-Smialowska, Z. 1986. *Pitting Corrosion of Metals*. Houston, TX: National Association of Corrosion Engineers: 19.
- Tamaki, K., S. Tsujikawa, and Y. Hisamatsu. 1990. Development of a new test method for chloride stress corrosion cracking of stainless steel in dilute NaCl solutions. *Advances in Localized Corrosion*. H.S. Isaacs, U. Bertocci, J. Kruger, and S. Smialowska, eds. Houston, TX: National Association of Corrosion Engineers: 207-214.
- Thompson, N.G., and B.C. Syrett. 1992. Relationship between conventional pitting and protection potentials and a new, unique pitting potential. *Corrosion* 48 (8): 649-659.
- Thompson, N.G., J.A. Beavers, and C.L. Durr. 1992. *Potentiodynamic Polarization Studies on Candidate Container Alloys for the Tuff Repository*. NUREG/CR-5708. Washington, DC: U.S. Nuclear Regulatory Commission.

- Treybal, R.E. 1980. *Mass-Transfer Operations*. New York, NY: McGraw-Hill.
- Tsujikawa, S., T. Shinihara, and Y. Hisamatsu. 1985. The role of crevices in comparison to pits in initiating stress corrosion cracks of type 316 stainless steel in different concentrations of  $MgCl_2$  solutions at 80 °C. *Corrosion Cracking*. V.S. Goel, ed. Metals Park, OH: American Society for Metals: 35-42.
- Tsujikawa, S., Y. Sone, and Y. Hisamatsu. 1987. Analysis of mass transfer in a crevice region for a concept of the repassivation potential as a crevice-corrosion characteristic. *Corrosion Chemistry Within Pits, Crevices, and Cracks*. A. Turnbull, ed. London: Her Majesty's Stationary Office: 171-186.
- Turnbull, A. 1993. Modelling of environment assisted cracking. *Corrosion Science* 34: 921-960.
- Turnbull, A., and M. Psaila-Dombrowski. 1992. A review of electrochemistry of relevance to environment-assisted cracking in light water reactors. *Corrosion Science* 33: 1925-1966.
- Urquidi-Macdonald, M., and D.D. Macdonald. 1987. Theoretical distribution functions for the breakdown of passive films. *Journal of the Electrochemical Society* 134 (1): 41-46.
- U.S. DOE. 1989. *Yucca Mountain Project Reference Information Base, Chapter 1, Section 3, Item 1, Version 4, Revision 0, Release Date 2/1/89*. 1-3.
- U.S. DOE. 1993a. *Yucca Mountain Site Characterization Project Waste Package Plan, Revision 1*. YMP/90-62. Washington, DC: U.S. Department of Energy, Office of Civilian Radioactive Waste Management.
- U.S. DOE. 1993b. *Yucca Mountain Site Characterization Project Waste Package Implementation Plan, Revision 0*. YMP/92-11. Washington, DC: U.S. Department of Energy, Office of Civilian Radioactive Waste Management.
- U.S. DOE. 1993c. *Yucca Mountain Site Characterization Project Reference Information Base, Revision 2*. YMP/93-02, Chapter 3, Section 1, Item 1. Washington, DC: U.S. Department of Energy, Office of Civilian Radioactive Waste Management.
- van Brakel, J., and P.M. Heertjes. 1974. Analysis of diffusion in microporous media in terms of a porosity, a tortuosity, and a constrictivity factor. *International Journal of Heat Mass Transfer* 17: 1093-1103.
- Vaniman, D.T., M.H. Ebinger, D.L. Bish, and S.J. Chipera. 1992. Precipitation of calcite, dolomite, sepiolite and silica from evaporated carbonate and tuffaceous waters of southern Nevada, USA. *Water-Rock Interaction*. Kharaka and Maest, eds. 687-691.
- Vermilyea, D.A. 1972. A theory for the propagation of stress corrosion cracks in metals. *Journal of the Electrochemical Society* 119: 405-407.

- Vermilyea, D.A. 1977. A film rupture model for stress corrosion cracking. *Stress Corrosion Cracking and Hydrogen Embrittlement of Iron Base Alloys*. R.W. Staehle, J. Hochmann, R.D. McCright, and J.E. Slater, eds. Houston, TX: National Association of Corrosion Engineers: 208-217.
- Vetter, K.J. 1967. *Electrochemical Kinetics. Theoretical and Experimental Aspects*. New York, NY: Academic Press.
- Walter, R.J., and W.T. Chandler. 1973. *Influence of Gaseous Hydrogen on Metals. Final Report*. NASA CR-124410. Canoga Park, CA: Rocketdyne Division of Rockwell International.
- Walton, J.C., and S.K. Kalandros. 1992a. *TWITCH—A Model for Transient Diffusion, Electromigration, and Chemical Reaction in One Dimension — Version 1.0*. CNWRA 92-019. San Antonio, TX: Center for Nuclear Waste Regulatory Analyses.
- Walton, J.C., and S.K. Kalandros. 1992b. *MARIANA—A Simple Chemical Equilibrium Module — Version 1.0*. CNWRA 92-020. San Antonio, TX: Center for Nuclear Waste Regulatory Analyses.
- Walton, J.C., and B. Sagar. 1988. Modeling performance of steel containers in high-level waste repository environments: Implications for waste isolation. *Radioactive Waste Management and the Nuclear Fuel Cycle* 9 (4): 323-347.
- Wanner, H., and I. Forest, eds. 1992. *Chemical Thermodynamics of Uranium*. Nuclear Energy Agency. Organisation for Economic Co-operation and Development (OECD). Amsterdam, The Netherlands: North-Holland Publishing Co.
- Watson, M.K., and J. Postlethwaite. 1990. Numerical simulation of crevice corrosion of stainless steel and nickel alloys in chloride solutions. *Corrosion* 46: 522-530.
- Will, F.G. 1976. *The Oxygen Electrode: A Critical Assessment*. Report No. 76CRD2 76. Schenectady, NY: General Electric Co.
- Williams, D.E., C. Westcott, and M. Fleischmann. 1985a. Stochastic models of pitting corrosion of stainless steels. I. Modeling of the initiation and growth of pits at constant potential. *Journal of the Electrochemical Society* 132: 1796-1804.
- Williams, D.E., C. Westcott, and M. Fleischmann. 1985b. Stochastic models of pitting corrosion of stainless steels. II. Measurement and interpretation of data at constant potential. *Journal of the Electrochemical Society* 132: 1804-1811.
- Zimmerman, R.M., and M.L. Blanford. 1986. Expected thermal and hydrothermal environments for waste emplacement holes based on G-tunnel heater experiments. *27th U.S. Symposium on Rock Mechanics*. H. Hartman, ed. Littleton, CO: Society of Mining Engineers, Inc. 874-882.

## **APPENDIX A**

Table A-1. Pit initiation, repassivation, and crevice repassivation potentials of types 304/304L stainless steels as a function of chloride concentration and temperature from literature

Chloride, M	$E_p$ , mV, 20°C	$E_p$ , mV, 40°C	$E_p$ , mV, 60°C	$E_p$ , mV, 80°C	$E_p$ , mV, 150°C	$E_{rp}$ , mV, 20°C	$E_{rp}$ , mV, 55°C	$E_{rp}$ , mV, 80°C	$E_{rp}$ , mV, 90°C	$E_{rp}$ , mV, 150°C	$E_{rc}$ , mV, 20°C	$E_{rc}$ , mV, 55°C	$E_{rc}$ , mV, 80°C	$E_{rc}$ , mV, 90°C	Ref
0.00028					200										1
0.00028												410		110	2
0.00028												360			3
0.0005	750										-180				4
0.00283	460	350	270	220	80										1
0.00283												70			3
0.00283												110		-240	2
0.005	680										-280				4
0.01	620										-220				4
0.01						50									5
0.01					-40					-380					6
0.014														-290	2
0.02						50									5
0.0283												-120			3
0.0283														-300	2
0.0283		200		65	0										1
0.034	700		400			40	-30								5

**Table A-1. Pit initiation, repassivation, and crevice repassivation potentials of types 304/304L stainless steels as a function of chloride concentration and temperature from literature (cont'd)**

Chloride, M	$E_p$ , mV, 20°C	$E_p$ , mV, 40°C	$E_p$ , mV, 60°C	$E_p$ , mV, 80°C	$E_p$ , mV, 150°C	$E_{rp}$ , mV, 20°C	$E_{rp}$ , mV, 55°C	$E_{rp}$ , mV, 80°C	$E_{rp}$ , mV, 90°C	$E_{rp}$ , mV, 150°C	$E_{rc}$ , mV, 20°C	$E_{rc}$ , mV, 55°C	$E_{rc}$ , mV, 80°C	$E_{rc}$ , mV, 90°C	Ref
0.05					-160					-420					6
0.05	500										-280				4
0.05													-190		7
0.05	230														8
0.064	230														1
0.08	650		300			0	-120								5
0.1	200	50		0	-200										9
0.1		100		80	-100										9
0.1					-200					-430					6
0.1			-20	-60	-160										10
0.15	620		280			-50	-150								5
0.21	170	80	0												1
0.38	500					-120									5
0.4	320										-370				4
0.5													-380		7
0.5	160														11
0.5	360	240	60	-90	-340	-50	-140	-230	-240	-440	-320	-340	-390	-400	12

**Table A-1. Pit initiation, repassivation, and crevice repassivation potentials of types 304/304L stainless steels as a function of chloride concentration and temperature from literature (cont'd)**

Chloride, M	$E_p$ , mV, 20°C	$E_p$ , mV, 40°C	$E_p$ , mV, 60°C	$E_p$ , mV, 80°C	$E_p$ , mV, 150°C	$E_{rp}$ , mV, 20°C	$E_{rp}$ , mV, 55°C	$E_{rp}$ , mV, 80°C	$E_{rp}$ , mV, 90°C	$E_{rp}$ , mV, 150°C	$E_{rc}$ , mV, 20°C	$E_{rc}$ , mV, 55°C	$E_{rc}$ , mV, 80°C	$E_{rc}$ , mV, 90°C	Ref
0.536	100	40	-60	-110											1
0.63	450		150			-200	-300								5
1	400					-250									5
1	280														4
1	70														13
2					-440					-480					6
2.83												-120			2
3	10				-360										14
3.45													-410		7
4	-190	-250	-300	-350	-350										15
5.64	230														4

**Table A-2. Pit initiation, repassivation, and crevice corrosion potentials of alloy 825 in various chloride solutions from the literature**

Chloride, M	$E_p$ , mV 30°C	$E_p$ , mV 50°C	$E_p$ , mV 60°C	$E_p$ , mV 95°C	$E_{rp}$ , mV 30°C	$E_{rp}$ , mV 50°C	$E_{rp}$ , mV 60°C	$E_{rp}$ , mV 80°C	$E_{rp}$ , mV 95°C	$E_{rc}$ , mV 20°C	$E_{rc}$ , mV 55°C	$E_{rc}$ , mV 80°C	$E_{rc}$ , mV 90°C	Ref
0.283	864	606		418	-1	46								16
0.283					-20									16
0.0283	817	572	678	626	165	196	38	-10	82					16
0.0283				699		38			-46					16
0.0283				691					-35					16
0.0283				467					-26					16
0.0283				669					135					16
0.0283				690					-48					16
0.0283				699					-42					16
0.0283				679					-63					16
0.00283									366					16
0.00283									669					16
0.00283									688					16
0.00283									656					16
0.00283									672					16
0.00283									417					16
0.00283									309					16

Table A-2. Pit initiation, repassivation, and crevice corrosion potentials of alloy 825 in various chloride solutions from the literature (cont'd)

Chloride, M	$E_p$ , mV 30°C	$E_p$ , mV 50°C	$E_p$ , mV 60°C	$E_p$ , mV 95°C	$E_{rp}$ , mV 30°C	$E_{rp}$ , mV 50°C	$E_{rp}$ , mV 60°C	$E_{rp}$ , mV 80°C	$E_{rp}$ , mV 95°C	$E_{rc}$ , mV 20°C	$E_{rc}$ , mV 55°C	$E_{rc}$ , mV 80°C	$E_{rc}$ , mV 90°C	Ref
0.00283										758			158	17
0.00566									415					16
0.00566									152					16
0.00566									377					16
0.00566									335					16
0.00846									34					16
0.00846									103					16
0.00846									51					16
0.0283										58			-112	17
0.283										18			-122	17
0.05												-10		7
0.5				269					12					16
0.5												-100		7
0.5	1050		230		1030		0							18
3.45												-320		7
4			56	-7		-61	-61		-200					16

A-5

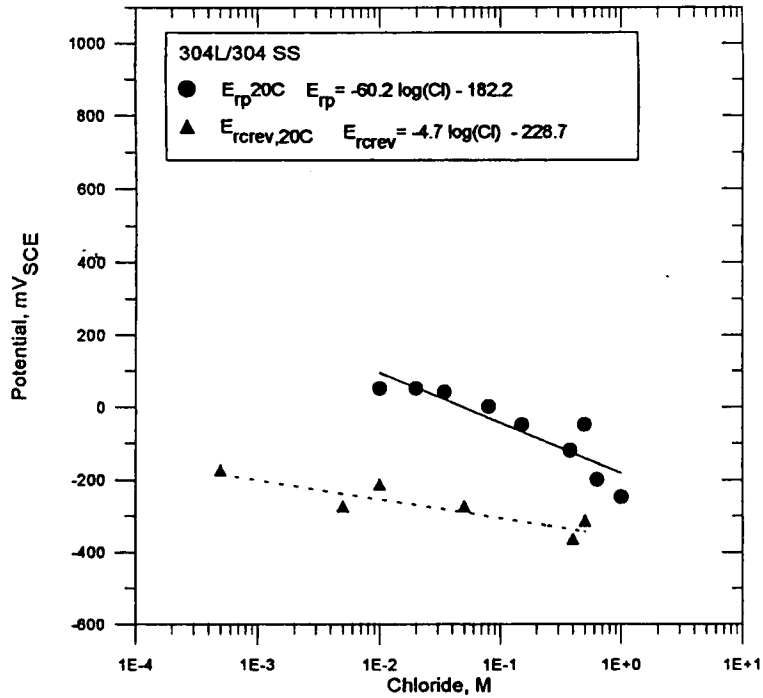


Figure A-1. The effect of chloride concentration on the pit and crevice repassivation potentials of types 304/304L stainless steels at room temperature

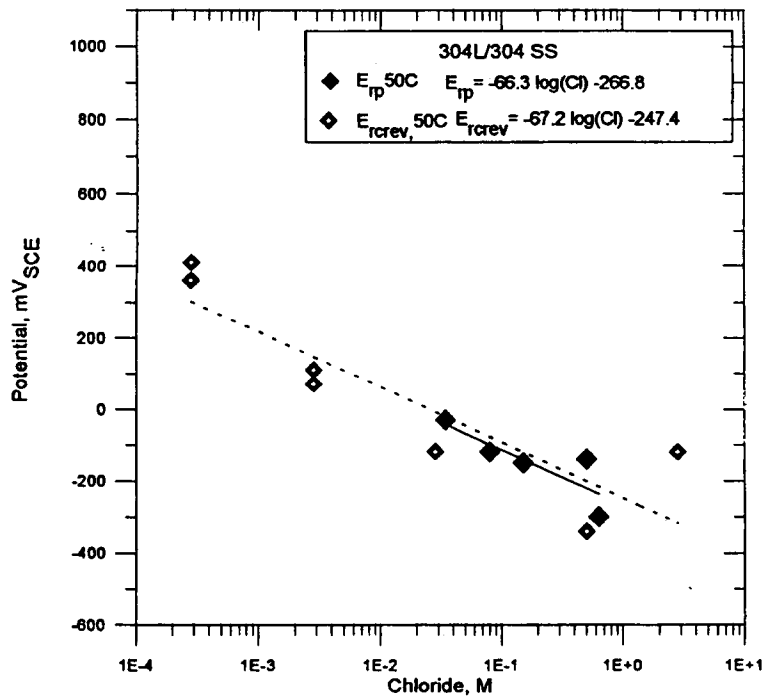


Figure A-2. Effect of chloride concentration on the repassivation potentials for pitting and crevice corrosion of types 304/304L stainless steels at 50 °C

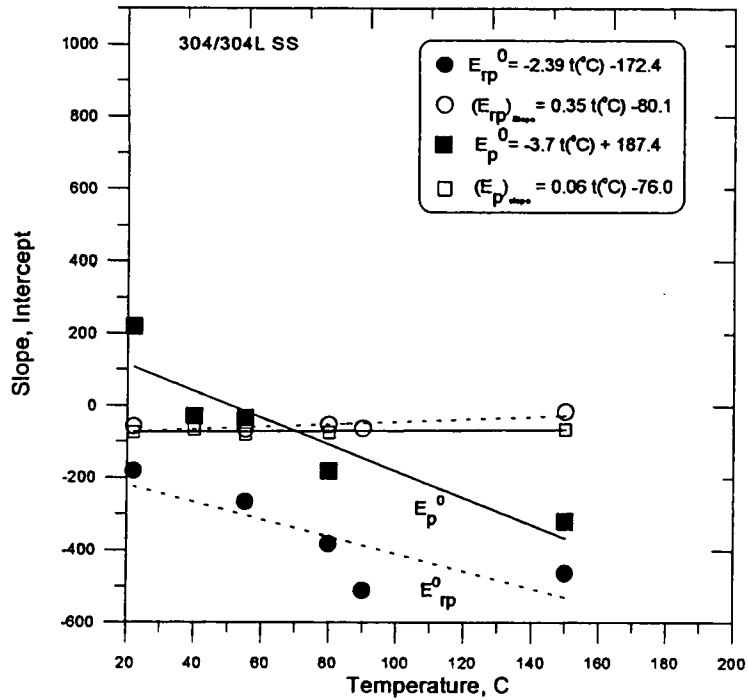


Figure A-3. The effect of temperature on the slope and intercept of the critical potential-log (chloride) relationship for types 304/304L stainless steels

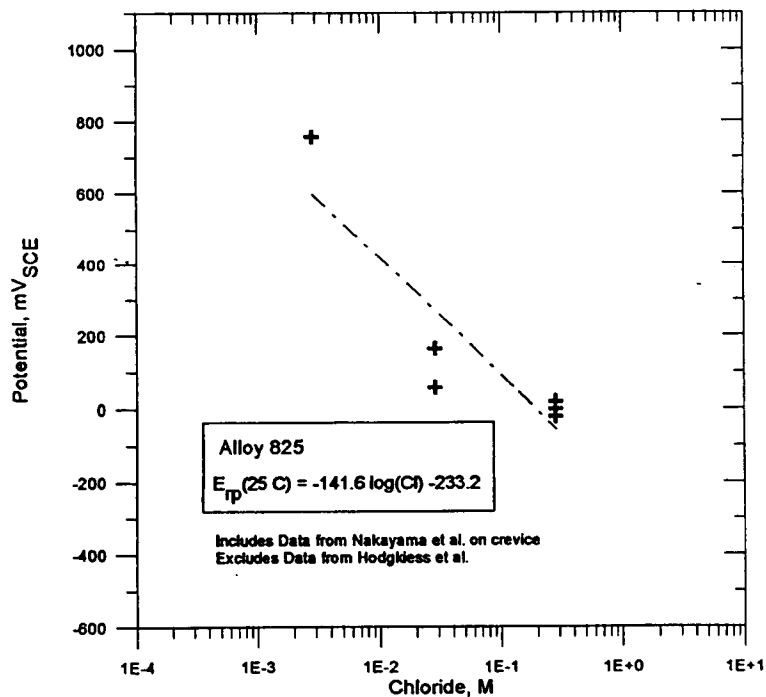


Figure A-4. The effect of chloride concentration on the pit repassivation potential of alloy 825 at 25 °C

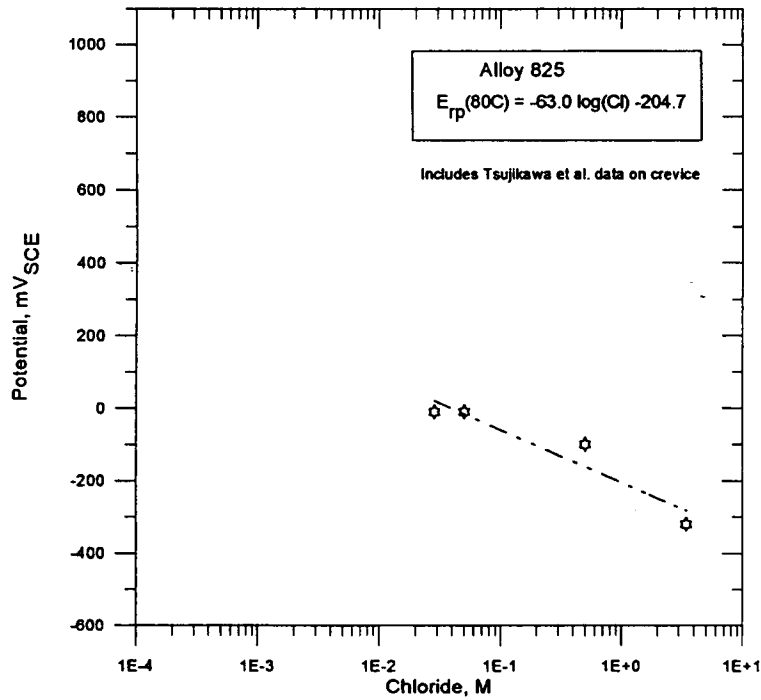


Figure A-5. The effect of chloride concentration on the repassivation potential for alloy 825 at 80 °C

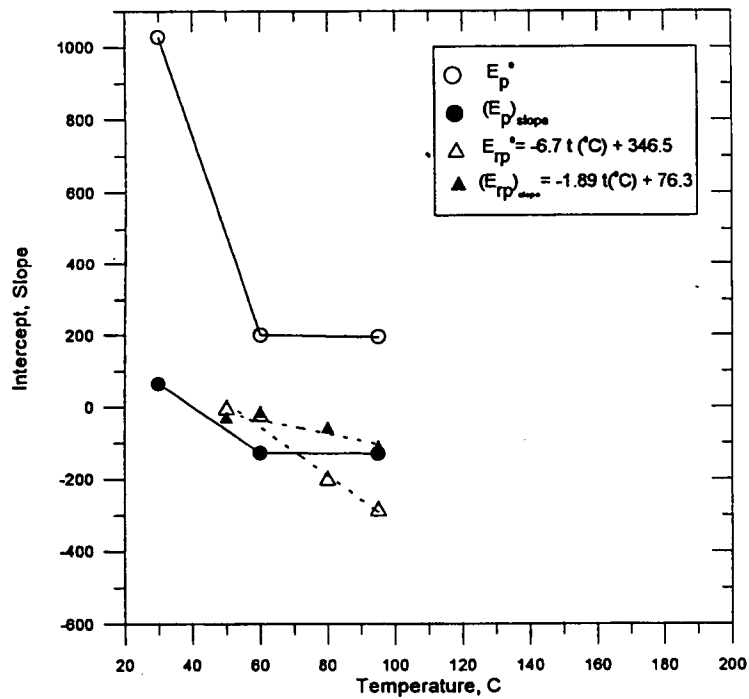


Figure A-6. The slope and intercept of the critical potentials-log (chloride) plots at various temperature for alloy 825

## REFERENCES

1. Wang, J.H., C.C. Su, and Z. Szklarska-Smialowska. 1988. Effects of Cl concentration and temperature on pitting of AISI 304 stainless steel. *Corrosion* 44 (10): 732-737.
2. Nakayama, G., H. Wakamatsu, and M. Akashi. 1992. Effects of chloride, bromide, and thiosulfate ions on the critical conditions for crevice corrosion of several stainless steels as a material for geologic disposal packages for nuclear waste. *Scientific Basis for Nuclear Waste Management XVI*. Pittsburgh, PA: Materials Research Society. 294: 323-328.
3. Kosaki, A., and Komada, H. 1991. Crevice corrosion resistivity assessment of carbon steel and stainless alloys. *Structural Mechanics in Reactor Technology*. Tokyo, Japan: Atomic Energy Society of Japan and The International Association for Structural Mechanics in Reactor Technology, e.v. Vol. SD1. 13/1. 259-264.
4. Lee, Y.H., Z. Takehara, and S. Yoshizawa. 1981. The enrichment of hydrogen and chloride ions in the crevice corrosion of steels. *Corrosion Science* 21: 391-397.
5. Azzerri, N., F. Mancina, and A. Tamba. 1982. Electrochemical prediction of corrosion behavior of stainless steels in chloride containing water. *Corrosion Science* 22 (7): 675-687.
6. Yashiro, H., and K. Tanno. 1990. The effect of electrolyte composition on the pitting and repassivation behavior of AISI 304 stainless steel at high temperature. *Corrosion Science* 31: 485-490.
7. Tsujikawa, S., and S. Okayama. 1990. Repassivation method to determine critical conditions in terms of electrode potential, temperature and NaCl concentration to predict crevice corrosion resistance of stainless steels. *Corrosion Science* 31: 441-446.
8. Bogaerts, W., A. Van Haute, M. Brabers, P. Vanslembruck, and D. Kennis. 1981. Influence of Cl, HCO<sub>3</sub>, and SO<sub>4</sub> on the corrosion of Fe-Cr-Ni alloys in hot water systems. *Metallic Corrosion. Proceedings of 8th International Congress on Metallic Corrosion*. Frankfurt, Germany: DECHEMA: 1887-1892.
9. Fujii, T. 1975. Pitting corrosion and temperature dependence of pitting potentials for stainless steels in chloride solutions at elevated temperatures. *Corrosion Engineering* 24: 183-188.
10. Bogaerts, W., and A.A. Van Haute. 1985. Chloride pitting and water chemistry control in cooling or boiler circuits. *Corrosion Science* 25 (12): 1149-1161.
11. Shibata, T., and H. Takamiya. 1986. Effect of pH and Cl on the stochastic process of pitting corrosion of Mo containing stainless steels. *Critical Issues in Reducing the Corrosion of Steels*. Houston, TX: National Association of Corrosion Engineers: 17-27.

12. Yashiro, H., K. Tanno, H. Hanayama, and A. Miura. 1990. Effect of temperature on the crevice corrosion of type 304 stainless steel in chloride solution up to 250 °C. *Corrosion* 46 (9): 727-733.
13. Wilde, B.E., and E. Williams. The relevance of accelerated electrochemical pitting tests to the long-term pitting and crevice corrosion behavior of stainless steels in marine environments. *Journal of the Electrochemical Society* 118 (7): 1057-1062.
14. Andresen, P.L. 1983. *The Effects of Aqueous Impurities on Intergranular Stress Corrosion Cracking of Sensitized Type 304 Stainless Steel*. EPRI-NP-3384. Palo Alto, CA: Electric Power Research Institute.
15. Posey, F.A., A.A. Palko, and A.L. Bacarella. 1978. *Corrosivity of Geothermal Brines Progress Report for Period Ending September, 1977*. ORNL/TM-6308. Oak Ridge, TN: Oak Ridge National Laboratory.
16. Cragolino, G.A., and N. Sridhar. 1991. Integrated waste package experiments. *Report on Research Activities for Calendar Year 1990*. W.C. Patrick, ed. NUREG/CR-5817. CNWRA 90-01A. San Antonio, TX: Center for Nuclear Waste Regulatory Analyses: 5-1 to 5-39.
17. Nakayama, G., and M. Akashi. 1993. Localized corrosion prediction for nuclear waste disposal container materials. *High-Level Radioactive Waste Management*. La Grange Park, IL: American Nuclear Society: 1761-1769.
18. Hodgkiess, T., and S. Rigas. 1983. A comparison of the corrosion resistance of some higher-alloy stainless steels in seawater at 20-100 °C. *Desalination*. 44: 283-294.

462.2 --- T199310180003  
Engineered Barrier System  
Performance Assessment Codes  
(EBSPAC) Progress Report -  
October 1, 1992, through